Title
Perfluorophenylazide Photochemistry for Modification of Materials

Author
Aguilar, Stephanie

Publication Date
2020

Peer reviewed|Thesis/dissertation

UNIVERSITY OF CALIFORNIA

Los Angeles

Perfluorophenylazide Photochemistry for Modification of Materials

A dissertation submitted in partial satisfaction of

the requirements for the degree Doctor of Philosophy

in Chemistry

by

Stephanie Aguilar

2020

ABSTRACT OF THE DISSERTATION

Perfluorophenylazide Photochemistry for Modification of Materials

by

Stephanie Aguilar

Doctor of Philosophy in Chemistry

University of California, Los Angeles

Professor Richard B. Kaner, Chair

Polymeric materials are proposed for applications in a variety of fields including and not limited to: biomedical applications, electronics, biosensor devices and water treatment. Covalent functionalization of these materials provides an effective means to adjust surface properties. These covalent approaches benefit more than noncovalent alternatives because they are more robust, creating stable attachment of groups with specific functional properties. Specifically, photoinitiated grafting can be performed under mild reaction conditions and low temperatures with high selectivity compared to other grafting techniques. Perfluorophenylazide (PFPA) chemistry has been used as a coupling agent for fluorinated phenylazide, which are capable of forming stable covalent bonds to sp^2 or sp^3 hybridized carbons or nitrogens. Phenylazides are popular because they are relatively simple to prepare, have fast kinetics, possess high reaction efficiencies, are easy

to store and can covalently link organic or inorganic materials. We propose to synthesize PFPA polymers and small molecules to graft a variety of materials to enhance the materials surface properties. These materials include polymers, semiconductor surfaces, metals, carbons and metal oxide surfaces. The surface properties altered include increased hydrophilicity and conductivity, lowered surface roughness, and reactivity of the surface. We have successfully modified a variety of surfaces and enhanced specifically the rejection and fouling capability of water purification membranes and a variety of other materials. In conclusion, we were able to successfully synthesize a variety of polymers and small molecules for modification of water purification membranes.

The goals of this dissertation are to investigate perfluorophenylazide chemistry and its use in a variety of materials to create covalently bonded coatings to enhance materials properties. Chapter 1 provides an introduction, while Chapter 2 compiles detailed performance of a tetraaniline coating on ultrafiltration membranes with respect to anti-fouling properties. Chapter 3 briefly describes a project investigating the synthesis and properties of the octamer of aniline. Chapter 4 discusses a collaborative project in creating polymer coatings on nanofiltration membranes to enhance divalent ion rejection. In Chapter 5, ethyleneimine and sulfonates are coated onto polypropylene separators used in lithium-sulfur batteries to enhance the capacity of the batteries by preventing polysulfide migration. In Chapter 6, zwitterions are coated onto polydimethylsiloxane to prevent biofouling in biomedical devices.

The dissertation of Stephanie Aguilar is approved.

William M. Gelbart

Yang Yang

Chong Liu

Richard B. Kaner, Committee Chair

University of California, Los Angeles

2020

Dedicated to my loving parents.

TABLE OF CONTENTS

LIST OF FIGURES

LIST OF TABLES

ACKNOWLEDGEMENT

First and foremost, I would like to thank my parents for the support they have always given me. I am very thankful for their encouragement and support in letting me be anything I wanted to be. I never would have made it this far if it wasn't for all the sacrifices they made for their kids. I also want to thank my loving sisters and nephews for always being there for me when I needed them the most. I want to thank my husband, Dr. Javier Pazos for always being there during the good and bad times of a PhD and for understanding that getting a doctorate requires a lot of time and patience.

I would like to thank my advisor, Professor Richard B. Kaner for guiding me throughout this process. I appreciate your willingness to listen to my ideas, the kindness, encouragement, and patience you always gave me. I would also like to thank my committee members Professor Chong Liu, Professor William Gelbart and Professor Yang Yang for their advice and support throughout my graduate studies.

I would like to thank all the past and present members of the Kaner group for their friendship and support. I have made some lifelong friends in this group and I appreciate the supporting environment. I would like to thank the the USA/China Clean Energy Research Center for Water-Energy Technologies (CERC-WET) and UCLA Eugene V. Cota-Robles Fellowship for financial support.

VITA

2016-2020	Graduate Student with Prof. Richard B. Kaner University of California, Los Angeles Los Angeles, California
2020	UCLA Chemists Association Dissertation Award in Inorganic Chemistry University of California, Los Angeles Los Angeles, California
2019	ACS PMSE Graduate Student Travel Award PMSE Division, ACS Conference Fall 2019 San Diego, California
2019	Research Showcase Travel Award for ACS National Conference University of California, Los Angeles Los Angeles, California
2019	Emerging Researchers National Conference in STEM Travel Award Washington DC
2016	Eugene V. Cota-Robles Fellowship University of California, Los Angeles Los Angeles, California
2016	UCLA University Fellowship University of California, Los Angeles Los Angeles, California
2016	Competitive Edge Summer Research Fellowship University of California, Los Angeles Los Angeles, California
2015	Master of Science in Organic Chemistry University of Illinois at Chicago Chicago, Illinois
2011-2015	Graduate Student with Prof. Laura L. Anderson University of Illinois at Chicago Chicago, Illinois
2011	Undergraduate Student University of California, Irvine Irvine, California

CHAPTER 1. INTRODUCTION

Perfluorophenylazides (PFPA) are known for generating a highly reactive nitrene from an azide ($-N_3$) moiety that allows them to make chemical bonds with rather unreactive substrates. The nitrene group is activated thermally or with photo-excitation that expels nitrogen gas and affords a reactive singlet nitrogen that attacks –NH-, C=C, and C-H bonds (**Fig. 1**). A PFPA can be synthesized with a carbonyl in the *para* position relative to the nitrene group that enables the attachment of a variety of amine or alcohol terminated molecules, particles, or surfaces via amide or ester bond formation. The azide functional group is activated by photo-excitation producing a highly reactive singlet nitrene that can, for example, undergo C-H insertion within the hydrocarbon backbone of a polyamide membrane, thus creating a covalent bond between the polymer and the membrane. Via intersystem crossing, the singlet nitrene gives a triplet nitrene that dimerizes to a diazo-compound, or gives a ring expansion to an azepine.

Polymeric materials have been proposed for applications in a variety of fields including: biomedical applications, electronics, biosensor devices and water treatment. Covalent functionalization of these materials provides an effective means to adjust surface properties. These covalent approaches benefit more than noncovalent alternatives because they are more robust, creating stable attachment of groups with specific functional properties. Specifically, photoinitiated grafting can be performed under mild reaction conditions and low temperatures with high selectivity compared to other grafting techniques. PFPA chemistry has been used as a coupling agent for fluorinated phenylazides, which are capable of forming stable covalent bonds to sp^2 or sp^3 hybridized carbons or nitrogens.

This chapter will focus on the synthesis of PFPA polymers and small molecules that can be used to graft a variety of materials to enhance the materials surface properties. The surface

properties altered include increased hydrophilicity and conductivity, smooth surface roughness, and reactivity of the surface. We have successfully modified a variety of surfaces and enhanced specifically the rejection and antifouling capacity of water purification membranes. This study opens possibilities to alter the surface properties of a variety of materials with polymers and small molecules in a facile manner.

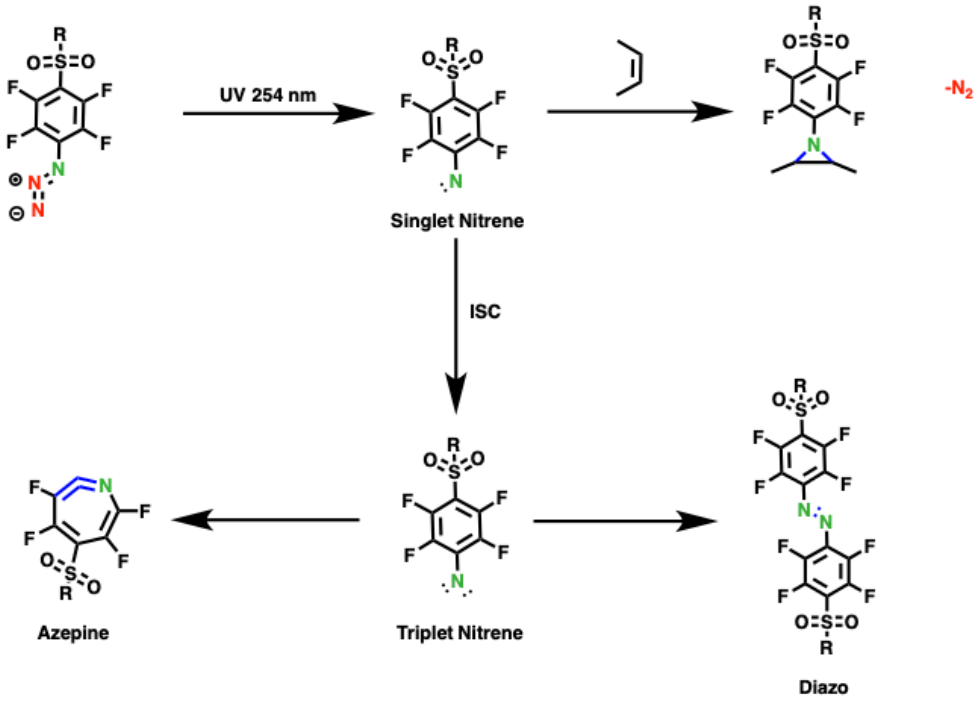

Figure 1-1. PFPA chemistry. The azide functional group is activated by photoexcitation, producing a highly reactive singlet nitrene that can undergo C-H insertion within the hydrocarbon backbone of a polyolefin like polyethylene, thus, creating a covalent bond between the polymer and the PFPA molecule. Intersystem crossing also occurs to give a triplet nitrene that dimerizes to a diazocompound, or gives a ring expansion to an azepine.

Chapter 2 discusses work carried out with tetraaniline (TANI), an oligomer of polyaniline.[1] Polyaniline is difficult to process because of its lack of solubility in common organic solvents.[2]

TANI is the smallest representative repeat unit of polyaniline and is known to have similar properties to polyaniline, but can be dissolved in common organic solvents for facile processing.[3] We wanted to take advantage of the hydrophilic and antibacterial properties that are associated with polyaniline on hydrophobic materials.[4] We reacted tetraaniline with PFPA and grafted it onto a variety of materials; a polyethersulfone, reduced graphene oxide, polyethylene terephthalate (PET), single walled carbon nanotubes and polystyrene. Polyethersulfones are used to make ultrafiltration membranes (UF). Coating the UF membranes is used to prevent bio-fouling from occurring during water purification processes. The PET films have high transparencies and low bio-adhesion that show great potential to apply this material for biomedical uses.

Chapter 3 discusses using the octamer of aniline instead of polyaniline. Polyaniline (PANI) is a conducting polymer that has unique acid/base doping/de-doping properties. Controlled doping of PANI leads to enhanced conductivity due to the formation of charge carriers that can move under the influence of external potential and in the Coulombic field of counter-ions distributed between the chains. Doping of PANI leads to the emeraldine oxidation state, that is the conductive state. However, PANI is limited in its defects that lower conductivity. Aniline oligomers also have unique acid/base doping chemistry.[13] They are smaller than polyaniline and can be made as well-defined molecules, with the smallest oligomer possessing acid/base doping chemistry being tetra-aniline (TANI). Twice the length of TANI is the aniline octamer (OANI). OANI should have higher conductivity compared to TANI and just as high or higher than PANI because of its ordered structure. OANI was synthesized via palladium catalyzed amination and purified using a Soxhlet extractor. Doping of OANI was monitored via UV-Vis with hydrochloric acid (HCl) to show that optimum doping occurs at a concentration of 0.29 mM.

Chapter 4 discusses how PFPA photochemistry can be used to graft charged copolymers on polyamide nanofiltration membranes (NF). NF membranes can be used to treat ground, surface, and waste water or used as a pretreatment for desalination.[5] Here we demonstrate how a membrane's surface charge can be altered by grafting different electrostatically varying copolymers on to commercial membrane surfaces for enhancing ion separation performance. The membranes performances in terms of divalent cation separation with copolymer containing positively charged quaternary ammonium ions, a negatively charged sulfonate and an essentially neutral zwitterion indicate that: a) the sulfonated polymer induces robust Coulombic exclusion of divalent anions as compared to the negatively charged native membrane surface on account of its higher negative charge; b) the positively charged ammonium coating induces exclusion of cations more effectively than the native membrane; and significantly, c) the zwitterion polymer coating, which reduces the surface roughness and improves the wettability in spite of its near neutral charge, enhances exclusion of both divalent cations and anions on account of aperture sieving by the compact zwitterion polymer that arises from its ability to limit the size of ions that transport through the polymer. The outcomes thereby inform new pathways to achieve size- and charge-based exclusion of ionic, molecular, and other species contained in liquid streams.

In Chapter 5, PFPA-ethyleneimine small molecules were used to modify polyolefin separators for lithium ion (LiB) and lithium sulfur (LiS) batteries. Separators are one of the important components that make up a LiB or LiS battery.[10] The function of a separator is to act as a physical barrier for the electrolyte as well as an electrolyte reservoir for ion transport. An ideal separator should have porous properties, high chemical and thermal stability, high wettability, and most importantly, it should prevent the diffusion of electrode components.[11] One of the major limitations of LiS batteries is the "shuttle effect" caused by dissolved polysulfide species, the

discharge product of Li_2S from lithium anode deterioration due to passivation and the formation of a solid electrolyte interphase (SEI) layer.[12] We attempted to trap these large-chain polysulfides by modifying polypropylene/polyethylene separators with two PFPA-ethyleneimine and PFPA-methylated ethyleneamine small molecules. Polysulfide diffusion tests were performed to test the separators ability to trap polysulfides before they pass through the separator. PFPA-ethyleneimine showed diffusion of polysulfides after 24 hours, while PFPA-methylated ethyleneimine showed no diffusion after 48 hours. Capacity loss over time was compared for the native separator relative to the modified separators with the small molecules. Both PFPA-methylated ethyleneimine and PFPA-ethyleneimine showed enhanced capacity retention compared to the control.

Chapter 6 discusses zwitterion chemistry. Zwitterions have no net charge; two of the main types of zwitterions are sulfoxybetaine and carboxybetaine.[6] The sulfoxbetaine has a quaternary amine (positive charge) and a sulfoxide (negative charge), while the carboxybetaine has a quaternary amine and a carboxy group (negative charge).[7] These non-ionic species are known to have less adsorption/absorption of foulants, compared to charged species.[8] Zwitterions specifically have been studied because they tend to create a strong water layer that surrounds them, preventing any adhesion by being more hydrophilic than a neutral substrate. Two zwitterions were synthesized and grafted on polydimethylsiloxane (PDMS) to create a hydrophilic surface to prevent bacterial adhesion. The mechanism for preventing protein or bacterial adhesion by the zwitterion brush is due to steric repulsion, i.e. the restriction on the number of zwitterion conformations and the high local osmotic pressure that results from protein insertion into the zwitterion layer.[9] The two zwitterions both showed superhydrophilicity in water contact angle measurements compared to the native material. Cell adhesion studies were carried out to test if the polymer coatings would resist bacterial adhesion to prevent biofilm formation. A 24-hour fibroblast cell culture and

live/dead staining was performed to show their performance with bio-adhesion in the modified PDMS compared to the unmodified. Both zwitterion grafted polymers showed no live cells and very few dead ones compared to the native PDMS. There was virtually no adhesion and ability to grow and reproduce, and the small number of cells that did adhere were dead. The native PDMS exhibited over 100% cell adhesion showing that the cells reproduced over the 24-hour period studied.

1.1 REFERENCES

(1.1) Lin, C. W.; Aguilar, S.; Rao, E.; Mak, W. H.; Huang, X.; He, N.; Chen, D.; Jun, D.;

Curson, P. A.; McVerry, B. T.; et al. Direct Grafting of Tetraaniline: Via Perfluorophenylazide Photochemistry to Create Antifouling, Low Bio-Adhesion Surfaces. *Chem. Sci.* **2019**, *10*, 4445–4457.

(2) Baker, C. O.; Huang, X.; Nelson, W.; Kaner, R. B. Polyaniline Nanofibers: Broadening Applications for Conducting Polymers. *Chem. Soc. Rev.* **2017**, *46*, 1510–1525.

(3) Wang, Y.; Tran, H. D.; Liao, L.; Duan, X.; Kaner, R. B. Nanoscale Morphology, Dimensional Control, and Electrical Properties of Oligoanilines. *J. Am. Chem. Soc.* **2010**, *132*, 10365–10373.

(4) Nezakati, T.; Seifalian, A.; Tan, A.; Seifalian, A. M. Conductive Polymers: Opportunities and Challenges in Biomedical Applications. *Chem. Rev.* **2018**, *118*, 6766–6843.

(5) Abdel-Fatah, M. A. Nanofiltration Systems and Applications in Wastewater Treatment: Review Article. *Ain Shams Eng. J.* **2018**, *9*, 3077–3092.

(6) Shao, Q.; Jiang, S. Molecular Understanding and Design of Zwitterionic Materials. *Adv. Mater.* **2015**, *27*, 15–26.

(7) Zheng, L.; Sundaram, H. S.; Wei, Z.; Li, C.; Yuan, Z. Applications of Zwitterionic Polymers. *React. Funct. Polym.* **2017**, *118*, 51–61.

(8) Rana, D.; Matsuura, T. Surface Modifications for Antifouling Membranes. *Chem. Rev.* **2010**, *110*, 2448–2471.

(9) Zhao, X.; Zhang, R.; Liu, Y.; He, M.; Su, Y.; Gao, C.; Jiang, Z. Antifouling Membrane Surface Construction: Chemistry Plays a Critical Role. *J. Memb. Sci.* **2018**, *551*, 145–171.

(10) Deng, N.; Kang, W.; Liu, Y.; Ju, J.; Wu, D.; Li, L.; Hassan, B. S.; Cheng, B. A Review on Separators for Lithium Sulfur Battery: Progress and Prospects. *J. Power Sources* **2016**, *331*, 132–155.

(11) Marija Kirchhöfer, A.; von Zamory, J.; Paillard, E.; Passerini, S. Separators for Li-Ion and Li-Metal Battery Including Ionic Liquid Based Electrolytes Based on the TFSI− and FSI− Anions. *Int. J. Mol. Sci. Int. J. Mol. Sci* **2014**, *15*, 14868–14890.

(12) Chang, C.-H.; Chung, S.-H.; Manthiram, A. Ultra-Lightweight PANiNF/MWCNT-Functionalized Separators with Synergistic Suppression of Polysulfide Migration for Li–S Batteries with Pure Sulfur Cathodes. *J. Mater. Chem. A* **2015**, *3*, 18829–18834.

(13) Javadi, H. H. S.; Treat, S. P.; Ginder, J. M.; Wolf, J. F.; Epstein, A. J. Aniline Tetramers: Comparison with Aniline Octamer and Polyaniline. *J. Phys. Chem. Solids* **1990**, *51*, 107–112.

CHAPTER 2 PFPA-TANI on Ultrafiltration Membranes

Reprinted (adapted) with permission from (Lin, C.-W.; Aguilar, S.; Rao, E.; Mak, W.H.; Huang, X.; Jun, D.; He, N.; Chen, D.; Curson, P.; McVerry, B.T.; Hoek, E.M.V.; Huang, S.-C.; Kaner, R.B. "Direct Grafting of Tetraaniline via Perfluorophenylazide Photochemistry to Create Antifouling, Low Bio-Adhesion Surfaces" *Chemical Science*, 2019, 10, 4445-4457. DOI: 10.1039/C8SC04832K).

2.1 INTRODUCTION

2.1.1 Polyaniline

Polyaniline, a well-studied conjugated polymer known for its simple acid/base doping/de-doping chemistry and facile synthesis,[1–5] has been widely applied to chemical gas sensors for ammonia detection,[4,6] chemical and electrochemical actuators,[7,8] non-volatile memory devices,[9] supercapacitors,[10] water filtration membranes,[11] anticorrosive coatings,[12] tissue engineering,[13] *etc*.[14,15] In the realm of coatings,[16,17] and membranes,[11,18–21] researchers often blend polyaniline with other matrix materials in order to obtain the hydrophilic and antibacterial characteristics of polyaniline at the surface.[22–26] However, low solubility and gelation of polyaniline during processing, have hindered the development of improved materials.[27,28] Therefore, grafting polyaniline onto other materials is crucial in order to achieve more robust coatings and functionalize surfaces for enhanced performance.[29,30] Due to difficulties in processing polyaniline, chemically grafting polyaniline is often performed by functionalizing end groups with amines,[31–33] amidation reactions with carboxylic groups,[34–37] diazotization reactions with diazonium salts,[38–40] and nitrogen doping[41] followed by oxidative polymerization. However, such modification processes require chemically inert and mechanically strong materials in order to sustain the harsh pretreatments. In addition, the abovementioned methods are only suitable for materials within the

micro- and nanoscale regime, which limit the feasibility of modifying large surfaces with such hydrophilic, pH-responsive, and antibacterial polyaniline.

2.1.3 Ultrafiltration Membranes

Another application that could greatly benefit from a coating that prevents bio-fouling is ultrafiltration (UF) membranes. Typical commercial UF membranes are made of polyethersulfone (PES), polyvinylidene fluoride (PVDF), polysulfone (PSF), polypropylene (PP), or polyurethane (PU).[42,43] The hydrophobic nature of these matrix polymers leads to protein adherence to their surfaces and the proliferation of bacteria.[44,45] Additionally, the accumulation of both organic and inorganic foulants on membrane surfaces over time, *i.e.* fouling, can severely lower the permeation flux and the filtration efficiency, often damaging the membranes.[46–50] In order to surmount these problems, scientists and engineers have already developed a couple rule-of-thumbs for designing antifouling membranes. First, hydrophilic membrane surfaces have been suggested as a method to form a few-molecule-thick hydration nanolayer, which may prevent foulant adhesions and cake formation. Second, stimuli-responsive polymers grafted onto membrane surfaces can undergo a coil-to-globule transition to "release" the accumulated foulants when exposed to a stimulus during washing cycles.[42,43,51,52]

2.1.4 Polyaniline-based UF membranes

To date, all the reported polyaniline-based filtration membranes are formed by blending polyaniline with base polymers. For instance, in 2008, Fan *et al.* reported a UF membrane made

by blending polyaniline with PSF, doubling the pure water flux compared to a pristine PSF membrane and lessening the flux decline.[11,18] Since then, other researchers have reported UF membranes composed of polyaniline blended with base polymer, including PES, PSF, PVDF, *etc*.[21,53–57] Blending-in polyaniline enhances the membrane's hydrophilicity, thereby decreasing the flux decline and improving the flux recovery. Even more hydrophilic membranes were reported by further mixing CNTs into polyaniline-blended UF membranes; however, bovine serum albumin (BSA) rejection decreased due to the formation of larger porosity in these membranes.[58–60] McVerry *et al.* and Zhao *et al.* incorporated self-doped sulfonated polyaniline (SPANI) into PSF and PVDF UF membranes, respectively, with superior hydrophilicity. The zwitterionic nature of SPANI resulted in a high flux recovery and high BSA rejection rate.[20,61]

2.1.5 Limitations of Polyaniline UF Membranes

The blending strategy mentioned above is straightforward but has several limitations: 1) The processability of polyaniline during membrane casting needs to be improved as polyaniline only appears dispersible in dimethyl sulfoxide (DMSO) and *N*-methyl-2-pyrrolidone (NMP). 2) The crucial pore size of the composite membranes that directly affects the water flux and rejection rate has to be tuned experimentally by trial and error. 3) The mechanical properties of the resultant composite membranes are strongly dependent on the intrinsic properties of polyaniline and the percentage blended in. As polyaniline possesses a more rigid backbone,[62,63] the flexibility of its membranes are limited. 4) The confined polyaniline chains embedded in composite membranes cannot undergo a coil-to-globule transition when treated with acids in order to actively repel foulants. In order to graft polyaniline onto membranes or attach bridging groups to polyaniline through chemical reactions, dissolving polyaniline in DMSO or NMP is inevitable. However, DMSO and NMP are strong organic solvents that can readily dissolve and destroy the base UF

membranes during the modification process. Hence, grafting polyaniline onto membrane surfaces without damaging the base UF membranes has so far been unsuccessful.

2.1.6 Oligioaniline used instead of Polyaniline in UF Membranes

We report a newly synthesized molecule, 4-azidotetrafluorobenzoyl tetraaniline (ATFB-TANI), which can be used to couple tetraaniline (TANI) to other materials. TANI, the smallest representative repeat unit of polyaniline, is known to have similar properties to polyaniline, but can be readily dissolved in common organic solvents for facile processing.[64–66] This bridging group is based on the solid foundation of perfluorophenylazide photochemistry,[30] which can undergo addition and insertion reactions when exposed to UV light.[67–71] Thus, with the assistance of perfluorophenylazide, TANI can now be covalently photografted onto carbon nanotubes (CNTs) and reduced graphene oxide (rGO) without pretreatments. Furthermore, large area modifications through dip-coating and spray-coating on polyethylene terephthalate (PET) films with high transparencies and low bio-adhesions show great potential to apply this material for biomedical uses.

Here we report the first oligo/polyaniline modified filtration membranes via photografting ATFB-TANI onto commercially available PES UF membranes. The modified membrane surfaces show enhanced hydrophilicity and improved performance in terms of antifouling ability, BSA rejection, and preventing bio-adhesions. This fast, facile, and non-destructive modification process offers a new route to graft conducting oligoanilines and can serve as the initiator for further polymerization as well.

2.2 Experimental Section

2.2.1 Materials

Polyether sulfone **(**PES) UF membranes were purchased from Synder Filtration (LX, 300 kDa). Aniline dimer, ferric chloride hexahydrate, bovine serum albumin (BSA) (heat shock fraction, pH = 7, ≥98%), sodium azide (NaN_3), acetone, sodium hydroxide (NaOH), methanol, triethylamine (NEt_3), 4-dimethylaminopyridine (DMAP), dichloromethane (DCM), ammonium hydroxide, and deuterated dimethyl sulfoxide (d_6-DMSO) were purchased from Sigma Aldrich. *Escherichia coli (E. coli)*, Luria-Bertani (LB) broth, and *S. Epidermidis* were purchased from ATCC. Graphite powder (SP-1 325) for making graphite pellets was purchased from Bay Carbon Inc. The multi-walled carbon nanotubes (MWCNTs) (outer diameter >50 nm; length = 10-20 μm; purity >95 wt%) were purchased from Cheap Tubes. Polystyrene Petri dishes were purchased from Fisher Scientific. Polyethylene terephthalate (PET) films (PP2950) were purchased from 3M. All chemicals were used as received.

2.2.2 ATFB-TANI Synthesis

Tetraaniline. Tetraaniline (TANI) was synthesized through a modified method.[72,73] Aniline dimer, *N*-phenyl-1,4-phenylenediamine powders (1.89 g, 7 mmol, 1 equiv.) were rapidly stirred with hydrochloric acid (50 mL, 0.1 M) for 30 min in a 250 mL round bottom flask. Ferric chloride hexahydrate (2.76 g, 15 mmol, 2.1 equiv.) was dissolved in hydrochloric acid (50 mL, 0.1 M) and quickly poured into the round bottom flask followed by an additional 50 mL of 0.1 M hydrochloric acid. The reaction was stirred at room temperature for about two hours. The precipitate was centrifuged and washed with 0.1 M hydrochloric acid multiple times (at least 3 times with 50 mL per wash) in order to fully remove iron ions. The precipitate was then mixed with ammonium

hydroxide (50 mL, 2.0 M) and acetone (300 mL) for 30 min resulting in a bright blue solution. The solution turns gray if the iron ions are not completely removed during the hydrochloric acid wash. The acetone was removed using a rotory evaporator. The dispersion was then centrifuged and washed with DI water several times until the supernatant pH became neutral. The powder was collected after the precipitate was rinsed out with ethanol and air dried overnight, producing a blue solid with a 65% yield. The Matrix Assisted Laser Desorption/Ionization (MALDI) spectrum of TANI is presented in **Figure S3**.

4-Azidotetrafluorobenzoate. NaN_3 (0.154 g, 2.38 mmol, 1.07 equiv.) and pentafluorobenzoate (0.499 g, 2.21 mmol, 1 equiv.) were mixed together in a solution of acetone (20 mL) and water (7 mL) and refluxed for 10 hours. The mixture was cooled and water (20 mL) was added to form a white precipitate. The precipitate was then filtered and washed with $CHCl_3$ (3 times) and left to dry to produce a white solid (82% yield). ^{19}F NMR (400 MHz; $CDCl_3$): δ 138.858 (m, 2F), 151.113 (m, 2F).

4-Azidotetrafluorobenzoic acid. 4-Azidotetrafluorobenzoate (0.473 g, 2.12 mmol, 1 equiv.) was dissolved in methanol (10 mL). A 20% NaOH solution (0.8 mL) was added slowly to a stirring solution of 4-azidotetrafluorobenzoate and then stirred overnight. The reaction was next cooled to 0 ºC in an ice bath and slowly acidified with 2 N HCl to reach a pH < 1, then extracted with $CHCl_3$ (3 times) and dried to produce a white solid (yield = 89%). ^{19}F NMR (400 MHz; D_6-acetone): δ 141.323 (m, 2F), 151.660 (m, 2F).

ATFB-TANI. 4-Azidotetrafluorobenzoic acid (0.552 g, 2.35 mmol, 1 equiv.), trimethylamine (0.260 g, 2.58 mmol, 1.1 equiv.) and 4-dimethylaminopyridine (0.287 g, 2.35 mmol, 1 equiv.) were dissolved in 10 mL of DCM. TANI (1.11 g, 3.05 mmol, 1.3 equiv.) was then added and stirred for 48 hours at room temperature. The reaction mixture was then washed with

DI water (3 times). After evaporation under reduced pressure, a violet solid product (yield = 84%) was collected and used without further purification. The product was stored in the dark before use. ^{19}F NMR (400 MHz; D_6-acetone): δ 137.357 (m, 2F), 150.801 (m, 2F).

2.2.3 Modification

The commercial PES membranes were soaked in DI water, renewed every few hours, for at least two days in order to remove the chemicals added for transportation and storage. First, solutions of 1.0 mM and 2.0 mM ATFB-TANI in ethanol were prepared. The unmodified membranes were quickly rinsed with ethanol in order to remove any residual water that may lead to uneven modifications. The membranes were then dipped into the ATFB-TANI ethanol solution for one minute before irradiation with a handheld UV light (254 nm) for one minute. The UV-treated membranes were rinsed with ethanol and DI water, respectively. The grafted membranes were soaked in DI water for another 24 hours before use. In order to modify the Petri dishes, 0.5 mL of 2.0 mM ATFB-TANI solution was pipetted onto a Petri dish and gently swirled. The Petri dish was exposed to UV light for 90 seconds before rinsing with ethanol several times. The graphite pellets were made by compressing graphite powders with a hydraulic press at 10,000 lb.; ~0.2 mL of 2.0 mM ATFB-TANI solution was then drop-cast on top of the pellets followed by UV treatment for one minute, rinsing with ethanol and then DI water. The multi-walled carbon nanotubes (MWCNTs) were dispersed in a 2.0 mM ATFB-TANI ethanol solution (300 μg mL^{-1}). The dispersion was ultrasonicated with a tip-ultrasonication processor (Ultrasonics FS-300N, 20% power) in an ice bath for 10 min. The well-dispersed solution (2.5 mL) was exposed to UV light for 3 minutes, followed by drop-casting onto a glass slide and gentle rinsing with ethanol in order

to remove the unreacted ATFB-TANIs. The TEM samples were prepared by tapping TEM grids on the glass slide. The graphene oxide (GO) was synthesized through a modified Hummer's method, as reported elsewhere.[73] As described previously,[74] a GO aqueous solution was mixed with ascorbic acid and after vacuum filtration, the ascorbic acid was rinsed out and dried in a 100 ºC oven overnight. The reduced GO (rGO) film was ultrasonicated with 2.0 mM ATFB-TANI ethanol solution for 1 minute, followed by UV treatment for 3 minutes. The PET films were dipped into ATFB-TANI solutions for 10 seconds and exposed to UV light for another minute, rinsed with ethanol and air dried. The spray-coatings on SWCNT films and the UCLA pattern on the PET film with stencil masks were carried out by spraying 2.0 mM solution with an Image® Dual Action airbrush. The airflow rate was 5 standard cubic feet per minute (SCFH) with approximately 1 mL of solution sprayed out per minute.

2.2.4 Membrane Performance Testing

To measure fouling, membranes were placed in a stainless holder. A feed tank was connected to a mechanical pump, which flowed feed solutions across the membrane with an effective area of 17 cm^2. A pressure gauge was placed between the pump and the membrane holder to monitor the input pressure. The output after membrane filtration was monitored with a flow meter, and its readings were recorded by a connected computer. The membranes were first compacted with DI water at 50 psi until the flow reached a steady value. The fouling test began by introducing 1.0 g/L of BSA solution for 45 minutes. The flow decline percentage was calculated based on the equation:

$$\text{Flow Decline (\%)} = (1 - J_f / J_i) \times 100\%$$

where J_f is the flux after 45 min of fouling, and J_i is the equilibrated flux after compaction. After fouling, the feed tank was refilled with DI which was flowed across the membrane for 5 minutes in a washing procedure, before carrying out the next fouling cycle. The flow recovery percentage is defined as:

$$\text{Flow Recovery (\%)} = J_R / J_i \times 100\%$$

where J_R is the flux reading after 5 min of DI washing. It should be noted that the inlet pressure was not tuned after its original setting to 50 psi during membrane compaction; therefore, the flux fluctuations may be attributed to both the accumulation of foulants and the change in transmembrane pressures (TMP).

The BSA rejection performance testing on the UF membranes was conducted in a stainless-steel dead-end stirred filtration cell (Sterlitech Corp., Kent, WA) with an active membrane area of approximately 110 cm^2. The stirred cell was filled with DI water and pressurized. The water flow rate was recorded using a digital flow meter (FlowCal 5000, Tovatech LLC, South Orange, NJ). The membrane was then compacted at 50 psi until the flow rate was stable, approximately 1 hour for each membrane. BSA rejection of each membrane was characterized by filling the stirred cell with 1.0 g/L of BSA solution and pressurized it at 50 psi. The BSA rejection rate was calculated through the equation:

$$R = 1 - A_p / A_f$$

where A_p and A_f are the absorbance values of the permeate solution and the feed solution at a wavelength of 279 nm, respectively.

2.2.5 Bacterial and BSA Adhesion Testing

The antifouling properties of the ATFB-TANI modified membranes were investigated by a bacterial adhesion experiment using *E. coli* as a model organism. *E. coli* cell cultures were suspended in Luria-Bertani broth for 24 hours at 35 ºC. 1 cm^2 samples of modified and unmodified membranes were then soaked in the *E. coli* suspension (~1 $x10^7$ CFU/ mL) at 37 ºC while shaken at 35 rpm for 24 hrs. The samples were then removed from the suspension and rinsed with a 1 M PBS solution to remove any unbound cells. Membrane samples were then immersed and stained in a SYTO 9 dye solution (live/dead Baclight Bacterial Viability Kit) for 20 minutes. The samples were again rinsed with the 1 M PBS solution. The samples were then immersed in a propidium iodide solution (PI) for 20 minutes and again rinsed with the 1 M PBS solution. SYTO 9 labels nucleic acids of both live and dead cells, whereas PI only labels nucleic acids of dead cells. When both dyes are present, PI exhibits a stronger affinity for nucleic acids than SYTO 9 and therefore SYTO 9 is displaced on the nucleic acids of dead cells. Images were then taken using a fluorescence microscope using different filters to view the SYTO9 and PI dyes. For BSA adhesion test, the green fluorescence protein (GFP) BSA was dissolved in DI water (concentration equals to 50 μg/mL), and samples of the membranes were immersed in that solution and placed in an incubator at 37 ºC and 50 rpm. After 24 hours, the samples were removed, rinsed with DI water and imaged using a fluorescent microscope. Image analysis was performed using ImageJ. The surface coverage values were quantified by dividing the number of colored pixels by the total number of pixels.

2.2.6 Characterization

The synthesized TANI was characterized by a Bruker UltraFlex Matrix Assisted Laser Desorption/Ionization (MALDI-TOF) spectrometer with 2,5-dihydroxybenzoic acid (DHB) as the matrix. NMR spectra were carried out on a Bruker AV300. Electrospray ionization mass

spectrometry (ESI-MS) in methanol solvent was utilized to determine the composition of ATFB-TANI by comparison to Leucine Enkephalin. During ESI-MS characterization, a signal for ATFB-TANI $(C_{31}H_{21}N_7F_4O)^+$ was observed at 583.1748 m/z and had an isotope pattern consistent with C, H, N, and O incorporation. The observed high-resolution ESI-MS for ATFB-TANI differed from the calculated masses by 0.7 ppm. UV-vis spectra were taken on a Shimadzu UV-3101 PC UV-vis-NIR scanning spectrometer with quartz cuvettes. The membrane topographies were investigated using a Bruker Dimension FastScan Probe Microscope (SPM) with silicon tips on nitride levers (Bruker Scanasyst-air). The root-mean-square roughness and the image process were carried out by the software NanoScope Analysis. The conventional contact angles were measured through a First 10 Ångstroms Contact Angle Goniometer. The captive bubble contact angles were measured through a homemade setup where the membranes were clamped on glass substrates. The membrane was then faced down and immersed into a transparent acrylic box. Air bubbles were placed through a U-shape needle connected to a syringe. The transmission electron microscopy (TEM) images were collected on a Tecnai TF20 TEM (FEI Inc.) operated under low dose mode. The electrical performances of PET films were measured via a probe station HP 4155B using toothless alligator clips as the metal contacts. The measured Amperes were corrected to zero at zero voltage. The attenuated total reflectance infrared (ATR-IR) spectra were acquired on a PerkinElmer Spectrum One spectrometer equipped with a universal ATR sampling accessory. The pH values of TANI dispersions (optical images) were calibrated by a pH meter (Mettler Toledo). For measuring the zeta potentials, around 4 mg of aniline tetramer and polyaniline nanofibers, synthesized by interfacial polymerization, were sonicated and vortexed until the powders were well-dispersed. 1.0 M $HCl_{(aq)}$ and 1.0 M $NaOH_{(aq)}$ (PanReact AppliChem) were used to adjust each

solution to a total volume of about 15 mL with the desired pH value. The zeta potential values were measured via a Malvern Zetasizer Nano-ZS.

2.3 Results and Discussions

In order to graft TANI onto large scale membrane surfaces without ruining the base polymer membranes, perfluorophenylazide was applied due to its fast and non-destructive photochemistry. As shown in **Figure 1a**, TANI and 4-azidotetrafluorobenzoic acid (ATFB) were stirred under basic conditions for 48 hours in order to complete the coupling reaction. The azides on ATFB-TANI form phenylnitrenes after being exposed to UV light, and the nitrene radicals can undergo

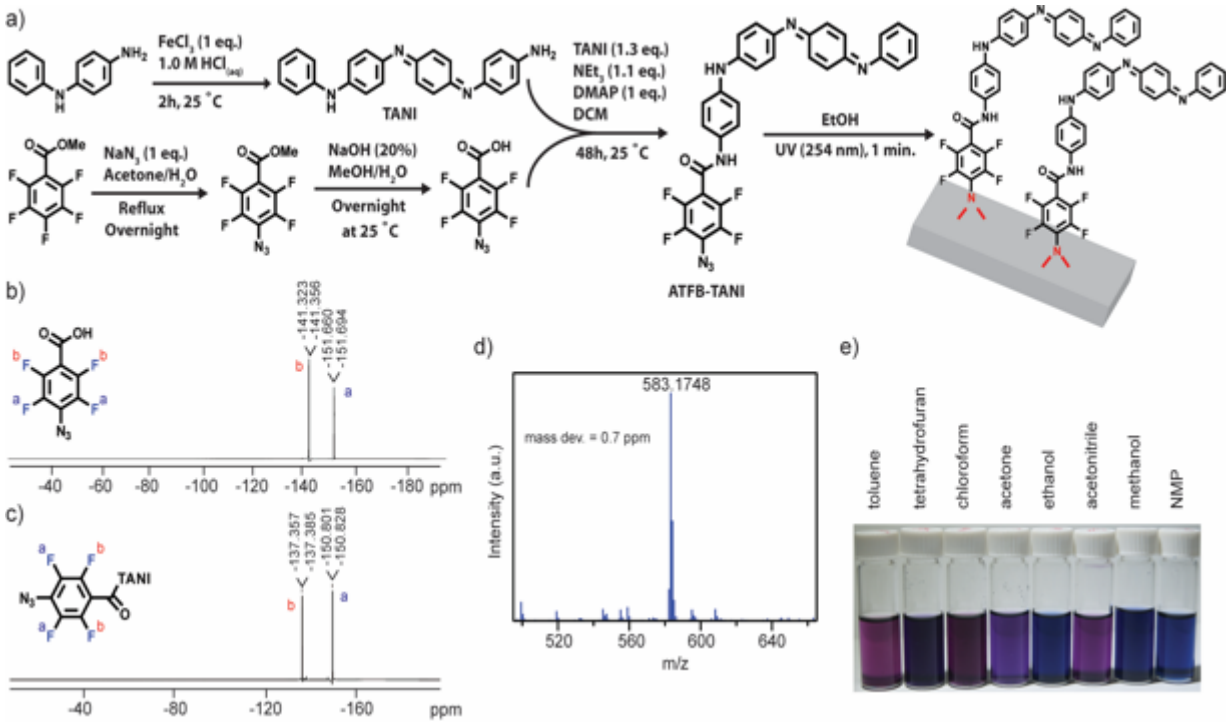

Figure 2-1. The synthesis procedure and characterizations of 4-azidotetrafluorobenzoyl-tetraaniline (ATFB-TANI). (a) ATFB-TANI was synthesized by coupling tetraaniline (TANI) with 4-azidotetrafluorobenzoic acid (ATFB). The ATFB-TANI can be covalently grafted onto the substrates by utilizing azide photochemistry. The ^{19}F-NMR spectra of (b) ATFB and (c) ATFB-

TANI. (d) Electrospray ionization (ESI) spectrum showing the molar mass of ATFB-TANI is 0.7 ppm away from the calculated value. (e) Photo showing ATFB-TANI can be dissolved in common organic solvents.

C=C addition and C-H and N-H insertion reactions.[75] The synthesized ATFB-TANI complex was confirmed by the peak shifts observed in ^{19}F-NMR (**Figure 1c**) when compared to the ATFB starting molecule (**Figure 1b**), along with the electrospray ionization (ESI) spectrum with a mass observed within 0.7 ppm of the expected mass (**Figure 1d**). As a small molecule, ATFB-TANI can be dissolved in a wide range of organic solvents, including toluene, tetrahydrofuran, chloroform, acetone, ethanol, acetonitrile, methanol, and NMP, as shown in **Figure 1e** with the color differences being attributed to solvatochromism.[64,76] The relatively high solubility of ATFB-TANI in common organic solvents compared to polyaniline indicates its advantageous processability. In this report, we chose ethanol as the solvent to carry out modifications, mainly due to its low toxicity, high solubility toward ATFB-TANI, low solubility toward polyethersulfone membranes, and high miscibility with water.

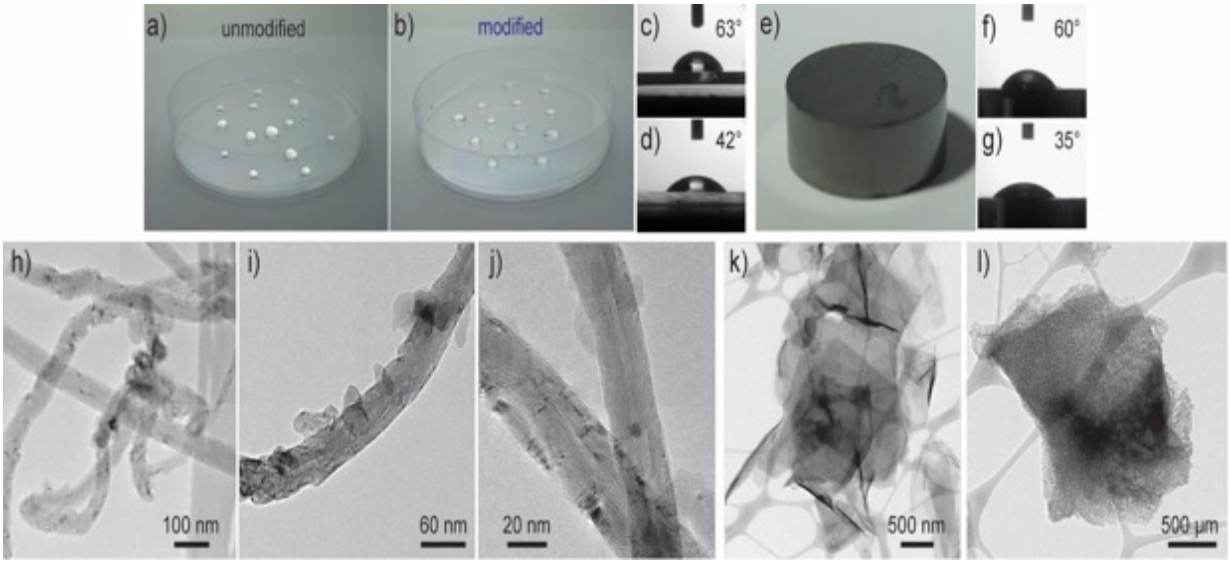

Figure 2-2. Images of water droplets on (a) an unmodified and (b) a modified polystyrene-based petri dish. The contact angles of (c) unmodified and (d) modified petri dish are 63º and 42º, respectively. The contact angle of (e) a compressed graphite pellet decreases from (f) 60 º to (g) 35 º after modification. The transmission electron microscopy (TEM) bright field images of (h) unmodified, (i, j) modified multi-walled carbon nanotubes (MWCNTs) and (k) unmodified and (l) modified reduced graphene oxide (rGO).

2.3.1 ATFB-TANI modified into different materials

Here we demonstrate that facile surface modification using ATFB-TANI can be applied to several important materials. In **Figure 2a,b**, a lab grade Petri dish made of polystyrene becomes more hydrophilic after modification as indicated by water droplets spreading out and a very faint blue color. The water droplet contact angle as measured by a goniometer decreased from 63º to 42º (**Figure 2c,d**). Analogously, a modified compressed graphite pellet also exhibits a decreased contact angle (**Figure 2f,g**) indicating increased hydrophilicity (**Figure 2e**). Furthermore, the ATFB-TANI molecule provides a simple way to graft TANI onto carbon nanotubes (CNTs) (**Figure 2h)** and reduced graphene oxide (rGO) (**Figure 2k)**. Conventionally, grafting polyaniline onto CNTs or GO/rGO requires surface functional groups via harsh chemical pre-treatments in order to obtain active sites for chemical grafting or polymerization.[35,41,77] Here, conducting TANI is successfully chemically grafted onto these materials via a non-destructive photochemical method (**Figure 2i**,**j**,**l**).

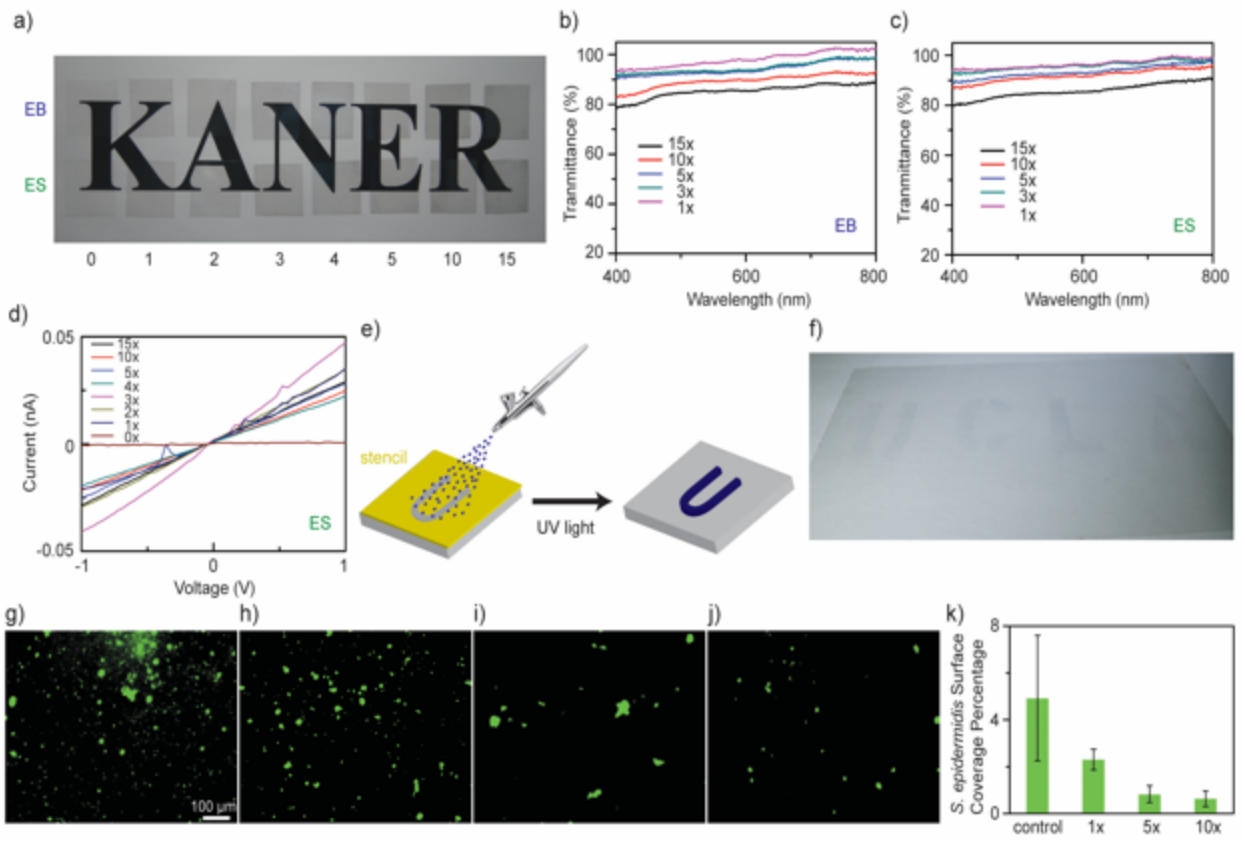

Figure 2-3. (a) Undoped (EB) and HCl doped (ES) polyethylene terephthalate (PET) films with different numbers of modifications showing their transparencies. UV-vis spectra show the transmittances of (b) undoped and (c) doped PET films with a pristine PET film as the reference. (d) The measured I-V curves of a pristine PET film and modified PET films after doping. (e) A schematic showing (f) a UCLA pattern by spray-coating ATFB-TANI solutions on top of a 13.5 cm x 8.0 cm PET film through stencil masks, followed by UV light exposure. Microscopic images showing the surface coverage of *Staphylococcus epidermidis* on the (g) unmodified, (h) 1, (i) 5, and (j) 10 times modified PET films, along with (k) a statistics bar graph. ((g-j) are under the same magnification.)

2.3.2 Spray Coating ATFB-TANI on PET Films

Since ATFB-TANI can dissolve in common organic solvents, large-scale modifications are possible. **Figure 3a** shows polyethylene terephthalate (PET) films subjected to an increasing number of dip-coatings. The coating process was performed by repeated dip-coating, UV light exposure, and ethanol washing. Both undoped (EB) and doped (ES) PET films show a gradual decrease in the transparency as the number of coating layers is increased. The percent transmittance of both EB and ES PET films is around 95% for a monolayer, and about 80% after 15 layers of modification (**Figure 3b,c**). The sheet resistances of the doped conducting PET films decrease from around 10^{11} Ω/sq (**Figure S1**) to 10^{9} Ω/sq. (**Figure 3d**). The high sheet resistances may be explained by the rather sparse grafting density, and short chains of TANI that do not greatly enhance carrier hopping.[78] The modified films show similar sheet resistances, implying that the ATFB-TANI molecules grafted onto previous layers may react with those on pre-modified molecules, resulting in the loss of some conjugation for the pre-existing layers.

Spray-coating combined with stencil masks is a method often used for large scale patterning. The schematic in **Figure 3e** demonstrates how ATFB-TANI molecules dissolved in an ethanol solution can be airbrushed onto PET films using stencil masks to form a "UCLA" pattern. This achieves a highly transparent UCLA patterned coating after exposure to UV light and an ethanol rinse, as shown in **Figure 3f**. Such a facile, fast, and non-destructive method for modification to produce materials with high transparency could prove useful for biomedical applications such as artificial skin. The idea is to prevent common infections such as those caused by *Staphylococcus epidermidis* (*S. epidermidis*).[79–81] Adhesion tests on both modified and unmodified PET films were carried out by exposure to *S. epidermidis*. The observed images with stained cells on unmodified (**Figure 3g**), and one, five, and ten-fold modified (**Figure 3h,i,j**) PET films show a readily noticeable drop in the number of cells adhered. A statistical bar graph reveals

that the surface coverage percentage of *S. epidermidis* drops approximately 50% from the unmodified to the more modified films (**Figure 3k**).

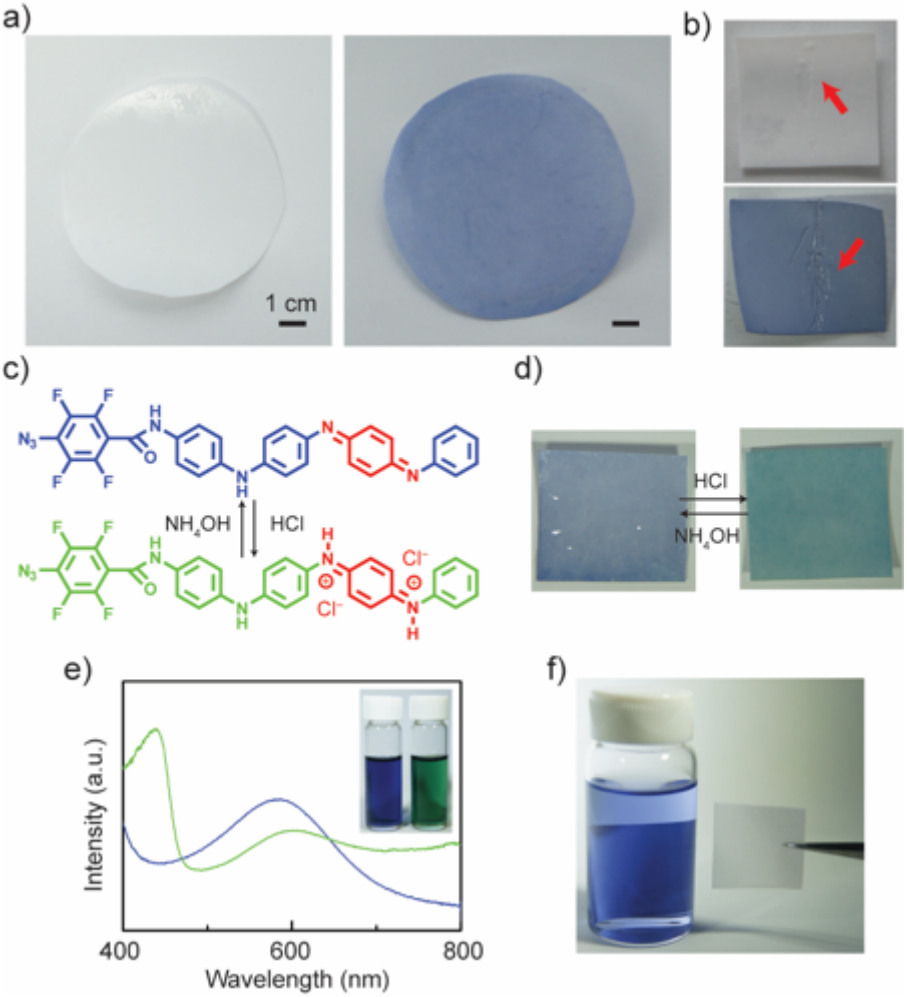

Figure 2-4. (a) Photographs of unmodified (left) and modified (right) polyethersulfone (PES) membranes. (b) Scratches are easily seen on the modified membrane (bottom) compared to the unmodified one (top). The (c) ATFB-TANI molecule and (d) the modified membrane can be protonated and deprotonated when treated with acids and bases. (e) The UV-vis spectra and photo (inset) of undoped (blue) and doped (green) ATFB-TANI dissolved in dimethyl sulfoxide (DMSO). (f) UV light treated TANI stained membranes showed colorless after rinsing in a vial of ethanol.

2.3.3 Grafting ATFB-TANI onto UF Membranes

Next, we grafted TANI onto polyethersulfone (PES) UF membranes. The unmodified UF PES membranes appear white, while the modified membranes exhibit a light blue color even after rinsing with DI water and ethanol (**Figure 4a**). Unlike the modification of colored materials, one can directly observe the modification of these initially transparent membranes as they develop a blue hue. The colored modification also makes any surface imperfections on the membrane readily visible (**Figure 4b)**. Similar to aniline oligomers and polyaniline, ATFB-TANI can undergo a doping/de-doping process by treating with acids/bases. During the doping process, the imine nitrogens in the blue emeraldine base form become protonated, forming the green emeraldine salt form with the positively charged backbone surrounded by counter-anions to balance the charge (**Figure 4c**).[82] The modified membrane can be reversibly protonated with acid and deprotonated with base, switching from the blue emeraldine base form to the green emeraldine salt form (**Figure 4d**). Note that the color change of the modified membranes takes a slightly longer time, about 3 to 5 seconds more, than protonating/deprotonating in solution. The reason is simply due to the slower diffusion rate of the dopants in solids when compared to liquids. **Figure 4e** shows the UV-vis spectra of both the blue emeraldine base (EB) and the green emeraldine salt (ES) forms of ATFB-TANI dissolved in DMSO. Similar to TANI, the broad peak at ~600 nm can be attributed to the benzenoid to quinoid excitation transition, while the sharper peak for emeraldine salt at ~440 nm can be attributed to the allowed optical transition from the highest occupied molecular orbital (HOMO) to the higher bipolaron state.[64,83–85]

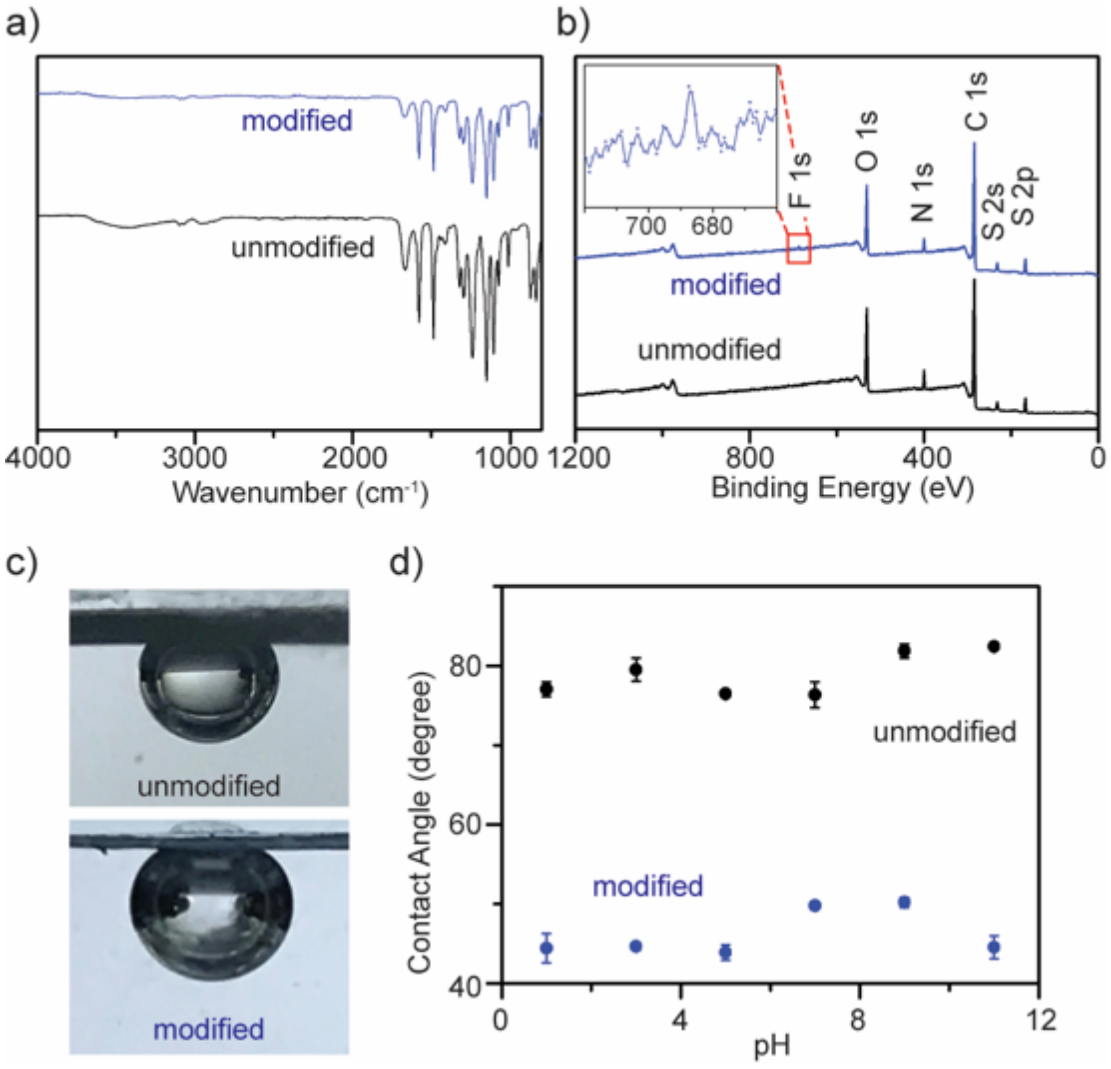

Figure 2-5. (a) ATR-IR spectra of both modified and unmodified PES membranes. (b) X-ray spectroscopy (XPS) spectra and F 1s spectra (inset) of the modified and unmodified membrane surfaces. (c) Captive bubble images under deionized water, and (d) contact angles under different pH aqueous solutions of modified and unmodified membranes.

2.3.4 Characterizing ATFB-TANI grafted UF Membranes

To confirm the chemical grafting of ATFB-TANI onto the membrane surfaces, we performed the same modification procedure with TANI instead of ATFB-TANI in an ethanol solution. Without the assistance of azides, the TANI modified membrane after the treatment of

UV light maintained its unaltered white color after rinsing with ethanol (**Figure 4f**). In contrast, the ATFB-TANI modified PES membrane remained blue after rinsing with ethanol, indicating that the blue color of ATFB-TANI modified membranes is not stained, and the ATFB-TANI is successfully grafted on by photochemistry. Attempting a more careful examination using attenuated total reflectance infrared (ATR-IR) spectroscopy did not show the difference between the unmodified and modified membranes (**Figure 5a**), likely due to the small amount of ATFB-TANI attached. Hence, a more sensitive and precise surface technique, such as X-ray photoelectron spectroscopy (XPS), was needed. The XPS spectra, as shown in **Figure 5b**, cannot clearly differentiate the azide signal at 406.5 eV due to the existence of a high nitrogen signal from the commercially available unmodified membranes. However, the fluorine peak at 687.6 eV is evident, revealing that a small amount of ATFB-TANI has indeed been grafted onto the membrane.[86–88]

2.3.5 Captive Bubble

Due to the high-water permeability of these membranes, their hydrophilicity was examined using a captive bubble contact angle goniometer. A previous study showed that TANI decorated polymeric films possess lower contact angles.[89] The contact angle of TANI/water is comparatively smaller than PES/water, resulting in more rounded air bubbles, *i.e.* lower contact angles, for modified membranes (**Figure 5c**). Although the contact angle of modified membranes is expected to change when exposed to acids because of the protonation of the imine nitrogens, the contact angles observed were consistently around 30 degrees different between unmodified and modified membranes at various pH values, as can be seen in **Figure 5d**. This phenomenon can be explained by the insignificant differences in contact angle due to the very small amount of surface modification. The relatively more hydrophilic nature of the modified surfaces at different pH

values indicates that these membranes are capable of being operated under harsh conditions. Polyaniline films may also possess increased roughness which can affect the contact angle measurement;[90] TANI, as a small molecule, slightly decreases the surface roughness, from 9.64 nm to 4.24 nm for the unmodified and modified membranes, respectively.

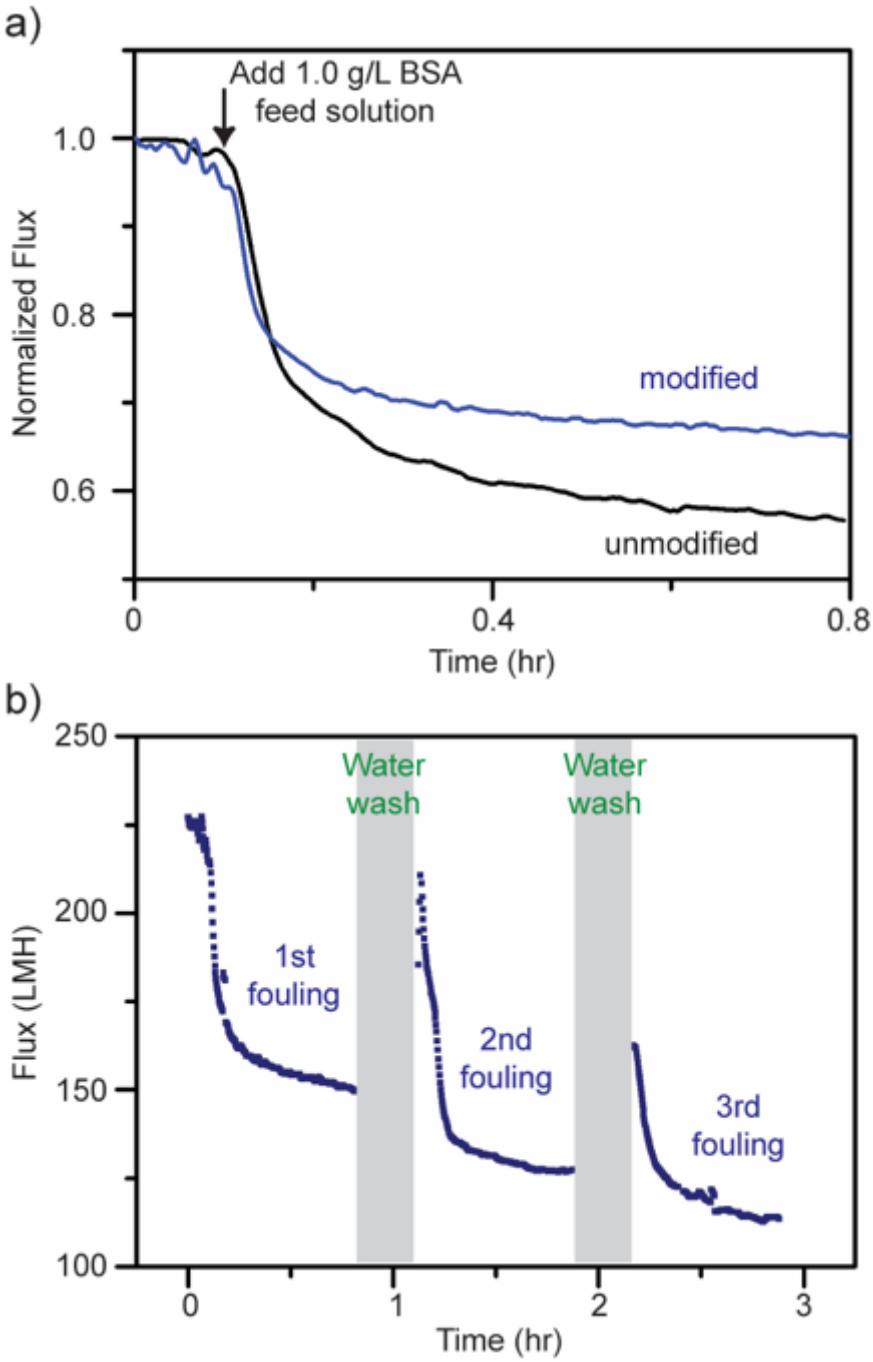

Figure 2-6. (a) Flux decline for unmodified and modified membranes after adding bovine serum albumin (BSA). (b) Flux declines and recoveries of a modified membrane after three cycles of fouling and water washing.

2.3.6 Antifouling Performance

To evaluate their antifouling properties, the membranes were subjected to a 1.0 g/L of bovine serum albumin (BSA) solution with a pressure of 50 psi. The membranes were first compacted with deionized (DI) water until the permeation flux reached equilibrium. After exposure to the 1.0 g/L BSA feed solution, the permeation flux decreased dramatically due to the formation of a cake layer during the fouling process.[43] As shown in **Figure 6a**, the modified membrane exhibited a smaller flux decline after 45 minutes of BSA fouling compared to the unmodified one. The reason may be the more hydrophilic surfaces created after modification; however, the improvement is not significant likely due to the high pressure (50 psi) applied. As mentioned above, the hydrophilic surfaces of the modified membranes form a few-nanometer-thick hydration layer that prevents the adhesion of foulants directly onto the membrane surfaces. Thus, the foulant BSA will have lower adhesion forces to the modified membranes. Hence, the modified membranes were tested with cycles of fouling and water washes. The water wash should remove much of the accumulated BSA from the more hydrophilic membrane surfaces due to lower interaction forces and thus give a higher recovery rate. In **Figure 6b**, the modified membranes were repeatedly water washed for 5 minutes after 45 minutes of BSA fouling. Note that the water wash duration on the graph shows about 10 minutes because of the extra time spent on cleaning and filling the water tank. The flux recovery percentages were found to be 73.30%, 60.77%, and 56.59% for the first, second, and third fouling experiments, respectively, carried out on the modified membranes. Note that the average flux recovery of the modified membranes after three

times fouling (56.59%), is still superior to the first flux recovery of the unmodified membranes (51.79%). The flux recovery percentages decrease each cycle due to the irreversible fouling that is occurring from the BSA, preventing a full 100% recovery on both the modified and unmodified membranes.

2.3.7 Membrane Performance

In addition, the modified membranes possess a better BSA rejection rate of 97.53%, comparable to polyaniline composite UF membranes,[11,18,21] while the unmodified membranes possess a rejection rate of only 90.66%. Furthermore, the modified membranes have slightly higher water permeation flux compared to the unmodified membranes. This counter-intuitive increase in the permeation flux is likely due to slight swelling of the PES membranes induced by their immersion in ethanol during the modification process.[91] The performances of both unmodified and modified membranes are summarized in **Table I**.

Table 2-I. Summary of Membrane Performance

membrane	pure water permeability at 50 psi (LMH)	BSA rejection (%)	flux decline (%)	flux recovery (%)	contact angle at pH 7 (degree)	root-mean-square roughness (nm)
Unmodified	181	90.66	46.85	56.34	76.3	9.64
Modified	227	97.53	40.70	73.30	49.8	4.24

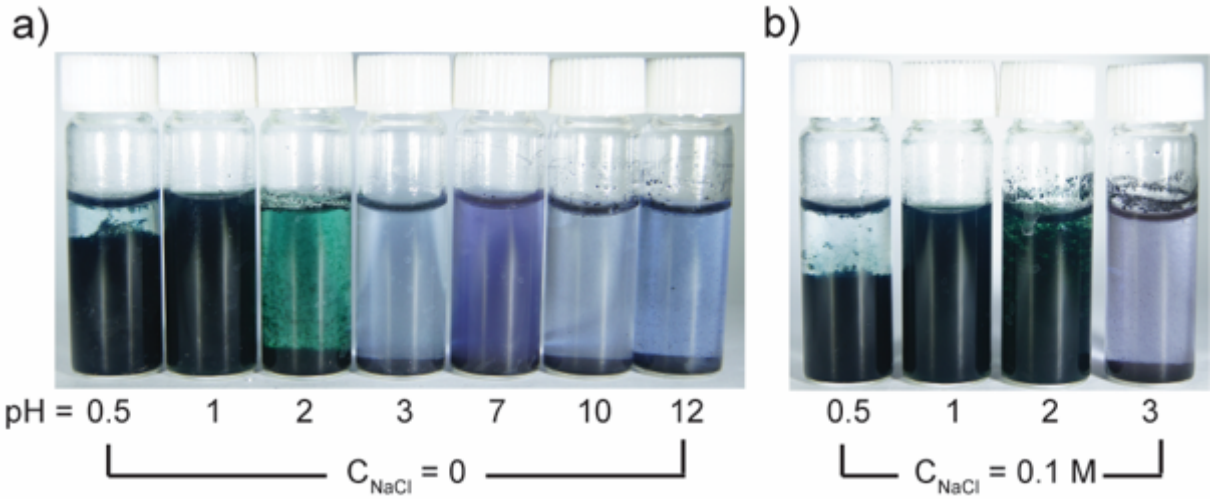

Figure 2-7. Optical images of TANI dispersed in aqueous solutions (2 mg/ml) at different pH and (b) with 0.1 M NaCl added after standing for 15 hours.

2.3.8 Washing Membranes at different pHs

Conjugated aniline oligomers can be protonated and deprotonated under different pH conditions. We performed fouling on modified membranes, followed by washing with water at different pH values. However, washing at different pHs did not give superior results to washing at neutral pH, indicating that the doping/de-doping of TANI did not effectively expel BSA during the wash cycle.[92] Based on the Derjaguin-Landau-Verwey-Overbeek (DLVO) theory,[93] polyaniline nanofibers are able to form stable colloids within a pH range from 2.2 to 3.5, while forming precipitates at pH values less than 1.5 and greater than ~5.[94] The pH responsive polyaniline nanofibers swell from a coiled state to a globule state when exposed to an appropriate pH environment. However, TANI only forms a stable dispersion in a solution of pH = 1 (zeta potential equals to 14.83 mV), as shown after 15 hours in **Figure 7a,** but has been observed to last for at least 6 months. The moderately destabilized TANI under pH = 0.5 and more stabilized

dispersion under pH = 2 after adding 0.1 M NaCl indicate that the TANI has a very narrow pH range for being stabilized in suspension (**Figure 7b**). Therefore, in order to have a responsive grafted TANI molecule, not only does the pH of the water wash have to be precisely 1, but also the interactions between TANI and BSA need to be taken into consideration.

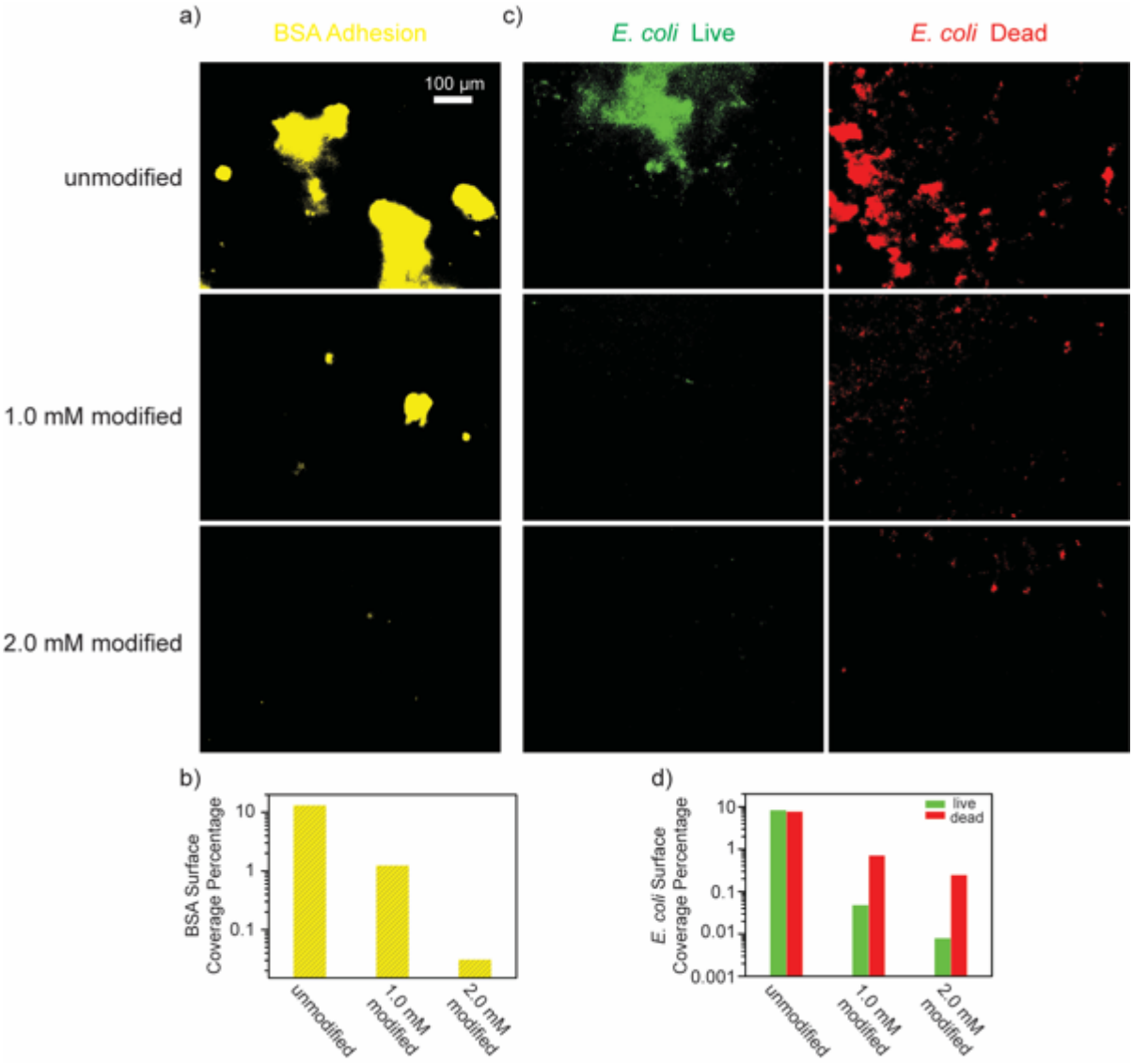

Figure 2-8. (a) BSA and (c) *E. coli* adhesion test microscopic images and (b, d) their surface coverage percentages of unmodified, 1.0 mM and 2.0 mM modified membranes. (All images share the same scale bar.)

2.3.9 BSA and E.Coli adhesion Test on UF Membranes

Another key indicator for evaluating membranes is the adhesion of microorganisms and the proliferation of bacteria on the membrane surfaces. As such, we performed experiments in which both unmodified and modified membranes were soaked in BSA solutions, and *E. coli* cultured in Luria-Bertani broth, followed by observing the surface coverage of BSA and *E. coli* adherence under a fluorescent microscope. Intermediately modified membranes (designated 1.0 mM modified) were also used in these tests in order to examine the effects of the ATFB-TANI attachment on the UF membranes. In **Figure 8a** it can be seen that the modified membranes show significantly lower BSA adhesion compared to the unmodified membranes. The quantified BSA surface coverage is 13.31%, 1.248% and 0.031% for the unmodified, 1.0 mM and 2.0 mM modified membranes, respectively (**Figure 8b**). The extremely low adhesions are believed to be due to the hydration layer created at the surface of the hydrophilic ATFB-TANI modified membranes. The low BSA adhesion also provides an explanation for the higher flux recovery and BSA rejection observed with the modified membranes. Note that we used pH neutral water for both membrane fouling tests and BSA adhesion testing, so the TANI is not positively charged enough to have a strong interaction with negatively charged BSA. Severe flux decline and very low flux recovery were observed when using hydrochloric acid (pH=1, 2) for membrane fouling testings.[92] On the other hand, although polyaniline has been reported as an antibacterial material,[22,57] we could not find any membrane filtration related studies with *E. coli*. As *E. coli* is known to have stronger interactions with hydrophobic materials,[95] we expected that the hydrophilic modification would prevent *E. coli* adhesion. As can be seen in **Figure 8d**, the live *E. coli* surface coverage for unmodified membranes is 8.36%, which drops dramatically for the 1.0 mM and 2.0 mM modified membranes to 0.048% and 0.008%, respectively. The dead *E. coli*

surface coverage was found to be 7.74%, 0.713%, and 0.248%, respectively. While these results do not suggest that TANI possesses antibacterial properties, they do indicate that only a small amount of modification is needed to dramatically lessen the adherence of *E. coli* by up to three orders of magnitude.

2.4 Conclusions

By synthesizing a novel ATFB-TANI molecule with a UV reactive azide group, a facile method for chemically grafting conjugated TANI onto important materials including graphite, carbon nanotubes, reduced graphite oxide and polymers is now available. Dip-coating or spray-coating with stencil masks leads to highly transparent, patterned, and low *S. epidermidis* adhesive PET films that show potential for low bio-adhesion coatings. Unlike conventional composite membranes, ATFB-TANI molecules can be grafted onto commercial polysulfone ultrafiltration membranes without complex pre-treatments. The TANI modified membranes exhibit increased hydrophilic surfaces, leading to low flux decline, high flux recovery, a high rate of BSA rejection, and low BSA and *E. coli* adhesions. The design concept of the ATFB-TANI molecule may inspire other modifications for grafting a variety of conjugated oligo/polymers to create hydrophilic and low bio-adhesion surfaces or to help with other materials suffering from processability issues.

2.5 References

(1) Heeger, A. J. Semiconducting and Metallic Polymers: The Fourth Generation of Polymeric Materials (Nobel Lecture)**. *Angew. Chemie Int. Ed.* **2001**, *40*, 2591–2611.

(2) Macdiarmid, A. G. "Synthetic Metals": A Novel Role for Organic Polymers (Nobel Lecture)**. *Angew. Chemie Int. Ed.* **2001**, *40*, 2581–2590.

(3) Shirakawa, H. The Discovery of Polyacetylene Film : The Dawning of an Era of Conducting Polymers (Nobel Lecture)**. *Angew. Chemie Int. Ed.* **2000**, *40*, 2574–2580.

(4) Huang, J.; Virji, S.; Weiller, B. H.; Kaner, R. B. Polyaniline Nanofibers : Facile Synthesis and Chemical Sensors. *J. Am. Chem. Soc.* **2003**, *125*, 314–315.

(5) Huang, J.; Kaner, R. B. A General Chemical Route to Polyaniline Nanofibers. *J. Am. Chem. Soc.* **2004**, *126*, 851–855.

(6) Virji, S.; Huang, J.; Kaner, R. B.; Weiller, B. H. Polyaniline Nanofiber Gas Sensors: Examination of Response Mechanisms. *Nano Lett.* **2004**, *4*, 491–496.

(7) Baker, C. O.; Shedd, B.; Innis, P. C.; Whitten, P. G.; Spinks, G. M.; Wallace, G. G.; Kaner, R. B. Monolithic Actuators from Flash-Welded Polyaniline Nanofibers. *Adv. Mater.* **2008**, *20*, 155–158.

(8) Gao, J.; Sansinena, J.-M.; Wang, H.-L. Fabrication and Characterization of Polyaniline Integrally Skinned Asymmetric Membranes for the Construction of Monolithic Chemical Actuators. *Mater. Res. Soc. Symp. Proc.* **2002**, *698*, 17–22.

(9) Tseng, R. J.; Huang, J.; Ouyang, J.; Kaner, R. B. Polyaniline Nanofiber/Gold Nanoparticle Nonvolatile Memory. *Nano Lett.* **2005**, *5*, 1–4.

(10) Snook, G. A.; Kao, P.; Best, A. S. Conducting-Polymer-Based Supercapacitor Devices and Electrodes. *J. Power Sources* **2011**, *196*, 1–12.

(11) Fan, Z.; Wang, Z.; Duan, M.; Wang, J.; Wang, S. Preparation and Characterization of Polyaniline/Polysulfone Nanocomposite Ultrafiltration Membrane. *J. Memb. Sci.* **2008**, *310*, 402–408.

(12) Tian, Z.; Yu, H.; Wang, L.; Saleem, M.; Ren, F.; Ren, P.; Chen, Y.; Sun, R.; Sun, Y.; Huang, L. Recent Progress in the Preparation of Polyaniline Nanostructures and Their Applications in Anticorrosive Coatings. *RSC Adv.* **2014**, *4*, 28195–28208.

(13) Guimard, N. K.; Gomez, N.; Schmidt, C. E. Conducting Polymers in Biomedical Engineering. *Prog. Polym. Sci.* **2007**, *32*, 876–921.

(14) Bhadra, S.; Khastgir, D.; Singha, N. K.; Lee, J. H. Progress in Preparation, Processing and Applications of Polyaniline. *Prog. Polym. Sci.* **2009**, *34*, 783–810.

(15) Li, D.; Huang, J.; Kaner, R. B. Polyaniline Nanofibers : A Unique Polymer Nanostructure for Versatile Applications. *Acc. Chem. Res.* **2009**, *42*, 135–145.

(16) Pud, A.; Ogurtsov, N.; Korzhenko, A.; Shapoval, G. Some Aspects of Preparation Methods and Properties of Polyaniline Blends and Composites with Organic Polymers. *Prog. Polym. Sci.* **2003**, *28*, 1701–1753.

(17) Prabhakar, P. K.; Raj, S.; Anuradha, P. R.; Sawant, S. N.; Doble, M. Biocompatibility Studies on Polyaniline and Polyaniline-Silver Nanoparticle Coated Polyurethane Composite. *Colloids Surfaces B Biointerfaces* **2011**, *86*, 146–153.

(18) Fan, Z.; Wang, Z.; Sun, N.; Wang, J.; Wang, S. Performance Improvement of Polysulfone Ultrafiltration Membrane by Blending with Polyaniline Nanofibers. *J. Memb. Sci.* **2008**, *320*, 363–371.

(19) Huang, X.; McVerry, B. T.; Marambio-Jones, C.; Wong, M. C. Y.; Hoek, E. M. V.; Kaner, R. B. Novel Chlorine Resistant Low-Fouling Ultrafiltration Membrane Based on a

Hydrophilic Polyaniline Derivative. *J. Mater. Chem. A* **2015**, *3*, 8725–8733.

(20) Zhao, X.; He, C. Efficient Preparation of Super Antifouling PVDF Ultrafiltration Membrane with One Step Fabricated Zwitterionic Surface. *ACS Appl. Mater. Interfaces* **2015**, *7*, 17947–17953.

(21) Zhao, S.; Wang, Z.; Wang, J.; Wang, S. Poly(Ether Sulfone)/Polyaniline Nanocomposite Membranes: Effect of Nanofiber Size on Membrane Morphology and Properties. *Ind. Eng. Chem. Res.* **2014**, *53*, 11468–11477.

(22) Gizdavic-Nikolaidis, M. R.; Bennett, J. R.; Swift, S.; Easteal, A. J.; Ambrose, M. Broad Spectrum Antimicrobial Activity of Functionalized Polyanilines. *Acta Biomater.* **2011**, *7*, 4204–4209.

(23) Tamboli, M. S.; Kulkarni, M. V; Patil, R. H.; Gade, W. N.; Navale, S. C.; Kale, B. B. Nanowires of Silver – Polyaniline Nanocomposite Synthesized via in Situ Polymerization and Its Novel Functionality as an Antibacterial Agent. *Colloids Surfaces B Biointerfaces* **2012**, *92*, 35–41.

(24) Liang, X.; Sun, M.; Li, L.; Qiao, R.; Chen, K.; Xiao, Q.; Xu, F. Preparation and Antibacterial Activities of Polyaniline/Cu0.05Zn0.95O Nanocomposites. *Dalt. Trans.* **2012**, *41*, 2804–2811.

(25) Zhang, Z.; Wei, Z.; Wan, M. Nanostructures of Polyaniline Doped with Inorganic Acids. *Macromolecules* **2002**, *35*, 5937–5942.

(26) Dhawale, D. S.; Salunkhe, R. R.; Jamadade, V. S.; Dubal, D. P.; Pawar, S. M.; Lokhande, C. D. Hydrophilic Polyaniline Nanofibrous Architecture Using Electrosynthesis Method for Supercapacitor Application. *Curr. Appl. Phys.* **2010**, *10*, 904–909.

(27) Yang, D.; Mattes, B. R. Polyaniline Emeraldine Base in N-Methyl-2-Pyrrolidinone

Containing Secondary Amine Additives: A Rheological Investigation of Solutions. *J. Polym. Sci. Part B Polym. Phys.* **2002**, *40*, 2702–2713.

(28) Yang, D.; Mattes, B. R. Investigation of Gel Inhibitor Assisted Dissolution of Polyaniline: A Case Study for Emeraldine Base, 2-Methyl-Aziridine, and N-Methyl-Pyrrolidone. *Synth. Met.* **1999**, *101*, 746–749.

(29) Orlando, J. J.; Burkholder, J. B.; McKeen, S. A.; Ravishankara, A. R. Atmospheric Fate of Several Hydrofluoroethanes and Hydrochloroethanes: 2. UV Absorption Cross Sections and Atmospheric Lifetimes. *J. Geophys. Res.* **1991**, *96*, 5013–5023.

(30) Roger, P.; Renaudie, L.; Le Narvor, C.; Lepoittevin, B.; Bech, L.; Brogly, M. Surface Characterizations of Poly(Ethylene Terephthalate) Film Modified by a Carbohydrate-Bearing Photoreactive Azide Group. *Eur. Polym. J.* **2010**, *46*, 1594–1603.

(31) Liu, J.; An, J.; Zhou, Y.; Ma, Y.; Li, M.; Yu, M.; Li, S. Preparation of an Amide Group-Connected Graphene-Polyaniline Nanofiber Hybrid and Its Application in Supercapacitors. *ACS Appl. Mater. Interfaces* **2012**, *4*, 2870–2876.

(32) Lai, L.; Yang, H.; Wang, L.; Teh, B.; Zhong, J.; Chou, H.; Chen, L.; Chen, W.; Shen, Z.; Ruoff, R. Preparation of Supercapacitor Electrodes through Selection of Graphene Surface Functionalities. *ACS Nano* **2012**, *6*, 5941–5951.

(33) An, J.; Liu, J.; Zhou, Y.; Zhao, H.; Ma, Y.; Li, M.; Yu, M.; Li, S. Polyaniline-Grafted Graphene Hybrid with Amide Groups and Its Use in Supercapacitors. *J. Phys. Chem. C* **2012**, *116*, 19699–19708.

(34) Kotal, M.; Thakur, A. K.; Bhowmick, A. K. Polyaniline-Carbon Nanofiber Composite by a Chemical Grafting Approach and Its Supercapacitor Application. *ACS Appl. Mater. Interfaces* **2013**, *5*, 8374–8386.

(35) Kumar, N. A.; Choi, H.; Shin, Y. R.; Chang, D. W.; Dai, L. Polyaniline-Grafted Reduced Graphene Oxide for Efficient Electrochemical. *ACS Nano* **2012**, No. 2, 1715–1723.

(36) An, J.; Liu, J.; Zhou, Y.; Zhao, H.; Ma, Y.; Li, M.; Yu, M.; Li, S. Polyaniline-Grafted Graphene Hybrid with Amide Groups and Its Use in Supercapacitors. *J. Phys. Chem. C* **2012**, *116*, 19699–19708.

(37) Li, Z. F.; Zhang, H.; Liu, Q.; Liu, Y.; Stanciu, L.; Xie, J. Covalently-Grafted Polyaniline on Graphene Oxide Sheets for High Performance Electrochemical Supercapacitors. *Carbon N. Y.* **2014**, *71*, 257–267.

(38) Liu, X.; Shang, P.; Zhang, Y.; Wang, X.; Fan, Z.; Wang, B.; Zheng, Y. Three-Dimensional and Stable Polyaniline-Grafted Graphene Hybrid Materials for Supercapacitor Electrodes. *J. Mater. Chem. A* **2014**, *2*, 15273–15278.

(39) Filimonov, V. D.; Trusova, M.; Postnikov, P.; Krasnokutskaya, E. A.; Lee, Y. M.; Hwang, H. Y.; Kim, H.; Chi, K. W. Unusually Stable, Versatile, and Pure Arenediazonium Tosylates: Their Preparation, Structures, and Synthetic Applicability. *Org. Lett.* **2008**, *10*, 3961–3964.

(40) Ziani-Cherif, H.; Imachi, K.; Matsuda, T. Preparation of Aryldiazonium-, Aryldiazo-, and Arylazido-Derivatized Copolymers and Their Surface Photografting. *Macromolecules* **1999**, *32*, 3438–3447.

(41) Haq, A. U.; Lim, J.; Yun, J. M.; Lee, W. J.; Han, T. H. Direct Growth of Polyaniline Chains from N-Doped Sites of Carbon Nanotubes. *Small* **2013**, *9*, 3829–3833.

(42) Rana, D.; Matsuura, T. Surface Modifications for Antifouling Membranes. *Chem. Rev.* **2010**, *110*, 2448–2471.

(43) Zhang, R.; Liu, Y.; He, M.; Su, Y.; Zhao, X.; Elimelech, M.; Jiang, Z. Antifouling

Membranes for Sustainable Water Purification: Strategies and Mechanisms. *Chem. Soc. Rev.* **2016**, *45*, 5888–5924.

(44) Koehler, J. A.; Ulbricht, M.; Belfort, G.; York, N. Intermolecular Forces between a Protein and a Hydrophilic Modified Polysulfone Film with Relevance to Filtration. *Langmuir* **2000**, *16*, 10419–10427.

(45) Fane, A.G.; Fell, C.J.D.; Suki, A. The Effect of PH and Ionic Environment on The Ultrafiltration of Protein Solutions with Retentive Membranes. *J. Memb. Sci.* **1983**, *16*, 195–210.

(46) Meng, F.; Chae, S.; Drews, A.; Kraume, M.; Shin, H. Recent Advances in Membrane Bioreactors (MBRs): Membrane Fouling and Membrane Material. *Water Res.* **2009**, *43*, 1489–1512.

(47) Le-clech, P.; Chen, V.; Fane, T. A. G. Fouling in Membrane Bioreactors Used in Wastewater Treatment. *J. Memb. Sci.* **2006**, *284*, 17–53.

(48) Guo, W.; Ngo, H.; Li, J. Bioresource Technology A Mini-Review on Membrane Fouling. *Bioresour. Technol.* **2012**, *122*, 27–34.

(49) Drews, A. Membrane Fouling in Membrane Bioreactors-Characterisation, Contradictions, Cause and Cures. *J. Memb. Sci.* **2010**, *363*, 1–28.

(50) Howe, K. J.; Clark, M. M. Fouling of Microfiltration and Ultrafiltration Membranes by Natural Waters. *Environ. Sci. Technol.* **2002**, *36*, 3571–3576.

(51) Dutta, Kingshuk; De, S. Smart Responsive Materials for Water Purification : An Overview. *J. Mater. Chem. A Mater. energy Sustain.* **2017**, *5*, 22095–22112.

(52) Magin, C. M.; Cooper, S. P.; Brennan, A. B. Non-Toxic Antifouling Strategies. *Mater. Today* **2010**, *13*, 36–44.

(53) Zhao, S.; Wang, Z.; Wei, X.; Zhao, B.; Wang, J. Performance Improvement of Polysulfone Ultrafiltration Membrane Using PANiEB as Both Pore Forming Agent and Hydrophilic Modifier. *J. Memb. Sci.* **2011**, *385–386*, 251–262.

(54) Teli, S. B.; Molina, S.; Calvo, E. G.; Lozano, A. E.; de Abajo, J. Preparation, Characterization and Antifouling Property of Polyethersulfone-PANI/PMA Ultrafiltration Membranes. *Desalination* **2012**, *299*, 113–122.

(55) Zhu, S.; Zhao, S.; Wang, Z.; Tian, X.; Shi, M. Improved Performance of Polyamide Thin-Film Composite Nano Filtration Membrane by Using Polyethersulfone/Polyaniline Membrane as the Substrate. *J. Memb. Sci.* **2015**, *493*, 263–274.

(56) Jiang, B.; Wang, B.; Zhang, L.; Sun, Y.; Xiao, X.; Yang, N.; Dou, H. Improvement of Antifouling Performance of Poly (L-Lactic Acid) Membranes through Incorporating Polyaniline Nanoparticles. *J. Appl. Polym. Sci.* **2017**, *44452*, 1–7.

(57) Zhao, S.; Huang, L.; Tong, T.; Zhang, W.; Wang, Z.; Wang, J.; Wang, S. Antifouling and Antibacterial Behavior of Polyethersulfone Membrane Incorporating Polyaniline@silver Nanocomposites. *Environ. Sci. Water Res. Technol.* **2017**, *3*, 710–719.

(58) Liao, Y.; Yu, D.; Wang, X.; Chain, W.; Li, X. Carbon Nanotube-Templated Polyaniline Nano Fibers: Synthesis, Flash Welding and Ultrafiltration Membranes. *Nanoscale* **2013**, *5*, 3856–3862.

(59) Duan, W.; Ronen, A.; Walker, S.; Jassby, D. Polyaniline-Coated Carbon Nanotube Ultrafiltration Membranes: Enhanced Anodic Stability for in Situ Cleaning and Electro-Oxidation Processes. *ACS Appl. Mater. Interfaces* **2016**, *8*, 22574–22584.

(60) Hudaib, B.; Gomes, V.; Zhou, C.; Liu, Z. Separation and Purification Technology Poly(Vinylidene Fluoride)/Polyaniline/MWCNT Nanocomposite Ultrafiltration

Membrane for Natural Organic Matter Removal. *Sep. Purif. Technol.* **2018**, *190*, 143–155.

(61) Mcverry, B. T.; Temple, J. A. T.; Huang, X.; Marsh, K. L.; Hoek, E. M. V; Kaner, R. B. Fabrication of Low-Fouling Ultrafiltration Membranes Using a Hydrophilic, Self-Doping Polyaniline Additive. *Chem. Mater.* **2013**, *25*, 3597–3602.

(62) Chen, S.; Lee, H. Structure and Properties of Poly(Acry1ic Acid)-Doped Polyaniline. *Macromolecules* **1995**, *28*, 2858–2866.

(63) Jaymand, M. Recent Progress in Chemical Modification of Polyaniline. *Prog. Polym. Sci.* **2013**, *38*, 1287–1306.

(64) Lin, C.; Li, R. L.; Robbennolt, S.; Yeung, M. T.; Akopov, G.; Kaner, R. B. Furthering Our Understanding of the Doping Mechanism in Conjugated Polymers Using Tetraaniline. *Macromolecules* **2017**, *50*, 5892–5897.

(65) Wang, Y.; Tran, H. D.; Kaner, R. B. Applications of Oligomers for Nanostructured Conducting Polymers. *Macromol. Rapid Commun.* **2011**, *32*, 35–49.

(66) Wei, Z.; Faul, C. F. J. Aniline Oligomers–Architecture, Function and New Opportunities for Nanostructured Materials. *Macromol. Rapid Commmunications* **2008**, *29*, 280–292.

(67) Keana, J. F. W.; Cai, S. X. New Reagents for Photoaffinity Labeling: Synthesis and Photolysis of Functionalized Perfluorophenyl Azides. *J. Org. Chem.* **1990**, *55*, 3640–3647.

(68) Pastine, S. J.; Okawa, D.; Kessler, B.; Rolandi, M.; Llorente, M.; Zettl, A.; Fréchet, J. M. J. A Facile and Patternable Method for the Surface Modification of Carbon Nanotube Forests Using Perfluoroarylazides. *J. Am. Chem. Soc.* **2008**, *130*, 4238–4239.

(69) Liu, L.-H.; Yan, M. Perfluorophenyl Azides: New Applications in Surface Functionalization and Nanomaterial Synthesis. *Acc. Chem. Res.* **2010**, *43*, 1434–1443.

(70) Brase, S.; Gil, C.; Knepper, K.; Zimmermann, V. Organic Azides: An Exploding Diversity of a Unique Class of Compounds. *Angew. Chemie Int. Ed.* **2005**, *44*, 5188–5240.

(71) Li, Z.; Ajami, A.; Stankevičius, E.; Husinsky, W.; Račiukaitis, G.; Stampfl, J.; Liska, R.; Ovsianikov, A. 3D Photografting with Aromatic Azides: A Comparison between Three-Photon and Two-Photon Case. *Opt. Mater. (Amst).* **2013**, *35*, 1846–1851.

(72) Shao, Z.; Rannou, P.; Sadki, S.; Fey, N.; Lindsay, D. M.; Faul, C. F. J. Delineating Poly(Aniline) Redox Chemistry by Using Tailored Oligo(Aryleneamine)s: Towards Oligo(Aniline)-Based Organic Semiconductors with Tunable Optoelectronic Properties. *Chem. Eur. J.* **2011**, *17*, 12512–12521.

(73) Li, R. L.; Lin, C. W.; Shao, Y.; Chang, C. W.; Yao, F. K.; Kowal, M. D.; Wang, H.; Yeung, M. T.; Huang, S. C.; Kaner, R. B. Characterization of Aniline Tetramer by MALDI TOF Mass Spectrometry upon Oxidative and Reductive Cycling. *Polymers (Basel).* **2016**, *8*, 401.

(74) Shao, Y.; El-Kady, M. F.; Lin, C. W.; Zhu, G.; Marsh, K. L.; Hwang, J. Y.; Zhang, Q.; Li, Y.; Wang, H.; Kaner, R. B. 3D Freeze-Casting of Cellular Graphene Films for Ultrahigh-Power-Density Supercapacitors. *Adv. Mater.* **2016**, 6719–6726.

(75) Liu, L. H.; Yan, M. Perfluorophenyl Azides: New Applications in Surface Functionalization and Nanomaterial Synthesis. *Acc. Chem. Res.* **2010**, *43*, 1434–1443.

(76) Liptay, V. W. Elektrochromie - Solvatochromie. *Angew. Chemie* **1969**, *81*, 195–206.

(77) Tsubokawa, N. Preparation and Properties of Polymer-Grafted Carbon Nanotubes and Nanofibers. *Polym. J.* **2005**, *37*, 637–655.

(78) Baughman, R. H.; ShackletteL.W. Conductivity as a Function of Conjugation Length: Theory and Experiment for Conducting Polymer Complexes. *Phys. Rev. B* **1989**, *39*,

5872–5886.

(79) Satpathy, S.; Sen, S. K.; Pattanaik, S.; Raut, S. Review on Bacterial Biofilm: An Universal Cause of Contamination. *Biocatal. Agric. Biotechnol.* **2016**, *7*, 56–66.

(80) Vuong, C.; Otto, M. Staphylococcus Epidermidis Infections. *Microbes Infect.* **2002**, *4*, 481–489.

(81) Otto, M. Staphylococcus Epidermidis - The "accidental" Pathogen. *Nat. Rev. Microbiol.* **2009**, *7*, 555–567.

(82) Jin-Chih, J.; Macdiarmid, A. G. "Polyaniline": Protonic Acid Doping of the Emeraldine Form to the Metallic Regime. *Synth. Met.* **1986**, *13*, 193–205.

(83) J.L., B.; G.B., S. Polarons, Bipolarons, and Solitons in Conducting Polymers. *Acc. Chem. Res.* **1985**, *18*, 309–315.

(84) Cao, Y.; Li, S.; Xue, Z.; Guo, D. Spectroscopic and Electrical Characterization of Some Aniline Oligomers and Polyaniline. *Synth. Met.* **1986**, *16*, 305–315.

(85) Epstein, A.; Ginder, J.; Zuo, F.; Bigelow, R.; Woo, H.; Tanner, D.; Richter, A.; Huang, W.-S.; MacDiarmid, A. Insulator-to-Metal Transition in Polyaniline. *Synth. Met.* **1987**, *18*, 303–309.

(86) Mcverry, B. T.; Wong, M. C. Y.; Marsh, K. L.; Temple, J. A. T.; Marambio-jones, C.; Hoek, E. M. V; Kaner, R. B. Scalable Antifouling Reverse Osmosis Membranes Utilizing Perfluorophenyl Azide Photochemistry. *Macromol. Rapid Commun.* **2014**, *35*, 1528–1533.

(87) Siegmann, K.; Inauen, J.; Sterchi, R.; Winkler, M. Spectroscopy on Photografted Polyethylene Surfaces Using a Perfluorophenyl Azide: Evidence for Covalent Attachment. *Surf. Interface Anal.* **2018**, *50*, 205–211.

(88) Siegmann, K.; Inauen, J.; Villamaina, D.; Winkler, M. Photografting of Perfluoroalkanes

onto Polyethylene Surfaces via Azide/Nitrene Chemistry. *Appl. Surf. Sci.* **2017**, *396*, 672–680.

(89) Guo, B.; Finne-wistrand, A.; Albertsson, A. Electroactive Hydrophilic Polylactide Surface by Covalent Modification with Tetraaniline. *Macromolecules* **2012**, *45*, 352–359.

(90) Zhou, P.; Li, J.; Yang, W.; Zhu, L.; Tang, H. Polyaniline Nanofibers: Their Amphiphilicity and Uses for Pickering Emulsions and On-Demand Emulsion Separation. *Langmuir* **2018**, *34*, 2841–2848.

(91) Kaeselev, B.; Kingshottb, P.; Jonsson, G. Influence of the Surface Structure on the Filtration Performance of UV-Modified PES Membranes. *Desalination* **2002**, *146*, 265–271.

(92) Wang, L. P.; Wang, W.; Di, L.; Lu, Y. N.; Wang, J. Y. Protein Adsorption under Electrical Stimulation of Neural Probe Coated with Polyaniline. *Colloids Surfaces B Biointerfaces* **2010**, *80*, 72–78.

(93) Hunter, R. J. *Foundations of Colloid Science*; Oxford University Press: New York, 1987.

(94) Li, D.; Kaner, R. B. Processable Stabilizer-Free Polyaniline Nanofiber Aqueous Colloids. *Chem. Commun.* **2005**, 3286–3288.

(95) Dorobantu, L. S.; Bhattacharjee, S.; Foght, J. M.; Gray, M. R. Analysis of Force Interactions between AFM Tips and Hydrophobic Bacteria Using DLVO Theory. *Langmuir* **2009**, *25*, 6968–6976.

CHAPTER 3: ANILINE OCTAMER

3.1 INTRODUCTION

3.1.1 Inherently Conducting Polymers

Inherently Conducting Polymers (ICPs) derive their conductivity from the presence of a conjugated electron system.[1] They have unique properties that include: a low energy optical transition, low ionization potential and high electron affinity.[2] ICPs are organic materials with electrical properties similar to metals and semiconductors.[1] In 1977, it was demonstrated that polyacetylene could obtain a level of conductivity similar to metals by a reaction with iodine vapor.[3] In 2000, the Nobel Prize was awarded to Alan MacDiarmid, Alan Heeger, and Hideki Shirakawa for their discovery of and contributions to conducting polymers.[4] They were able to produce conductive organic polymers using doping mechanisms that introduce charge carriers (electrons or holes) and give rise to polymers with metallic-like electrical properties.[4] This is significant because unlike their inorganic counterparts, organic conducting polymers are less expensive to produce, light weight, and more flexible. Extensive work has focused on polyaniline because it's thermally stable and shows good electrical conductivity.

Polyaniline is a conducting polymer that has unique acid/base doping/de-doping properties. It can be synthesized either by oxidative polymerization under acidic conditions or via electrochemical oxidation.[1] The three major oxidation states of polyaniline combined with its doping/de-doping mechanisms make it an ideal model for analyzing the stability and conductivity of ICPs (*i.e.* polyaniline is unique because not only can it be doped by a redox reaction, but it can undergo a direct acid doping reaction to achieve the conductive emeraldine state). Polyaniline is in its most reduced state as the leucoemeraldine base (LEB), half-oxidized in the emeraldine base

(EB) state (a semiconductor), and fully oxidized in the pernigraniline base (PG) state.[1] Conversion between the oxidation states can easily occur by using ammonium persulfate as the oxidizing agent or phenylhydrazine as the reducing agent, to cause a conversion between benzenoid and quinoid units in the polymer.[5]

3.1.2 Uses for Conducting Polymers

Conducting polymers can be used in electrical and electronic applications as insulating (dielectric) materials because of their very high resistivities in their un-doped or de-doped forms.[6] They can also provide electromagnetic shielding of electronic circuits, can be used as antistatic coating materials to prevent electrical discharge, can be used in organic light emitting diodes (OLEDS) as hole injecting electrodes and also for field-effect transistors to name but a few applications.[5,7]

3.1.3 Dopants

Doping is "raising the conductivity of certain organic polymers metallic levels by chemical or electrochemical 'pi doping' (oxidation), or 'n-doping' (reduction)".[8] Organic polymer doping is similar to the doping of inorganic semiconductors to achieve certain metallic properties where large increases in conductivity are observed.[8] When a conjugated polymer is synthesized, but not doped, it generally exhibits very low conductivities. When an electron is removed from the valence band, known as p-doping or an electron is added to the conduction band, known as n-doping, does the conducting polymer become highly conductive.[9] This doping phenomenon generates charge carriers that can move in an electric field. The positive (holes) and negative (electron) charges move to opposite electrodes.[10] This is the charge movement responsible for electrical conductivity. Doping in polyaniline occurs when the imine nitrogens become protonated with negatively

charged dopant anions that reside near the positively charged nitrogens.[2] Common dopants are camphor sulfonic acid (CSA), hydrochloric acid (HCl) and sulfuric acid (H_2SO_4).[11,12] Work done in the Kaner lab on oligoanilines regarding dopants has shown that TANI can self-assemble into nanostructures by varying the dopants and solvents by taking advantage of pi-pi stacking, hydrophobic interactions and hydrogen bonding, which are key elements for the self-assembly of many semiconductors and biomolecules.[13]

3.1.4 Polarons and Bipolarons in Conducting Polymers

PANI is a p-type semiconductor with holes and positively charged carriers. PANI in its bulk structure contains both crystalline (conductive) and amorphous (insulating) regions.[2] These ordered crystalline sites are conductive with the possibility for electron delocalization and hopping of charge carriers through the polaron structure, but are surrounded by insulating amorphous regions.[9] The bulk conductivity of PANI is dependent on three factors; the intramolecular, intermolecular and the intra-domain conduction.[7] Intermolecular conduction involves polarons for electronic hopping in the crystalline regions between polymer chains that are affected by inter-chain distances, the size of the region and the crystallinity of the ES state. Inter-domain conduction involves the interconnections between conductive crystalline regions in the amorphous regions. Intramolecular conduction is the movement of the charged carriers or holes along the conjugated chains.[2]

PANI obtains its conductivity in its polaron structure formed after oxidative doping of the (LEB) state or the protonation of the half oxidized EB state.[14] The controlled doping of PANI leads to enhanced conductivity due to formation of charge carriers that can move under the influence of an external potential and in the Coulombic field of counter-ions distributed between the chains.

For oxidative doping with ammonium persulfate (APS), doping electrons are removed from the LEB state to form radical cations (polarons).[15] For acid doping with HCl (strong protonic acid), the EB state is the starting point. The imine nitrogen atoms are preferentially protonated compared to the amine nitrogen atoms due to a large driving force for semiquinone formation from protonated imines, leading to the formation of a bipolaron.[16] Charge redistribution then occurs as an internal redox process that causes the polymer chains to end up with the same configuration after the oxidative doping. This can be done by converting the ES state back to the EB state via a strong base. The protonation of PANI-EB leads to the formation of polaron structures, where a current is carried by the holes. When PANI is in its perfect EB state, full doping will produce the maximum number of polarons and result in the highest conductivity achievable.[8] However, in the case of over doping, the formation of bipolarons (polarons/holes adjacent to each other) will cause a decrease in conductivity.[17] Therefore, acid doping is preferred over oxidative doping. There is no fear of over doping with an acid and also, EB is more stable to work with compared to LEB against oxidation (LEB will start to slowly oxidize into EB in air).[18]

Many of the issues in developing ICPs arise from the polymers limited solubility and lack of organization in the bulk form, ultimately limiting their use in electronic devices which require increased organization to favor carrier mobility.[18] PANI is not soluble in most organic solvents because of the pi-pi interactions that cause strong interactions between the polymer chains. Oligoanilines offer a solution to these problems by allowing for the formation of ordered structures, which retain polymer properties, through the process of crystallization, without having to add more synthesis steps by functionalizing polyaniline to help with its lack of solubility.[18]

3.1.5 Oligo(aniline)s

Oligo(aniline)s also have unique acid/base doping chemistry like PANI.[19] They are smaller and have more well-defined molecules, with the smallest oligomer that can have the acid/base doping/de-doping chemistry being tetraaniline (TANI).[20,21] Work done in the Kaner group has shown that increased conductivity arises out of noncovalent stacking between tetramers.[19] Therefore, nanoscale morphology and electrical properties can be controlled by manipulating noncovalent interactions between oligomers during crystallization. The self-assembly process is influenced by the solvent because the solvent to non-solvent ratio contribute to the degree of aggregation between oligomers.[19] The Kaner group has developed various crystal morphologies with TANI.[19] TANI can be synthesized to have different functionalities in its end groups. **Figure 1** shows the three different ways TANI can be used, which include, phenyl/amino (Ph/NH_2) capped (top), Phenyl/Phenyl (Ph/Ph) capped (middle), and amino/amino (NH_2/NH_2) capped (bottom). Ph/Ph TANI is the most stable of the three because it cannot produce any side products. In contrast, the amino functionalized TANIs can continue oxidative polymerization to produce higher oligomers. Ph/Ph TANIs are also symmetrical which is good for stacking and crystallization due to a limited number of degrees of freedom. Although much progress has been made in controlling morphologies and improving conductivity, other oligomers of aniline have yet to be explored. The electrical and physical properties of these oligomers will change as they increase in size. For example, the octamer of polyaniline is believed to share most of the same physical properties as the polymer itself. Understanding the chain length and physical properties is what drives this research.

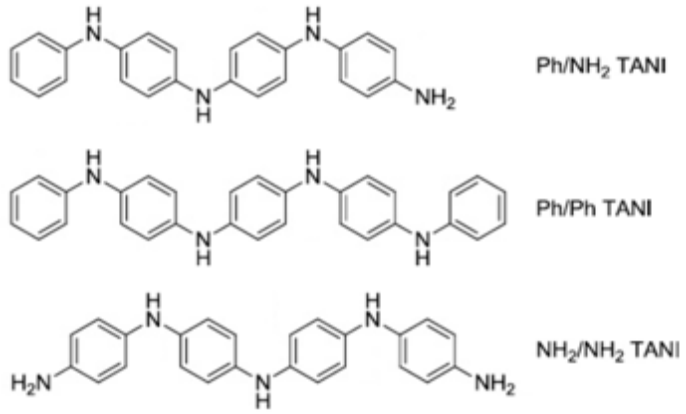

Figure 3-1. Three ways to use TANI, phenyl/amino-capped TANI (Top), phenyl-capped TANI (middle), and amino/amino-capped TANI (bottom).

Aniline oligomers are potentially a very favorable replacement for metallic conductors because of their lower costs, light weight and broader range of applications; e.g. in electronics, sensors and energy harvesting.[19,22] Aniline octamer (OANI) (**Figure 2**) contains eight aniline units (twice the length of TANI), offers a solution to the issues associated with polyaniline by allowing for the formation of ordered structures, which retain polymer properties, through the process of crystallization to obtain defined properties and functionality to determine the relationship between structure and properties.[19,23,24] Specifically, we believe OANI could allow for stronger stacking interactions and an increase in intermolecular order, resulting in higher crystallinity resulting in conductivity comparable to PANI itself, if not higher. It has been shown that by increasing crystallinity, the conductivity of PANI films increases significantly.[12]

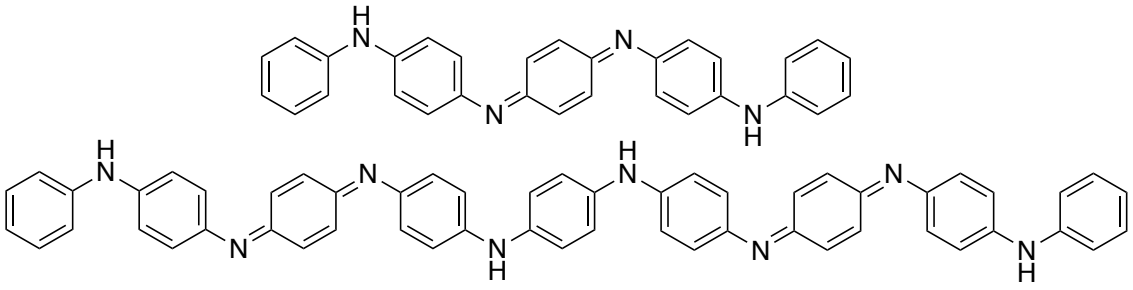

Figure 3-2. Phenyl-capped tetramer (top) and phenyl-capped octamer (bottom).

We focused on the morphological and dimensional control of the self-assembly process for doped OANI nanostructures. The conductivities achieved by the OANI structure should demonstrate marked improvements in conductivity for ICPs and could highlight the potential for future applications in various electrical devices. We base this believe on previous work by Mills *et al.* revealing that observing both a diamagnetic (bipolaron) as well as a paramagnetic (polaron) form of the TANI-ES state by varying the dopant concentration.[17] They also showed the effects for the doped states of OANI and diphenyl-p-phenylenediamine (DPPD) oligomers. However, they were not confident in their results which differed from computational results obtained from time-dependent density functional theory (TD-DFT) simulations.

Similar to TANI, the two main types of octamer that will be studied are the Ph/NH_2 (phenyl/amino-capped) and the Ph/Ph (phenyl-capped) octamer (**Figure 3**). The Ph/NH_2 OANI are used to study the chain length dependent properties of the oligomers because they can keep synthesizing higher oligomers. The phenyl capped OANI can be used to study the charge-storage mechanisms because they cannot undergo further reactions.

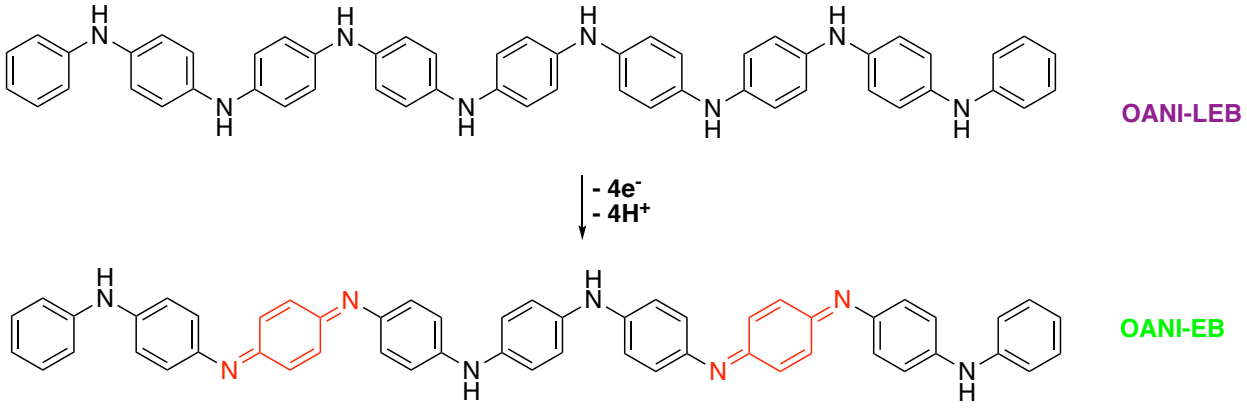

Figure 3-3. Oxidation of OANI-LEB to OANI-EB

3.1.6 Crystallization Techniques

Different crystallization techniques can be used to achieve a crystal structure; slow evaporation, slow cooling, vapor diffusion, liquid-liquid diffusion, and sublimation.[25] Crystallization is preceded by nucleation. Nucleation occurs either spontaneously or is started by vibration of particles. Small crystals will grow if the nucleation occurs too quickly. Good crystals typically grow very slowly, ranging from two to seven days if not longer. Crystals that grow within minutes or hours don't usually diffract well.[25]

3.2 Methods

3.2.1 Synthesis of TANI

Oxidative coupling was used to synthesize Ph/NH_2 TANI. A round bottom flask was charged with *N*-phenyl-1,4-phenylenediamine and HCl (0.1 M) and stirred for 30 minutes before quickly adding a solution of ferric chloride in HCl (0.1 M). The reaction was stirred for 2 hours at room temperature to obtain a dark green solution. The precipitate was washed 5 times with HCl (0.1 M) and collected by centrifugation in order to remove the excess ferric chloride. The precipitate was then treated with ammonium hydroxide (2.0 M) and acetone for 30 minutes. The acetone was removed under pressure and a violet solid was collected.

3.2.2 Synthesis of OANI

OANI was synthesized three different ways.

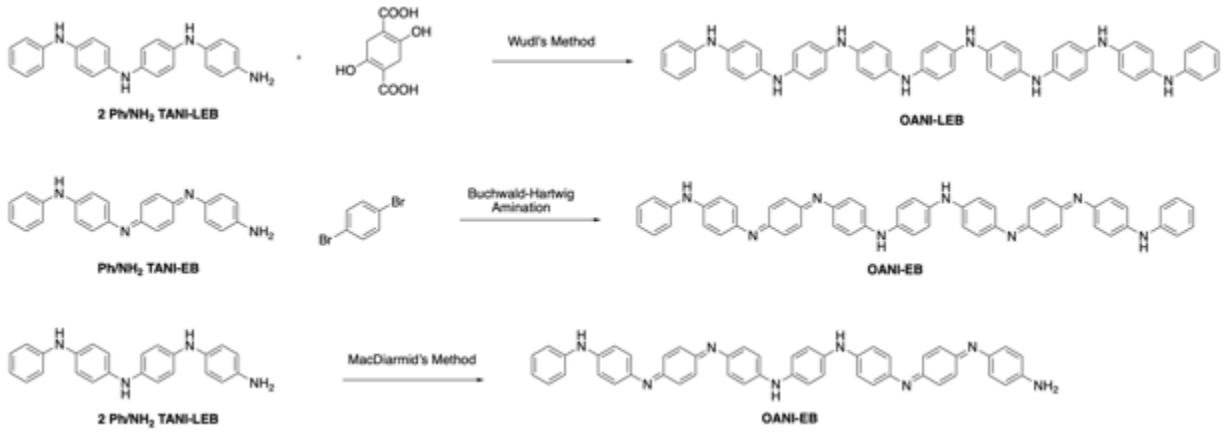

Figure 3-4. Wudl's method to obtain Ph/Ph OANI (top), Buchwald-Hartwig amination to obtain Ph/Ph OANI (middle) and MacDiarmid's method to obtain Ph/NH_2 OANI (bottom).

The first synthesis used the Wudl method, which is a condensation approach (**Figure 4, top**). This approach was only attempted once because of the dangerous mercury reagent required for the synthesis and the very low product yield. The two methods that were used more frequently were Buchwald-Hartwig amination and the MacDiarmid method. The amination reaction is a palladium catalyzed coupling reaction and the MacDiarmid method is simply oxidative coupling. The Buchwald-Hartwig amination reaction works by coupling two TANI molecules together. A Schlenk technique was used under argon gas. A slightly modified procedure was used for the reaction. In brief, a round bottom flask was charged with Ph/NH_2 TANI-EB, $Pd(dba)_2$, *rac*-BINAP, 1,4-dibromobenzene and sodium *tert*-butoxide in anhydrous THF. The reaction was heated to 90 ºC and stirred for 3 days. After 3 days, the reaction was cooled to room temperature and left open in air for 1 day. Deionized water was added to the reaction and THF was removed under reduced pressure. The product was collected by centrifugation and the precipitate was dissolved in DMF and HCl (2.0 M). The solution became doped, and went from a dark violet to a dark green color. DI water was added before the precipitate was collected by centrifugation. The solid was treated

with ammonium hydroxide (2.0 M) and acetone for 1 hour. The acetone was removed under reduced pressure and the solid was collected by centrifugation and oven dried for 24 hours. The product was a fine black powder (**Figure 5a**). However, when we attempted the synthesis, we were only able to obtain the Ph/NH_2 OANI. We also attempted to use Ph/NH_2 TANI-LEB instead of EB, but also obtained the same results. OANI-EB and also OANI-ES both dissolve in common organic solvents similarly. **Figure 5b** shows the deep violet color of OANI-EB in ethanol and the deep green color of OANI-ES.

3.3 Results and Discussion

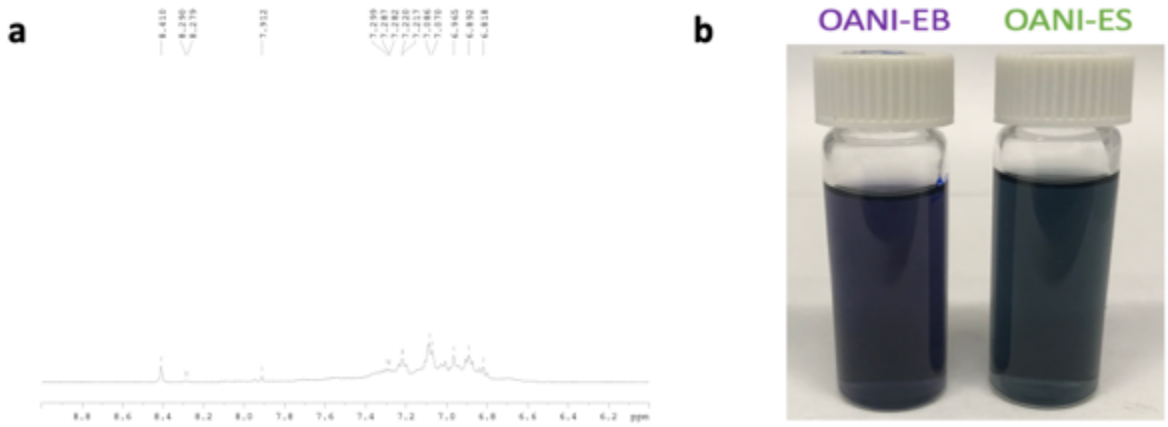

Figure 3-5. a) ^{1}H NMR of Ph/NH_2 OANI in its emeraldine base state in DMF; **b)** OANI-EB dissolved in ethanol (left) and OANI-ES doped in 0.1 M HCl in ethanol (right).

3.3.1 Matrix-assisted Laser Desorption Ionization Time-of-Flight (MALDI-TOF) Mass Spectrometry

MALDI-TOF mass spectrometry was carried out on a Bruker Ultraflex MALDI TOF-TOF. 1 mg of the dried samples were dissolved in 1 mL of ethanol. MALDI of the crude product after

Buchwald-Hartwig amination resulted in the Ph/NH_2 OANI with some tetramer and other smaller oligomers (**Figure 4**). To purify the mixture of oligomers, we used a Soxhlet extractor (**Figure 6)**. Removal of the smaller oligomers is a daunting task because the oligomers all share similar solubilities in common organic solvents. One method that was not attempted was column chromatography that can possibly also separate the oligomers from one another with varied solvent mixtures.

3.3.2 Soxhlet Extraction Purification

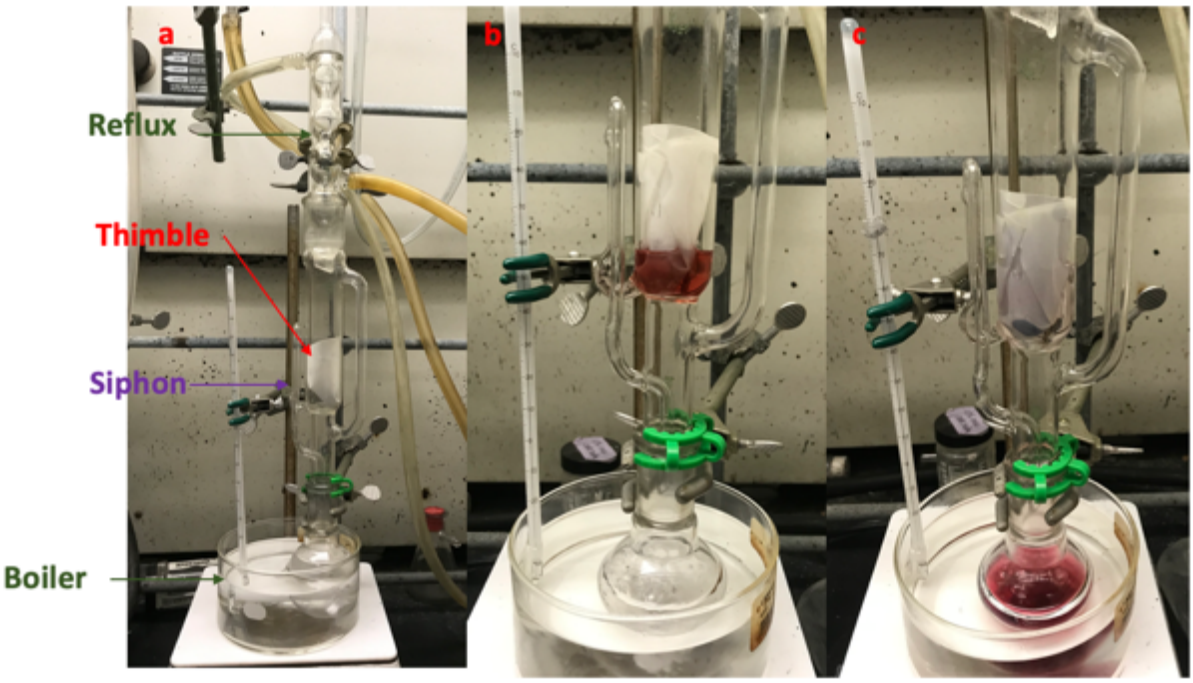

Figure 3-6: Soxhlet Extraction Setup: **a)** Start of the extraction; **b)** 3 hours after beginning extraction; and **c)** 24 hours after starting extraction.

A Soxhlet extraction apparatus was set up consisting of a condenser, extractor, distillation flask, and a homemade thimble made out of cellulose filter paper (**Figure 6**). The dried black product obtained from the OANI synthesis, described above, was placed into the thimble and the round bottom flask was filled with 75 mL of solvent (**Figure 6a**). Different solvents and reflux

temperatures were tested including (**Figures 6b, c**): cyclohexane (24 hours), 1:1 cyclohexane:diethyl ether (2 days), 1:1 cyclohexane: acetone (2 days), and cyclohexane (4 days). We obtained optimal results using cyclohexane for 4 days (**Figure 7)** and obtained pure OANI-EB. **Figures 7b, c** show the smaller oligomers dissolving into the solvent, while the OANI stays inside the thimble. Optimal results were obtained with the 1:1 cyclohexane:acetone (**Figure 7e**), while 1:1 cyclohexane:ethyl ether resulted in the ether also dissolving the octamer (**Figure 7c**). Cyclohexane resulted in poor separation over oligomers (**Figures 7b**).

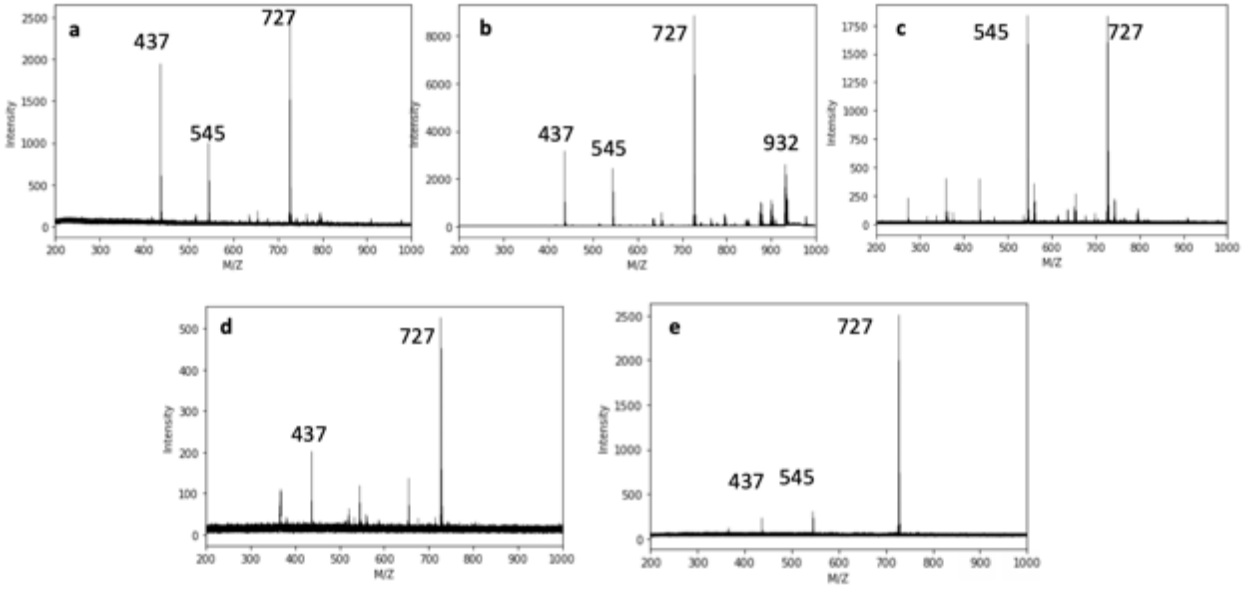

Figure 3-7. MALDI spectra of **a)** before Soxhlet extraction using Buchwald-Hartwig amination; **b)** cyclohexane after 24 hours; **c)** 1:1 cyclohexane:ethyl ether after 24 hours ;**d)** cyclohexane after 4 days; and **d)** 1:1 cyclohexane:acetone ether after 24 hours.

3.3.3 UV-Vis Spectra for the Doped States of OANI

We varied the concentration of HCl from 0.02-0.40 mM using a constant concentration of OANI (0.02 mM) and measured the UV-Vis absorption spectrum 24 hours after addition of the acid. We repeated this procedure using camphorsulfonic acid (CSA) as the dopant and varied the concentration from 0.20 mM- 1.00 mM. From the UV-Vis analysis of OANI-ES, we see the emergence of the polaron form occuring when the HCl dopant concentration is at 0.025 mM. The peak at 801 nm corresponds to the mono-protonated singlet state of phenyl capped OANI as computed from CAM-B3LYP and shown in **Figure 10**.

OANI-EB was doped at varied concentrations to determine how much acid is needed to dope the octamer. Immediately after the dopant was added, the solution turned green and over time the solution stabilized to a bluer color. As the dopant concentration was increased we observed dramatic color changes of OANI in ethanol starting from a dark blue to a lighter blue (**Figure 8**).

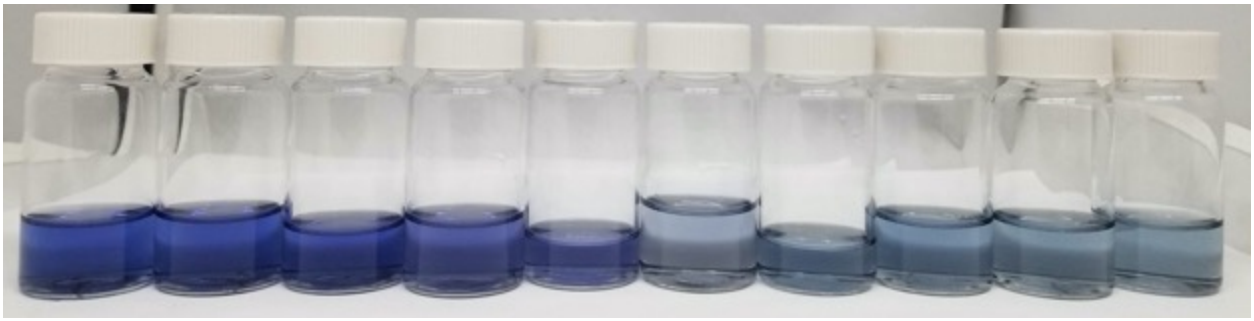

Figure 3-8. OANI (0.02 mM) doped with varying concentrations of HCl ranging from (0.02-0.4 mM) taken 24 hours after initial doping.

The UV-Vis spectrum for each sample was recorded on the following day in order to allow for the solution to stabilize. PANI-EB has a strong absorption at 343 and 626 nm, indicating the pi-pi* transition and the spectrum of the fully oxidized PG state with two absorption maxima at

320 and 528 nm. Similarly, when HCl is used as the dopant with OANI, the peaks at 317 and 589 nm represent the pi-pi* transition in the benzene ring and quinoid excitonic transition. These peaks decrease in intensity and the polaron to pi-pi* transition and the polaron to pi* transition peaks at 295 and 801 nm increases in intensity as the dopant concentration is increased to show OANI in the ES state (**Figure 9**). The peak around 801 nm begins to decrease as the concentration increases after reaching a maximum with the dopant concentration of 0.29 mM.

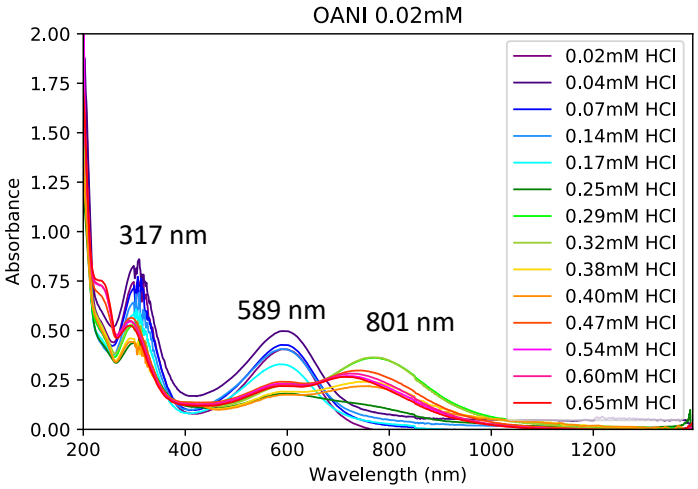

Figure 3-9. UV-Vis spectrum of OANI (0.02 mM) in solution with ethanol doped with varying concentrations of HCl (0.02-0.65 mM).

When CSA was used as the dopant, the peak at 801 nm did not decrease as the dopant concentration was increased. In addition, the peak at around 410 nm became more apparent (**Figure 10**). By better understanding the ES state, we will be able to control the conductive properties of the oligomer. From the UV-Vis spectra of the ES state under different dopant concentrations we are not able to observe all the bipolaronic and polaronic states of OANI previously reported for TANI. This may be due to the inability to find a suitable acid and range of dopant concentrations in the case of OANI.

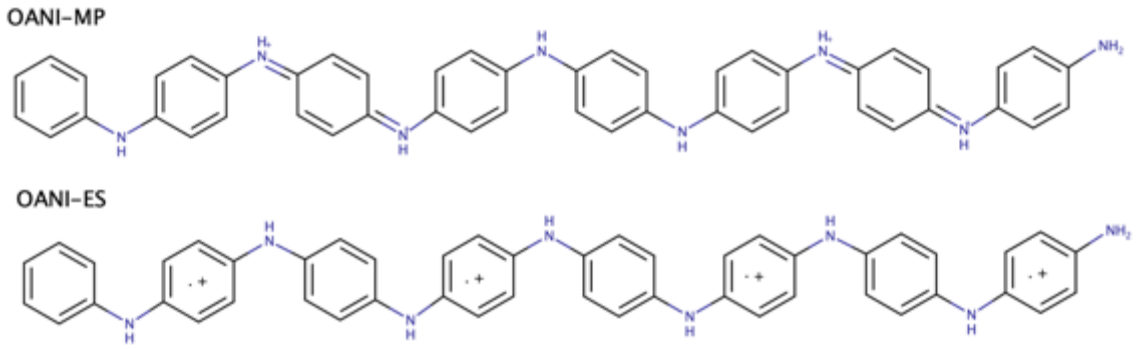

Figure 3-10. The different proposed emeraldine salt states of OANI. At low dopant concentrations, the mono-protonated (MP) state (top) is observed, and at high concentrations the fully protonated state may exist in a polaronic, paramagnetic state (bottom).

The peaks in the UV-Vis spectrum at 317 and 589 nm correspond to the EB state, and the emergence of the peak at 801 nm suggests the presence of the mono-protonated form (**Figures 10, 11**). The decrease in this peak past 0.29 mM HCl, suggests OANI is fully doped, however, from the color of the solution we have not yet fully doped the octamer even at these higher concentrations (**Figure 8**). When CSA was used as the dopant, we see similar peaks at around 317, 589, and 801 nm. In addition, the peak around 410 nm is more prominent, and the peak at 801 nm only increases as the dopant concentration increases, suggesting the large CSA may be a more suitable dopant (**Figure 11**).

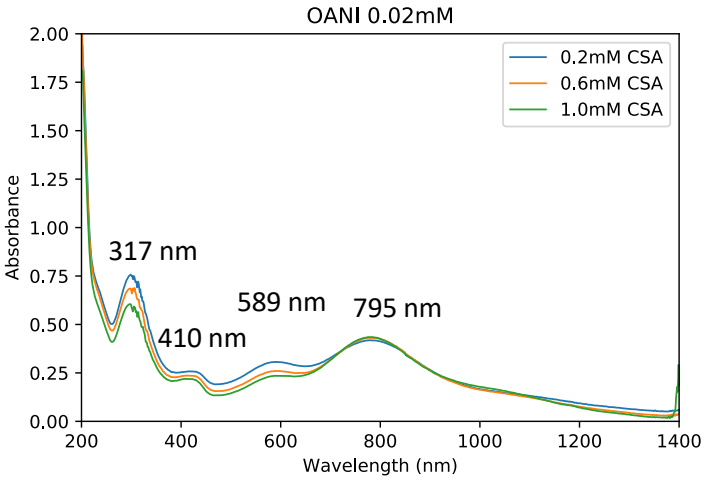

Figure 3-11. The UV-Vis spectrum of a 0.02 mM solution of OANI in ethanol doped with varying concentrations of CSA from 0.2-1 mM.

3.3.4 IR-Spectrum of Doped OANI

The infrared spectrum of OANI powder was measured using Attenuated Total Reflectance Fourier Transform Infrared (ATR-FTIR) spectroscopy. The infrared spectrum of CSA-doped OANI was measured by evaporating the solvent off of a solution of 0.02 mM OANI and 0.2 mM CSA in ethanol. The spectrometer baseline used ethanol as a blank before the fine powder was re-dissolved in a drop of ethanol and the IR was measured. The characterization of OANI by means of spectroscopic analysis remains a challenging task. The aromatic region is useful for distinguishing between the different oxidation states. The peaks corresponding to the -N-H groups are found within the 7.9-8.5 ppm region (**Figure 12a**). The difference peaks result from the different isomers, which differ in the location of the quinoid ring. Similar observations were made for the emeraldine base phenyl capped tetramer.[9] The formation of the ES state is seen in the IR spectrum by the disappearance of the C=N stretch which occurs at around 1500 cm^{-1} (**Figure 12b**).

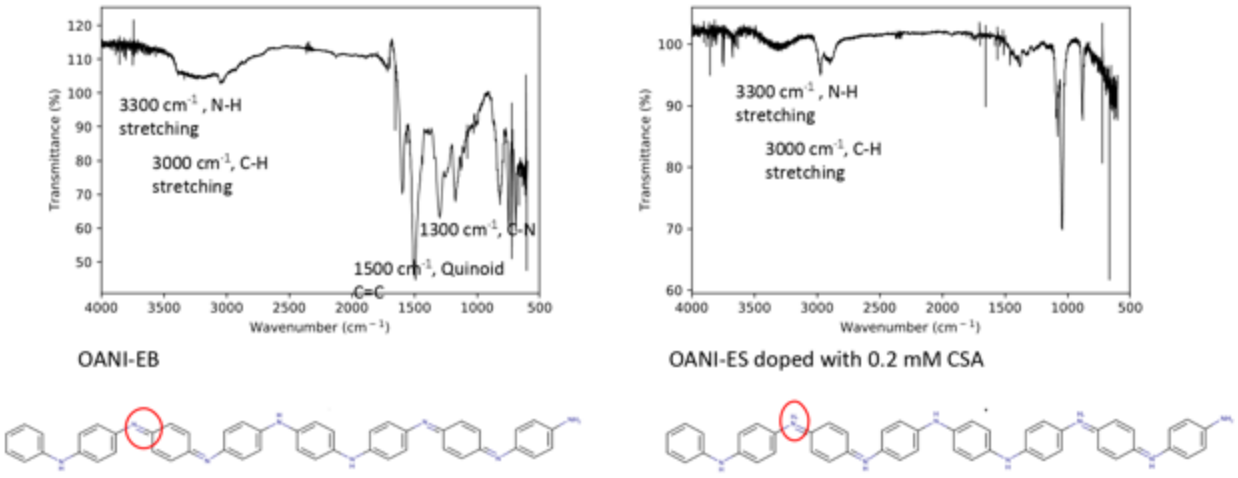

Figure 3-12. FT-IR spectra of **a)** OANI-EB and **b)** OANI-ES doped with 0.2 mM CSA.

3.3.5 Crystalizing Phenyl/Amine-Capped OANI

2 mg of OANI was dissolved in 1 mL of ethanol and 1.0 M HCl was added to give a final dopant concentration of 0.1 M and 1.0 M. The solution was left undisturbed for 7 days. Initially, both the 0.1 M and 1.0 M OANI solutions turned a dark green and had small particle chunks at the bottom of the vial, indicating OANI in the ES state. However, after 6 hours, the solution started to lose its dark green color and after 24 hours the solutions were both violet. After 7 days, the small particles chunks in solution looked even smaller and more like fine particles (**Figure 13**).

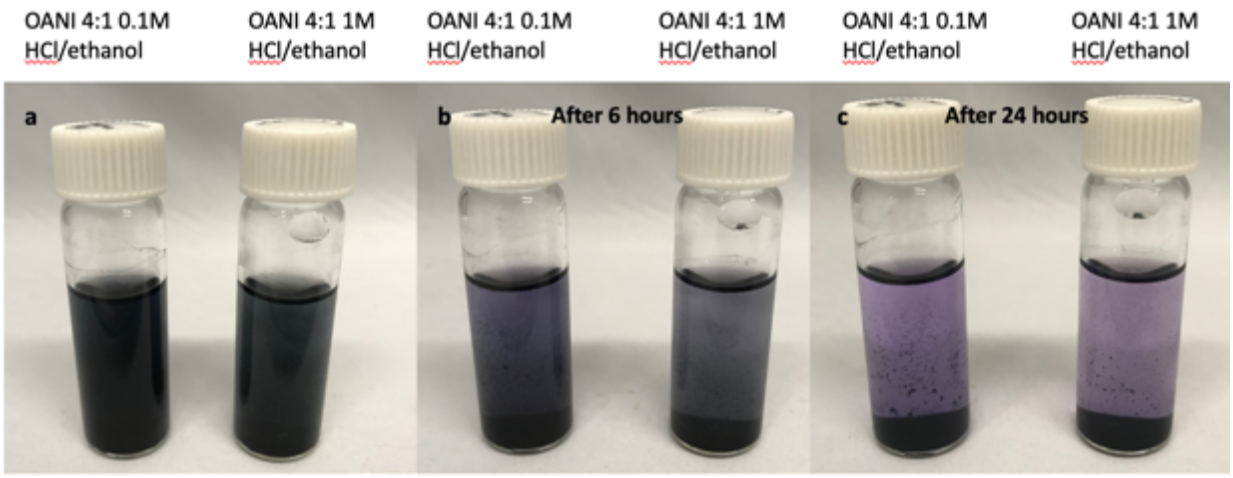

Figure 3-13. OANI doped in HCl in a 4:1 mixture of 0.1M HCl/ethanol and 4:1 1.0 M HCl/ethanol mixture: **a)** initial; **b)** after 6 hours; and **c)** after 24 hours.

3.3.6 Crystalizing Phenyl/Amine-Capped OANI Assisted by Sonification

2 mg of OANI was added to 5 mL of 0.1 M HCl and 1.0 M HCl. The solutions were sonicated for 4 minutes and then left undisturbed for 7 days (**Figure 14**). Initially, once OANI was added to the acidic media, the chunky OANI particles floated to the top and did not disperse into the HCl (OANI is not soluble in water). After being sonicated for 4 minutes, the 1.0 M HCl vial had some fine particles and the solvent turned a light green/blue and after 24 hours there was even more growth of fine particles and a deeper green/blue color. The 0.1 M vial looked unchanged after sonication and also after leaving it undisturbed for 7 days.

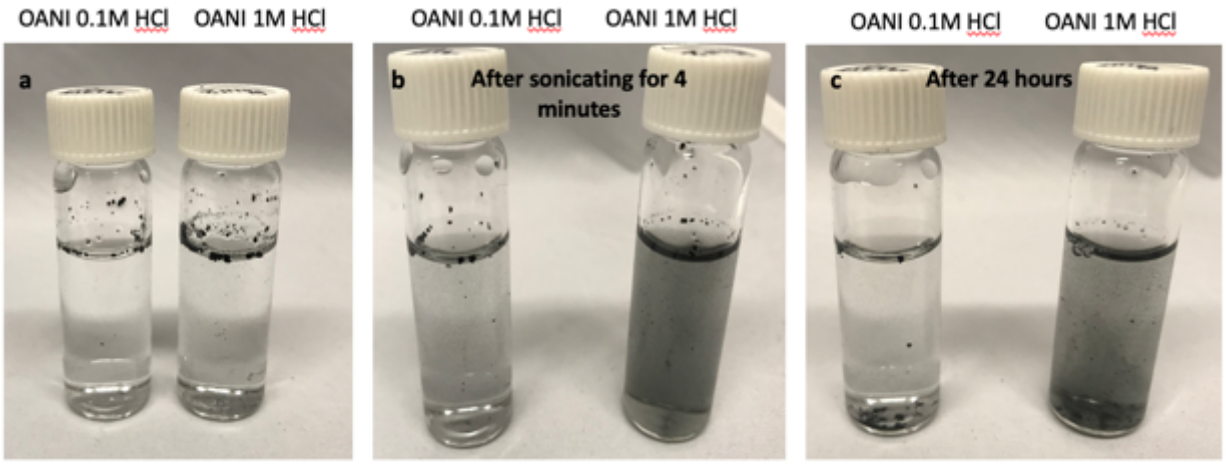

Figure 3-14. OANI doped in HCl in 0.1 M and 1.0 M HCl: **a)** initial; **b)** after sonicating for 4 minutes; and **c)** after 24 hours.

3.3.7 Scanning Electron Microscopy (SEM)

Samples under crystallization conditions were subjected to dialysis for 4 hours to remove excess HCl and the samples were then drop-cast onto a silicon wafer. SEM images of the samples subjected to crystallizing conditions show little change in morphology when compared to the bulk powder of OANI for these crystallization conditions (**Figures 15-18**). We will continue to monitor the samples for additional time and also consider different conditions. By combining the observations obtained from UV-Vis, we hope to explore the self-assembly process of the phenyl/amine octamer using different conditions and different dopants.

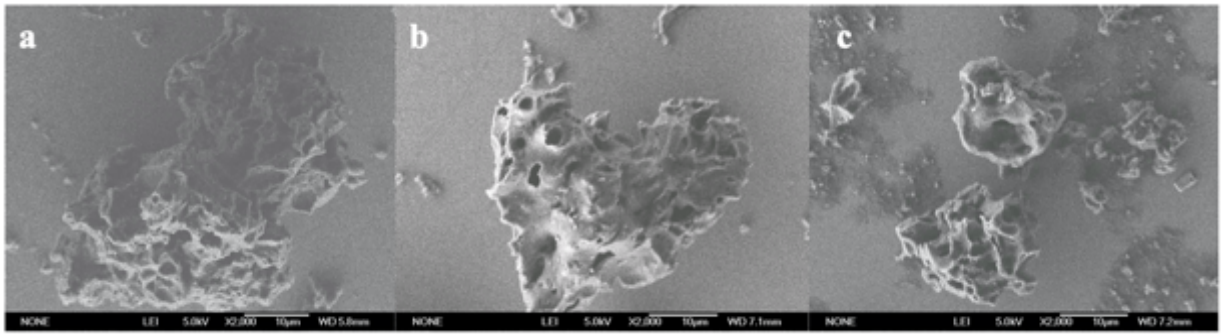

Figure 3-15. SEM of **a)** purified OANI; **b)** 1.0 M HCl after 7 days; and **c)** 1.0 M HCl in ethanol after 7 days.

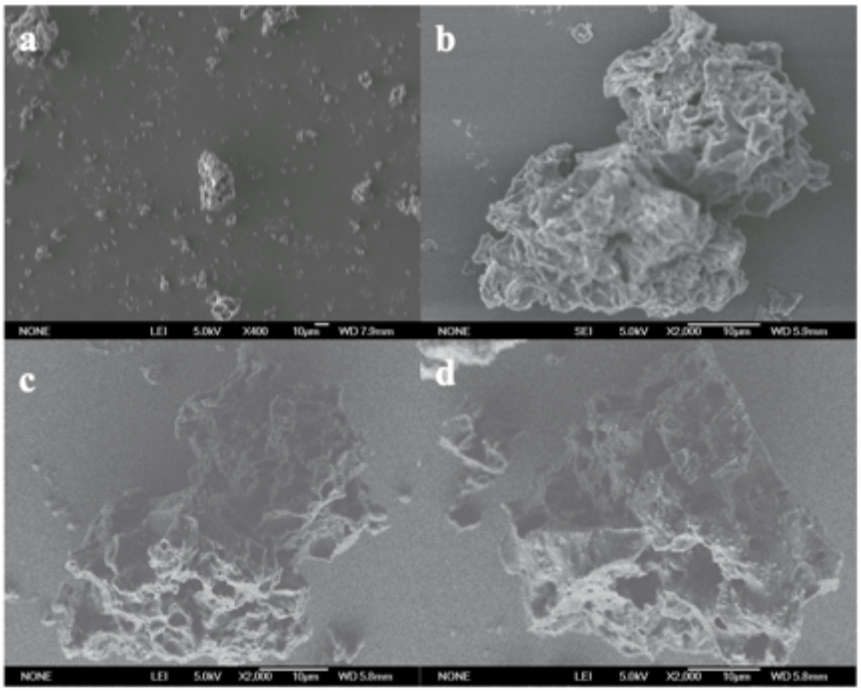

Figure 3-16. SEM of; **a)** purified OANI; **b)** 1.0 M HCl after 7 days; **c)** 1.0 M in ethanol after 7 days; **d)** 1.0 M in ethanol after 7 days.

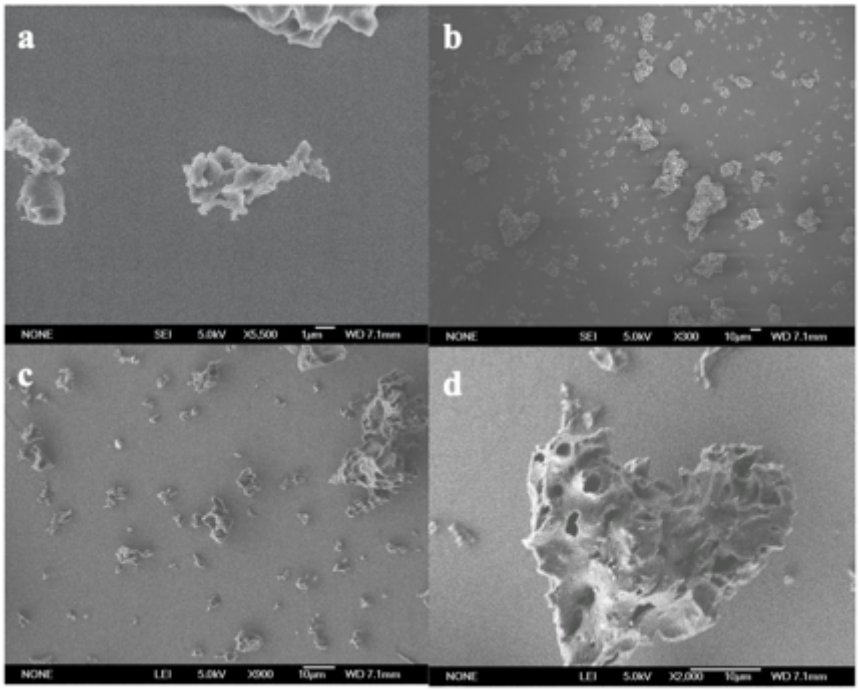

Figure 3-17. SEM of; **a-d)** 1.0 M HCl 7 days at different magnifications.

3.4 Conclusions

The octamer of aniline is a simple small molecule that can be easily synthesized with a variety of methods. The octamer can be easily purified Soxhlet extractor method with a 1:1 ratio of cyclohexane/acetone to obtain a pure compound. The solubility of OANI is very similar to that of TANI which shows its promise in its use in a variety of applications. Longer term experiments are needed to produce crystals for measuring potentially increased conductivity relative to the tetramer.

3.5 References

(1) Baker, C. O.; Huang, X.; Nelson, W.; Kaner, R. B. Polyaniline Nanofibers: Broadening Applications for Conducting Polymers. *Chem. Soc. Rev.* **2017**, *46*, 1510–1525.

(2) Louis, H.; Magu, T. O. *A Review on Conducting Polymers-Based Composites for Energy Storage Application*; 2019; Vol. 1.

(3) Shirakawa, H.; Louis, E. J.; MacDiarmid, A. G.; Chiang, C. K.; Heeger, A. J. *Synthesis of Electrically Conducting Organic Polymers: Halogen Derivatives of Polyacetylene, (CH)X*; 1977.

(4) Nezakati, T.; Seifalian, A.; Tan, A.; Seifalian, A. M. Conductive Polymers: Opportunities and Challenges in Biomedical Applications. *Chem. Rev.* **2018**, *118*, 6766–6843.

(5) Molapo, K. M.; Ndangili, P. M.; Ajayi, R. F.; Mbambisa, G.; Mailu, S. M.; Njomo, N.; Masikini, M.; Baker, P.; Iwuoha, E. I. *Electronics of Conjugated Polymers (I): Polyaniline*; 2012; Vol. 7.

(6) Dan, L. I.; Huang, J.; Kaner, R. B. Polyaniline Nanofibers: A Unique Polymer Nanostructure for Versatile Applications. *Acc. Chem. Res.* **2009**, *42*, 135–145.

(7) Bajpai, M.; Srivastava, R.; Dhar, R.; Tiwari, R. S. Review on Optical and Electrical Properties of Conducting Polymers. *Indian J. Mater. Sci.* **2016**, *2016*, 1–8.

(8) MacDiarmid, A. G.; Mammone, R. J.; Kaner, R. B.; Porter, S. J. The Concept of "doping" of Conducting Polymers: The Role of Reduction Potentials. *Phil. Trans. R. Soc. A* **1985**, No. 314, 3–15.

(9) Toušek, J.; Toušková, J.; Chomutová, R.; Křivka, I.; Hajná, M.; Stejskal, J. Mobility of Holes and Polarons in Polyaniline Films Assessed by Frequency-Dependent Impedance and Charge Extraction by Linearly Increasing Voltage. *Synth. Met.* **2017**, *234*, 161–165.

(10) Kausar, A. Review on Structure , Properties and Appliance of Essential Conjugated Polymers. *Am. J. Polym. Sci. Eng.* **2016**, *4*, 91–102.

(11) Tran, H. D.; D'Arcy, J. M.; Wang, Y.; Beltramo, P. J.; Strong, V. A.; Kaner, R. B. The Oxidation of Aniline to Produce "Polyaniline": A Process Yielding Many Different Nanoscale Structures. *J. Mater. Chem.* **2011**, *21*, 3534–3550.

(12) Tran, H. D.; Li, D.; Kaner, R. B. One-Dimensional Conducting Polymer Nanostructures: Bulk Synthesis and Applications. *Adv. Mater.* **2009**, *21*, 1487–1499.

(13) Wang, Y.; Liu, J.; Tran, H. D.; Mecklenburg, M.; Guan, X. N.; Stieg, A. Z.; Regan, B. C.; Martin, D. C.; Kaner, R. B. Morphological and Dimensional Control via Hierarchical Assembly of Doped Oligoaniline Single Crystals. *J. Am. Chem. Soc.* **2012**, *134*, 9251–9262.

(14) Miras, M. C.; Acevedo, D. F.; Monge, N.; Frontera, E.; Rivarola, C. R.; Barbero, C. A. *Organic Chemistry of Polyanilines: Tailoring Properties to Technological Applications*; 2008; Vol. 1.

(15) Wei, Y.; Hsueh, K. F.; Jang2, G.-W. *A Study of Leucoemeraldine and the Effect of Redox Reactions on the Molecular Weight of Chemically Prepared Polyaniline*; 1994; Vol. 27.

(16) Acevedo, D. F.; Salavagione, H. J.; Miras, M. C.; Barbero, C. A. *Synthesis, Properties and Aplications of Functionalized Polyanilines*; 2005; Vol. 16.

(17) Mills, B. M.; Shao, Z.; Flynn, S. R.; Rannou, P.; Lindsay, D. M.; Fey, N.; Faul, C. F. J. Tipping the Polaron-Bipolaron Balance: Concentration and Spin Effects in Doped Oligo(Aniline)s Observed by UV-Vis-NIR and TD-DFT. *Mol. Syst. Des. Eng.* **2019**, *4*, 103–109.

(18) Vaschetto, M. E.; Retamal, B. A. *Substituents Effect on the Electronic Properties of Aniline and Oligoanilines*; 1997; Vol. 101.

(19) Wang, Y.; Tran, H. D.; Kaner, R. B. Applications of Oligomers for Nanostructured Conducting Polymers. *Macromol. Rapid Commun.* **2011**, *32*, 35–49.

(20) Lyu, W.; Feng, J.; Yan, W.; Faul, C. F. Self-Assembly of Tetra(Aniline) Nanowires in Acidic Aqueous Media with Ultrasonic Irradiation †. *J. Mater. Chem. C* **2015**, *3*, 11945.

(21) Wei, Z.; Faul, C. F. J. Aniline Oligomers - Architecture, Function and New Opportunities for Nanostructured Materials. *Macromol. Rapid Commun.* **2008**, *29*, 280–292.

(22) Wang, Y.; Liu, J.; Tran, H. D.; Mecklenburg, M.; Guan, X. N.; Stieg, A. Z.; Regan, B. C.; Martin, D. C.; Kaner, R. B. Morphological and Dimensional Control via Hierarchical Assembly of Doped Oligoaniline Single Crystals. *J. Am. Chem. Soc.* **2012**, *134*, 9251–9262.

(23) Zhang, W. J.; Fen, J.; Macdiarmida, A. G. *Synthesis of Oligomeric Anilines*; 1997; Vol. 84.

(24) Javadi, H. H. S.; Treat, S. P.; Ginder, J. M.; Wolf, J. F.; Epstein, A. J. Aniline Tetramers: Comparison with Aniline Octamer and Polyaniline. *J. Phys. Chem. Solids* **1990**, *51*, 107–112.

(25) "Dirksen, J. A.; Ring, T. A. . Fundamentals of Crystallization: Kinetic Effects on Particle Size Distributions and Morphology. *Chem. Eng. Sci.* **1991**, *46*, 2389–2427.

CHAPTER 4. PFPA-Copolymers on Nanofiltration Membranes

Reprinted (adapted) with permission from (Aguilar, S.; Bustillio, S.; Xue, S.; Ji, C.; Rao, E.; Mak, W.H.; McVerry, B.T.; Callagon La Plante, E.; Simonetti, D.; Sant, G.; Kaner, R.B. "Enhancing polyvalent cation rejection using perfluorophenylazide-grafted-copolymer membrane coatings" *ACS Applied Materials and Interfaces,* 2020).

4.1 Introduction

4.1.1 Water Shortage

Global water shortage is one of the most serious challenges we face today.[1] Over one-third of the world's population lives in a water scarce country and this figure is predicted to rise by nearly two-thirds by 2025.[1,2] Nanofiltration (NF) has a separation effectiveness between reverse osmosis (RO) and ultrafiltration (UF), resulting in the ability to separate multivalent ions for water softening.[3] NF has many advantages over RO specifically because of its lower operating pressure, high retention of multivalent ions, high flux, and smaller energy consumption (1.0 – 2.2 kWh/m^3 for NF[4] and 2.5 – 4.0 kWh/m^3 for RO[4,5]).[3] NF membranes with low maintenance costs, 0.25 – 0.40 \$/m^3, can be used to treat ground, surface, and waste water or for pretreatment for desalination.[6] The membranes used are typically composed of polymeric materials and composites.[7] Polymeric materials find use in a variety of applications including: biomedical, electronics, biosensors and water treatment.[8–10] Covalent functionalization of these materials provides an effective means to adjust surface properties or to introduce steric or electrostatically stabilizing moieties. These covalent approaches are generally superior to non-covalent alternatives because they create stable attachment of groups with specific functional properties.[11] Surface grafting is one method of altering the chemical composition of the surface of a polymeric material without causing dramatic

morphological changes.[12] Either "grafted-to" or "grafted-from" can be achieved with end-functionalized polymer chains.[11] The grafting-to technique involves the synthesis of a polymer with a reactive end group that gets attached to the surface of a substrate, while grafting-from involves *in situ* polymerization of the monomer directly onto the surface of the substrate.[13] Grafting-to enables control over the molecular weight of the polymer enabling a low degree of grafting, which can be beneficial if a high degree of grafting can negatively impact the performance of the material being grafted. In contrast, grafting-from generally leads to a high degree of grafting.[11]

4.1.2 Grafting Techniques

Common grafting techniques include chemical grafting, ozone treatment, plasma treatment, gamma rays and UV irradiation.[11] Photo-initiated grafting can be performed under mild reaction conditions and low temperatures with high selectivity compared to other grafting techniques. Perfluorophenylazide (PFPA) chemistry has been used as a coupling agent for fluorinated phenylazide, which is capable of forming stable covalent bonds to sp^2 or sp^3 hybridized carbons or nitrogens.[13,14] Phenylazides are popular because they are simple to prepare, have fast kinetics, possess high reaction efficiencies, are easy to store and can covalently link organic or inorganic materials.[11,15] Functionalized PFPAs are particularly useful because they act as hetero-bifunctional coupling agents by bringing together molecules and materials via two reactive centers.[16] These materials include polymers, semiconductor surfaces, metals, carbon materials and metal oxide surfaces.[13,15] Phenylazide's photochemistry involves elimination of N_2 to give a singlet phenylnitrene; the process is initiated by light, heat or electrons within minutes.[16] Light activation of the PFPA is highly chemoselective, wherein only the photosensitive moieties (i.e., $-N_3$, azide) are activated and the rest of the structure is unaffected. The singlet phenylnitrene that is formed

upon light activation is a highly reactive intermediate that can undergo NH insertion (e.g., with polyamides), creating a covalent bond.[13] PFPA activation is fast and non-destructive, making it an ideal monomer for polymerization/grafting, while allowing precise control over the degree of grafting.

One possible material to alter via photo-grafting is a typical nanofiltration (NF) membrane which consist of polyamides that are negatively charged. With negatively charged membranes, the rejection mechanism is governed by steric effects (size exclusion), electrostatic effects (Donnan exclusion), and dielectric exclusion. NF is commonly used in water treatment on account of its ability to achieve a high rejection of polyvalent (as compared to monovalent) ions[1,17] However, NF membrane (ion) rejection decreases dramatically with salinity.[18,19] The lack of precise control during the industrial production of commercial membranes can cause a dramatic loss in solute retention.[3] Therefore, it is often sought to alter the surface electrostatic charge of a membrane to improve its rejection of different solutes by altering the functional groups and charge on the membrane's surface and also relying on dielectric exclusion.[20–22] Rather than apply temporarily ionized functional groups, it would be more beneficial to add fixed charges onto the membrane surface, for example, by application of a zwitterion. Zwitterions are believed to improve the hydrophilicity of membranes based on their ability to strongly attract and bind water molecules via electrostatic interactions.[23] Although zwitterions have shown promise for their high salt rejection capabilities,[24] the mechanisms by which they function remain poorly understood.[25] Thus, herein we report a facile approach to graft electrostatically charged copolymers including: (i) a positively charged PFPA-quaternary ammonium (PFPA-QA), (ii) a negatively charged PFPA-

[1] The top layer of a thin film composite (TFC) membrane is a selective barrier that is responsible for the solute rejection this is achieved via: (i) aperture sieving (depending on the spacing between polymer chains), and (ii) the Donnan effect (surface charge effects). Therefore, TFC's can retain polyvalent ions due to their large(r) hydrated size and charge, while permeating ions with a low(er) charge.

sulfonate (PFPA-S), and (iii) a near neutral PFPA-zwitterion (PFPA-Z) onto commercial NF membranes using phenylazide photochemistry. The goal is to develop polyamide NF membranes with charged functional groups that increase their ability for the rejection of divalent ions; and to explore the mechanism behind polyvalent ion rejection.

4.2 Experimental

4.2.1 Materials and Methods

Materials: [2-acrylamido-2-methyl-1-propanesulfonic acid, (3-acrylamidopropyl)trimethylammonium chloride, dimethylformamide (DMF), and chloroform were purchased from Sigma Aldrich. 99% calcium chloride ($CaCl_2 \cdot 2H_2O$), 99% sodium chloride (NaCl), 99% sodium sulfate (Na_2SO_4), 99% sodium carbonate (Na_2CO_3), 99% magnesium chloride ($MgCl_2$), 99% potassium chloride (KCl), 99% lithium chloride (LiCl), 99% aluminum chloride ($AlCl_3$), 99% chromium chloride ($CrCl_3$), sodium phosphate (Na_3PO_4) were obtained from Fisher Chemicals. N-(4-azido-2,3,5,6 tetraperfluorophenyl)sulfonamide propylmethylacylamide (PFPA-monomer) was purchased from Hydrophilix Inc. All solvents and chemicals were used as received unless stated otherwise. DOW FILMTEC™ Commercial NF90, molecular weight cut off (MWCO) 200 Da membranes and Synder Polyethersulfone (PES) Ultrafiltration membranes, MWCO 5000 Da were purchased from Sterlitech Corporation and soaked in DI-water prior to use. A CF-042 crossflow cell with an area of 42 cm^2 fitted with a Micropump was purchased from Sterlitech Corporation.

4.2.2 Synthesis and characterization of PFPA-copolymers

The PFPA-copolymers were synthesized by free radical polymerization using 2,2'-azo-bis-isobutyrylnitrile (AIBN) as a radical initiator, the PFPA monomer, and the corresponding

monomer, including: (i) [2-(methacryloyloxy)ethyl]dimethyl-(3-sulfopropyl)ammonium hydroxide (zwitterion), (ii) 2-acrylamido-2-methyl-1-propanesulfonic acid (sulfonate), and (iii) (3-acrylamidopropyl)trimethylammonium chloride (quaternary ammonium). Supporting information (SI). The copolymer synthesis description is described in the Supporting Information (Scheme S1-S3). Representative structures of these copolymers are shown in **Figure 1**. The ratios used for Comonomer:PFPA:initiator for the synthesis of the copolymers is 50:3:1 to obtain a Molecular Weight ~5,000 Da.

4.2.3 Characterization and Functionalization of Membranes

Functionalization of the polymeric membranes by surface modification was employed via surface grafting to improve the membranes' surface properties. Perfluorophenylazide photochemistry was used to create a covalent bond via N-H insertion between the polyamide membrane and the azide functional group on the PFPA-copolymers. Surface grafting allows a covalent attachment of polymer chains onto the membrane surface that avoids desorption that often occurs in other coating methods.

4.2.4 Membrane grafting with PFPA-copolymers

The commercial NF90 membranes were left to soak overnight in DI water to remove any chemicals that were added for transportation and storage. Once the membranes had been soaking, solutions of 2 mg/mL, 5 mg/mL and 10 mg/mL PFPA-copolymer in water were prepared. The PFPA-copolymer solution was then poured on top of the membrane and irradiated with a handheld UV light (254 nm) for one min. The UV-treated membranes were then rinsed with excess DI water to remove any unreacted copolymer or physically adsorbed polymer and side products, and then were left to soak in DI water until ready for use.

X-ray photo-electron spectroscopy (XPS, Kratos) was used to verify the chemical composition of the grafted polymers to ensure functionalization of copolymers with appropriate functional groups. The zeta potential of the membrane surfaces was characterized via streaming potential analyses (SurPASS, Anton Paar) to ensure the appropriate charges were on the modified surfaces.

The morphology of the membranes was characterized via scanning electron microscopy (SEM, JEOL, USA), and atomic force microscopy (AFM, Dimension ICON2-SYS, Bruker Nano Inc., USA) of before and after functionalization of membrane surface. The hydrophilicity and wettability of the membranes was characterized via contact angle goniometry. The pore size and volume of the PFPA-Z coated membrane was characterized via N_2-adsorption and Brunauer-Emmett-Teller (BET) analysis. More detailed procedures for each characterization method are noted in the Supplementary Information (SI).

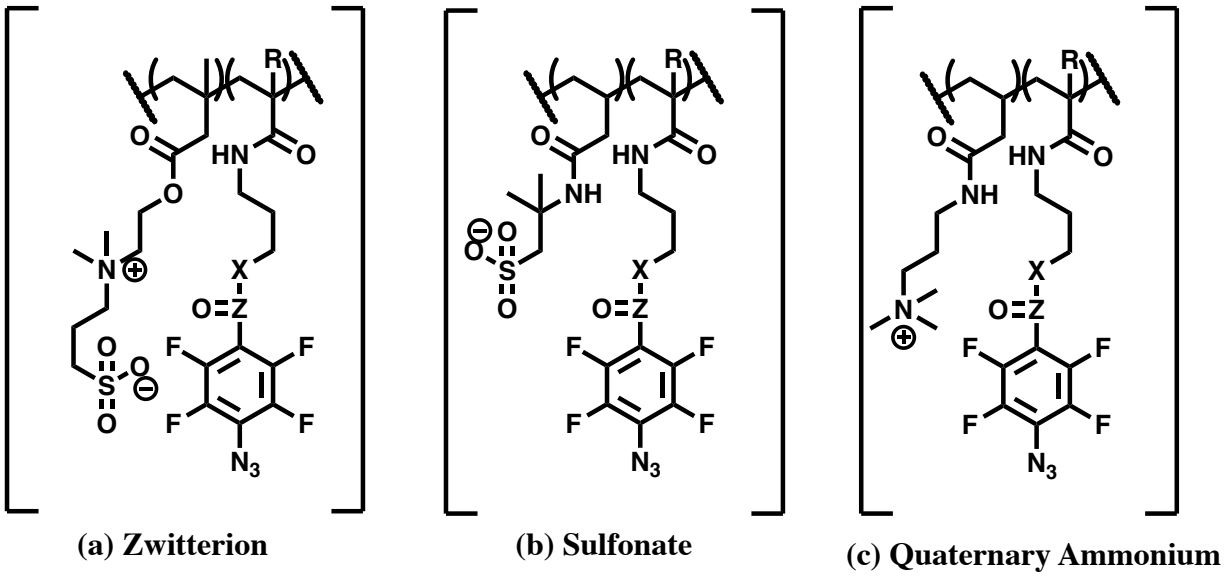

Figure 4-1. Representative structures of the perfluorophenylazide (PFPA) copolymers: **(a)** PFPA-Z (zwitterion), **(b)** PFPA-S (sulfonate), and **(c)** PFPA-QA (quarternary ammonium).

4.2.5 Cross-flow Cell and Dead-End Cell System

The NF membranes were characterized in a cross-flow cell using 5 mmol/L single-salt and mixed-salt solutions of equivalent ionic strengths unless otherwise stated. The cross-flow experiments were performed at: (a) low pressure (p = 4.8 bar), and (b) high pressure (p = 11 bar) at T = 25 ºC to account for the increase in the osmotic pressure with salt concentration. Each NF membrane was pressurized for 30 minutes using DI-water until a stable permeate flux was reached prior to introduction of the salt feed. Following each experiment, DI water was circulated for 30 minutes to clean the cross-flow cell. The concentrate flow rate was fixed at 8.5 litters per hour. The NF membranes were also examined using a dead-end filtration cell using 300 mL of a 10

mmol/L salt solution (p = 4.8 bar, T = 20 ºC). Herein, the feed solution was stirred at 18.33 Hz to minimize concentration polarization. The duration of the dead-end cell experiment was 6 hours. Designs for both experimental setups are shown in **Figure S1**.

4.2.6 Sample preparation and data analysis

All of the salts were dried for one hour at 70 °C prior to being used to create appropriate solutions. Solution samples were taken every 30 minutes from the feed and retentate streams for cross-flow cell experiments and filtered through 0.2 μm filters. The filtrate was then diluted in a 5% HNO_3 (v/v) matrix for Inductively Coupled Plasma-Optical Emission Spectroscopy (ICP-OES) analysis. The 5% HNO_3 matrix was made by diluting 70% HNO_3 with DI water. Prior to analysis, the ICP-OES was calibrated over ranges of relevance to the ions of interest using analytical-grade multi-ion standards. The extent of salt rejection (R, %) was calculated as follows: $R = 100\left[1 - \frac{C_p}{C_f}\right]$, where C_p and C_f are the concentrations (mmol/L) of the permeate and the feed solutions, respectively.

4.3 Results and Discussion

4.3.1 Membrane characterization

The surface elemental analysis of the PFPA-copolymer modified membranes was quantified and compared to the pristine NF90 membrane surface using X-ray photoelectron spectroscopy (XPS). The elemental compositions of the native and modified membranes show a distinct difference (**Fig. S2**) confirming the photo-grafting of the copolymers onto the polyamide membrane. The polyamide NF90 membrane shows binding energies of C at 290 eV, N at 400 eV, and O at 540 eV. The S_{2s} at 240 eV and S_{2p} at 190 eV on the NF90 are associated with the

polysulfone in the active layer.[26] The PFPA-Z, PFPA-S, and PFPA-QA all show a new fluorine peak. Fluorine is sensitively probed by XPS with the modified copolymers exhibiting a fluorine peak (F_{1s}) at 688 eV, indicating NH insertion onto the surface of the polyamide membrane as seen in **Figure S2**. The sulfonate (S_{2p}) peak at 180 eV on the PFPA-Z and PFPA-S correspond to the sulfonate groups, while the quaternary ammonium (N_{1s}) peak at 400 eV are verified on the PFPA-Z and PFPA-QA spectra.

Table 4-1. The surface properties of the native and PFPA-copolymer coated membrane surfaces.

Membrane	**Mean Roughness (S_a) (nm)**	**Contact Angle**
NF90	79.2±9	61±4º
PFPA-S	44.7±8	43±5º
PFPA-QA	37.3±9	34±3º
PFPA-Z	34.7±8	36±3º

Atomic force microscopy (AFM) of the native and modified membranes was used to ascertain the effects of membrane modification. The surface roughness of a membrane is important because it correlates with the total surface area with which ions may interact thus affecting the wettability of the material and the contact angle. Typically, when surface roughness decreases from modification, the wettability depends on the degree of wettability of the now smoother

material, indicating that roughness has a strong influence on wettability.[27,28] **Table 1** shows that the native NF90 membrane has a mean roughness (S_a) of 79.2±9 nm, while, in general, the modified membranes show a reduction in mean surface roughness of nearly 50%. PFPA-Z and PFPA-QA membranes feature a similar decrease in surface roughness as compared to the native NF90 and PFPA-S membranes. The surface roughness decrease signifies that the coating smooths the surface to create a more uniform membrane. A lower surface roughness may suggest a more hydrophilic character, due to a reduced propensity for Wenzel ("air trapping") effects, although hydrophilicity may be also be imposed by surface functional groups.[29,30] Therefore, contact angle measurements were used to assess the increase in surface hydrophilicity and wettability induced by grafting. The native NF90 membranes show a contact angle of 61±4º because the carboxylic and amine groups on their surfaces offer some potential for interaction with water via hydrogen bonding allowing for more wettability. The copolymer-modified membranes showed a much more wettability and hydrophilic character than the PFPA-S, PFPA-Z and PFPA-QA coatings producing contact angles of 43±5º, 36±3º, and 34±3º, respectively (**Table 1** and **Figs. S3b-d**). The PFPA-QA and PFPA-Z are postulated to produce the lowest contact angles because: (i) the quaternary ammonium cations (QAs) have polarity and possess two fixed water molecules of hydration, thus forming a hydration layer,[21,31] and (ii) the zwitterion sulfobetaine possesses six fixed water molecules around the QAs and the sulfonate thereby producing a more robust hydration layer that leads to a further reduced contact angle.[32,33]

The morphology of the native NF90 and the modified membranes following grafting (**Fig. S3**, middle) was examined via SEM. Generally speaking, there is no obvious change in the cross-sectional SEM images because the coating is applied only on the very near-surface region of the membrane (**Fig. S4**). It is observed that the native NF90 membrane has a rough surface as

compared to the modified membranes wherein a smooth polymer layer was produced on their surfaces (**Figs. S3c,d**, middle). Qualitatively, the PFPA-Z membrane shows the most obvious modification with a much smoother surface than the native membrane (**Figs. S3a,b**, middle). The zwitterion likely partially agglomerated in the aqueous solution during photo-grafting resulting in a non-uniform modification.[34,35]

To better understand how PFPA-Z grafting affected the surface attributes, pore size, and structure of the membranes, N_2-adsorption and BET analysis were used. Herein, the degree of grafting of PFPA-Z was varied using 2, 5 and 10 mg/mL of copolymer **(Table S1).** The lowest grafted amount of PFPA-Z produced a surface area of 32.2 m^2/g and a well-defined 1.7 nm micropore diameter. This indicates that the pore structure of polypiperazine-amide is still open after a slight surface modification because NF90 membranes typically feature a pore size of ~1 nm.[3] Interestingly, while the adsorption branch of 2-PFPA-Z exhibits substantial adsorption in the low-pressure range for P/P_0 from 0 to 0.4 (**Fig. S5a**); with increasing grafting, the 5-PFPA-Z and 10-PFPA-Z modifications only produce significant N_2 adsorption after $P/P_0 = 0.9$, which is considered to be macropore range. In turn, the 5-PFPA-Z and 10-PFPA-Z modifications result in a surface area of 7.56 m^2/g STP for the former and an almost nonporous structure for the latter (**Figs. S5c,d**). This indicates that the grafted polymer blocks the pore structure of the polypiperazine-amide resulting in a lower permeability and flux for the 5 and 10 mg/mL grafted PFPA-Zs.

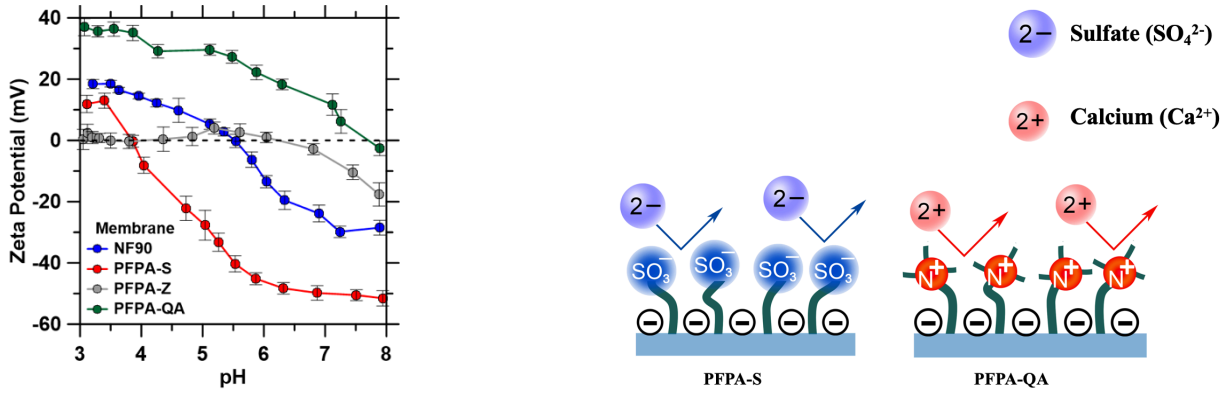

(a) **(b)**

Figure 4-2. (a) The zeta potential of the PFPA-copolymer coated membranes from acidic to mildly alkaline conditions (pH 3-8). (b) Positively and negatively charged membranes induce electrostatic repulsion thereby offering a basis to reject similarly charged ions.

A membrane's zeta potential (an indicator of surface charge) is influential in inducing Donnan exclusion effects, and is dictated by the functional groups present on the surface (see **Figure 2**). The surface charge originates from the pH dependent dissociation of ionic groups at the solid-solution interface.[12,22] Thus, Coulombic interactions between the membrane and ions affect transport of charged species through the membrane.[36] Neutral species interact with the membrane charge mostly through polarity effects; although steric effects affect the transport of both charged and uncharged species through the membrane.[11] Membrane charge influences the permeation of ions through NF membranes, because ions of increasing valence can be increasingly repelled by the electrostatic field of functional groups on the membrane surfaces.[22] The positively and negatively charged membranes therefore induce electrostatic repulsion to reject similarly charged ions. Thus, it may be anticipated that, all other parameters remaining fixed. A charged surface

may offer better rejection of ions than a neutral surface although divalent ion rejection is often noted to depend on the reversal of surface charges from either negative to positive or to a near neutral charge. The native NF90 features negative charge in circumneutral and alkaline environments (see **Figure 2**). Indeed, at pH 7, the zeta potential of the NF90 membrane and the PFPA-S modified membranes were -25 mV and -49 mV, respectively. The zeta potential of both membranes decreased with increasing pH due to the deprotonation of the carboxylic acid in the NF90 membrane and the sulfonate in the PFPA-S modified membrane. The zeta potential of the native NF90 membrane indicates that the carboxylic acid group within this membrane describes its electrokinetic behavior. On the other hand, for the PFPA-S coated membranes, the sulfonic acid groups ($-SO_3^-$) are strongly acidic and dissociate over the pH range considered. This dissociation explains the high surface charge density which will produce a high affinity for cations, and electronegative oxygen atoms in the water molecules. The PFPA-QA coated membrane features a zeta potential of +11 mV at pH 7; suggesting superior capacity for the rejection of positively charged cations (**Fig. 1c**). Interestingly, the PFPA-Z coating shows an isoelectric point (IEP) at pH 6.2 and a near-zero zeta potential from pH 3-6 which suggests an effectively uncharged membrane surface over this pH range (**Fig. 2**). This suggests that in effect, the positively charged quaternary ammonium group and the negatively charged sulfonate group, neutralize each other, when considered in the context of surface charge. With increasing pH, the membrane assumes a slight net negative charge indicating that the negative charge on the sulfonate is deprotonated in solution and can interact slightly more than the quaternary ammonium. Importantly however, the near-zero zeta potential may suggest that the PFPA-Z coating is likely to produce (ion) rejection on account of size exclusion rather than Coulombic effects in typical applications (i.e., pH < 8; see **Fig. 5c**).

4.3.2 Single salt rejection of modified membranes

Dead-end cell and Cross-Flow experiments were carried out to establish the single salt rejection behavior and Coulombic interactions of both Na_2SO_4 and $CaCl_2$ solutions, separately, for native and modified NF90 membranes (**Fig. 3**). **Figure 3** summarizes rejection performance, and permeate fluxes for compositions including: native NF90 membranes and PFPA-Z, PFPA-S and PFPA-QA coated membranes at a single grafting density of 10 mg/mL and across grafting density ranges of 3.03 - 13.86 μg/cm^2 for PFPA-Z (see **Fig. 3a,3c**). NF membranes typically have a rejection for divalent cations ranging from 75-to-90% and 80-to-90% for divalent anions.[11] This range in rejection arises due to the affinity between ions in solution and functional groups on the membrane surface that determine the membrane permselectivity. The native NF90 membrane has hydrophobic, negatively charged carboxylic acid groups on its surface that produce a zeta potential of -25 mV at pH 7 (**Fig. 2**). The negatively charged membrane will attract Na^+ ions (counter-ions), while allowing Cl^- and SO_4^{2-} (co-ions) to be repelled and allowing the transport of Na^+ ions through the membrane to the permeate, allowing it to maintain electroneutrality. When electrostatic interactions mainly govern separation selectivity, meaning the negatively charged carboxylates reject divalent anions because of the strong electrostatic repulsion between the negatively charged groups, dielectric exclusion has been found to have a strong effect on rejection with confined nanopores.[11,37,38] Consequently, the rejection of SO_4^{2-} is 94%.[39] This is similar to the PFPA-S copolymer which features negatively charged sulfonate groups. However, because the PFPA-S has a larger density of sulfonate groups and a (yet) lower zeta potential of -49 mV as compared to the native NF90 membrane, the rejection of SO_4^{2-} is even higher at 98% (**Fig. 3a**). The PFPA-S modified membrane exhibits 95% Ca^{2+} rejection, as compared to the 91% rejection for the native NF90 membrane (**Fig. 3a**). While the higher rejection of SO_4^{2-} is readily explained by (enhanced)

electrostatic repulsion; the increased rejection of divalent cations is postulated to be on account of a kinetic size exclusion effect that results from the reduction in the membrane's pore size with copolymer grafting along with diffusion playing a role in transport within the pores of the membrane.[38] The higher rejection rate of Na_2SO_4 compared to that of $CaCl_2$ can also be explained due to permeate electroneutrality in ions passaging through the membrane, with a higher passage of Cl^- ions. Cl^- ions permeate more readily than SO_4^{2-} because Cl^- has less electrostatic repulsion (smaller ionic charge) and less steric hinderance (smaller ionic radius).

The PFPA-QA coated membrane shows a positive zeta potential over the pH range of 3-7. As a result, it exhibits a divalent cation rejection of 98% because of the electrostatic repulsion between the QA group and Ca^{2+}-species in solution. PFPA-QA also obtained a high rejection of SO_4^{2-}, likely due to a slight attraction from the positive charge on the ammonium with the negative charge of the sulfonate, which hinders kinetic separations along with the more hydrophilic surface. These phenomena are also seen with PFPA-S and the high rejection of Ca^{2+}.

The PFPA-Z coated membrane obtained the highest SO_4^{2-} and Ca^{2+} rejection of 98% for each salt (**Fig. 3a**).

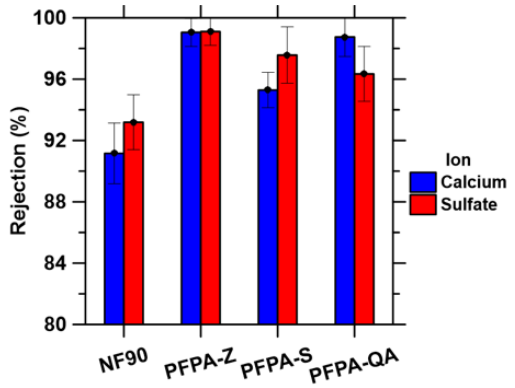

(a)

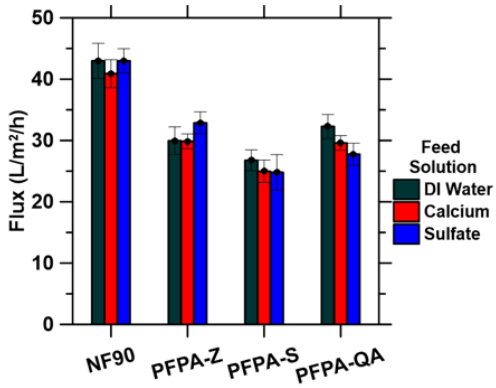

(b)

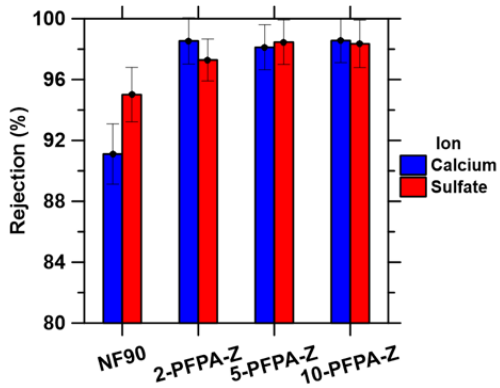

(c)

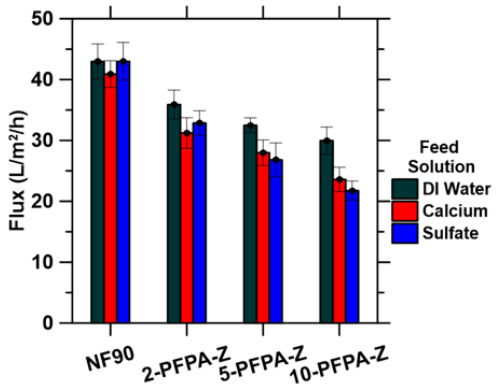

(d)

Figure 4-3. The ion rejection and permeate flux for the "10 mg/mL" PFPA-copolymers modified membranes as measuring using a dead-end cell using a feed solution consisting of 5 mM $CaCl_2$ and 5 mM Na_2SO_4 for single salt membrane **(a)** rejection and **(b)** permeate flux for $CaCl_2$ and Na_2SO_4 rejection with the different polymers. Also shown is single salt membrane performance for 5 mM $CaCl_2$ and 5 mM Na_2SO_4 **(c)** rejection, and **(d)** permeate flux for membranes grafted with different dosages of PFPA-Z.

Fig. 3b summarizes the permeate flux decline by grafting 10 mg/mL of the polymers on NF90 membranes. Ultimately, the coatings improve rejection but the flux is compromised. The

permeate flux decline was similar for all PFPA-Z, PFPA-S and PFPA-QA, with PFPA-Z having the best rejection of divalent salts; therefore, warranting more detailed study of the effects of the degree of grafting for the PFPA-Z coating. PFPA-S and PFPA-QA at lower grafting densities show an improved flux but did not improve rejection. However, the zwitterionic groups have an equal amount of cationic and anionic groups that are connected covalently and are therefore *macroscopically charge-neutral*. Zwitterions strongly hold on to water molecules via electrostatically induced hydration, thereby forming a hydration shell.[40,41] These zwitterionic hydration shells result in dense and tightly adsorbed water molecules.[23] This enhanced hydration is seen with a more hydrophilic surface, along with PFPA-QA (**Table 1**). Zwitterions can also have their polymer chains interacting with each other, thereby reducing charge screening by the ions in solution. On account of producing strong repulsions between the charges on the same chain (and ions in solution) and intramolecular repulsion between neighboring zwitterion chains, the PFPA-Z coating is able to achieve very high divalent ion rejection.[19]

Fig. 3c,d summarizes the Na_2SO_4 and $CaCl_2$ rejection and permeate flux for native NF90 and PFPA-Z coated membranes for grafting degrees of 3.03, 6.93 and 13.86 $\mu g/cm^2$ since the grafting density is an important parameter that affects permeability.[23] In general, a higher grafting density leads to greater permeation resistance and lower permeability via pore blockage, as evidenced by the N_2 adsorption data, which shows that increasing grafting reduces pore volume for pores smaller than 1.7 nm (**Fig S4**). The rejection of both Na_2SO_4 and $CaCl_2$ remained essentially constant around 98% beyond a co-polymer dosage (grafting density) of 2 mg/mL. This maximum in the separation performance indicates that, in fact, on account of the flux decrease that accompanies increasing grafting density, lower grafting densities are preferred to balance high rejection with high flux (**Fig. 3c,d**). Therefore, all further experiments were conducted at a grafting

density associated with a co-polymer dosage of 2 mg/mL. Lower grafting densities of 2 mg/mL of PFPA-S and PFPA-QA also result in improved flux, but do not enhance the rejection of divalent ions (95% and 94% rejection of SO_4^{2-} respectively; not shown). As such, while it is clear that charged membrane surfaces (NF90, PFPA-S, PFPA-QA) rely on Coulombic exclusion and dielectric exclusion to affect divalent cation rejection, it remains unclear how the (near) neutrally charged PFPA-Z coating ensures improved divalent ion rejection.

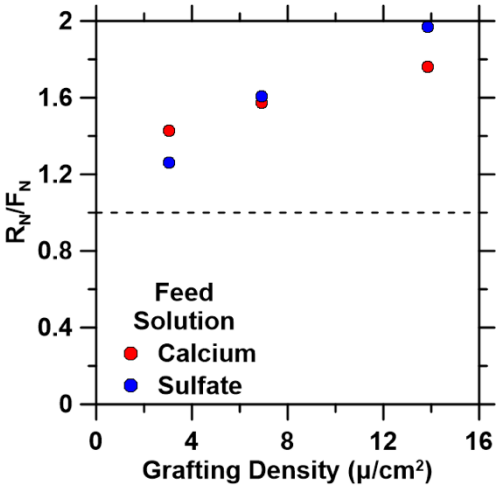

Figure 4-4. The ratio of normalized rejection to normalized flux for calcium and sulfate feed solutions as a function of the grafting density for PFPA-Z membranes.

Fig. 4 shows the ratio of normalized rejection to normalized flux (R_N/F_N) for PFPA-Z coated membranes, with respect to the performance of native NF90, as a function of varying grafting densities. Normalized ratios greater than 1 correspond to a decrease in performance of PFPA-Z membranes compared to native NF90 membranes because of significant reductions in permeate flux without a significant increase in ion rejection. The ratio R_N/F_N increases proportionally with increasing grafting density and is always larger than 1 for the grafting densities examined in this study. These results suggest that the improvement in rejection is not sufficient to

overcome the reduction in flux for NF90 membranes. PFPA-Z grafting should alternatively be performed on NF membranes that show smaller cation rejections but a larger permeate flux compared to NF90 membranes.

4.3.3 Effect of salt concentrations on membrane performance in a mixed salt solution

Treating high salinity wastes can present issues for membranes because rejections typically decrease with increasing ionic strength of the feed. Thus, the rejection performance of the PFPA-Z coating was examined for $CaCl_2$ solutions with ionic strengths ranging from 1 mM to 1 M, where ionic strengths were altered using the addition NaCl additions. But adding a second salt, NaCl not only increases the ionic strength, it tends to screen electrostatic interactions at these high concentrations, ultimately impacting ion rejection. Furthermore, Na^+ and Cl^- ions impact the transfer of divalent ions in competition (i.e., on account of the different diffusivities of different ionic species), due to a need to maintain electroneutrality in solution.[42] The screening of electrostatic interactions is observed with a decrease of Ca^{2+} rejection in the high ionic strength system (Fig. 5a). In general, Ca^{2+} ions in a mixed salt solution are more effective in charge neutralization and screening of the membranes functional groups (carbonyl groups for NF90, and quaternary ammonium and sulfonate groups in PFPA-Z) as compared to Na^+ in single salt systems, resulting in a decrease in Cl^- rejection. Under mixed salt conditions, the decrease in Na^+ rejection is due to maintaining electroneutrality of the permeate solution. The lower rejection of monovalent ions in the mixed salt system is due to the effectiveness of electrostatic repulsion of Cl^- revealing the importance of Donnan exclusion in salt mixtures rejections.[42] Therefore, typically the rejection of single salt systems decreases with an increase of salt concentration. In a mixed salt system, typically the electrostatic effect is therefore the major factor involved in separation in low salt concentrations, while steric-hindrance is typically the major factor at high salt concentrations.

Because of this, the rejection mechanism is mixed-salt systems in complex due to the different forces that can partake in the rejection, compared to a single salt system. PFPA-Z showed better rejection of Ca^{2+} because of its molecular sieving rejection mechanism (i.e., diffusion playing a role in the transport within pores) compared to the native NF90 that relied mostly on steric effects. Note that PFPA-Z has a near-neutral charge on its surface.

Fig. 5 shows the effect of increasing osmotic pressure at a fixed operating pressure of 11.0 bar on calcium rejection and permeate flux. An increase in ionic strength increases the osmotic pressure and consequentially decreases the permeate flux at constant pressure. Thus, as shown earlier (see **Figure 3a,c**), in dilute solutions (i.e., wherein the ratio of osmotic pressure to operating pressure, $\pi/P < 1$), calcium rejections remain constant at around 98%. As π/P exceeds unity, both the permeate flux and cation rejection decrease; although the decrease for $\pi/P < 3$ is more pronounced for the native NF90 membrane (see **Figure 4**). It is important to note that as $\pi/P > 3$ is in effect, the native NF90 and modified membranes show similar rejection performance and flux. **Fig. 5c** shows the ratio of normalized rejections to normalized flux for the PFPA-Z membrane with respect to the performance of native NF90 at each respective π/P ratio. As previously stated, normalized ratios greater than 1 correspond to a decrease in performance of PFPA-Z membranes compared to native NF90 membranes because the increase in ion rejections are not large enough to overcome the significant reductions in the permeate flux. Here, interestingly, $R_N/F_N \approx 1$ at the largest ionic strength studied. While the reasons for this are not completely clear, we postulate that this is on account of ions being forced through the surface coating, and the rejection produced is that attributable to kinetic/size exclusion effects associated with the thickness of the native NF90 membrane.

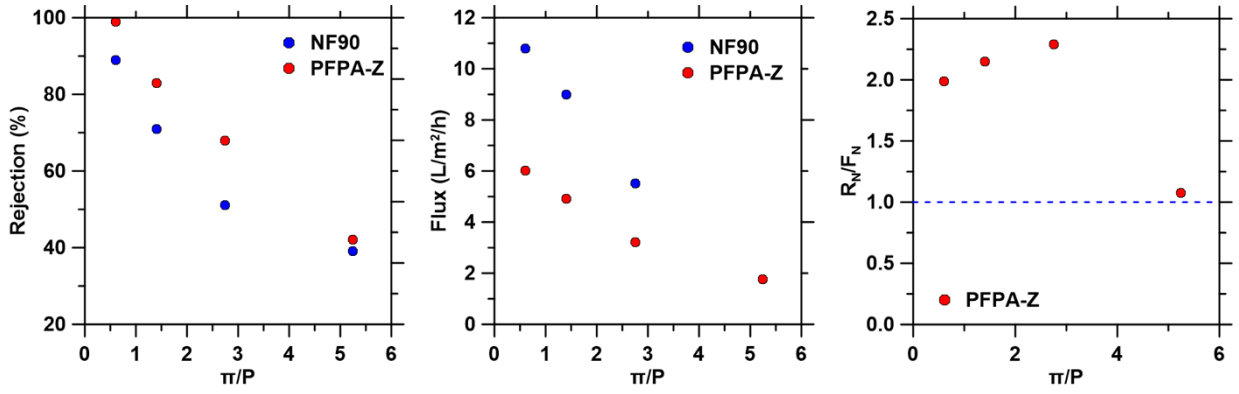

(a) **(b)** **(c)**

Figure 4-5. The effect of the ionic strength (osmotic pressure) of the feed stream on: **(a)** calcium rejection, **(b)** membrane flux, and **(c)** the ratio of normalized rejection to normalized flux across operating pressures of 11.0 bar The calcium concentration was fixed at 5 mM, while sodium (i.e., NaCl; up to 1000 mM) was used to alter the solution's osmotic pressure.

4.3.4 Aperture sieving

The rejection mechanism of zwitterion-coated membranes: Foremost, it is important to note that the native NF90 membrane is estimated to feature a pore size on the order of ~1 nm; which is much larger than the hydrated radii of typical ions (see **Figure 6** which shows that the ions with a relatively small ionic radii have higher hydration numbers and therefore larger hydrated radii).[43] Thus, from simply the perspective of size exclusion, such ions with a larger hydrated radii would be easier to remove as they hold their hydration shells more strongly. Coming back to the rejection mechanism of the PFPA-Z membrane modification, we carried out additional studies to determine if ion rejection was dependent on steric (hydrated ion radius) and/or electronic (field strength) attributes. Herein, the single salt rejection of a variety of monovalent, divalent and trivalent ions and the percentage of ions sorbed by the membrane in a static solution were used to establish the rejection mechanism (**Fig. 6**). (Pristine) NF membranes rely on both size and charge exclusion to

ensure high rejections of polyvalent anions (>90%) and comparatively lower rejections of polyvalent and monovalent cations (<90%). Herein, cations (counter-ions) are attracted, while anions (co-ions) are repelled because of the membrane's fixed charged surface. However, the PFPA-Z modified NF90 membrane presents near-neutral charge suggesting that it presents no fixed surface charges like the native NF90 membrane. Thus, at the IEP of a zwitterion, there is an overall charge balance in the polymer and the inter- and intra-chain interactions are maximized; resulting in a compact configuration.[44,45,46] A change in the pH of the solution alters (slightly) its surface charge and hence, the electrostatic interactions occurring with the ions in solution. This phenomenon has been shown to occur with a change in pH by the loss of a tightly bound hydration layer.[47] Therefore, single salts were allowed to interact with a freestanding solution of PFPA-Z to test the sequestering potential of the zwitterion without any influence of the polyamide membrane; and thereafter the rejection of the same ions was examined using PFPA-Z grafted NF membranes.

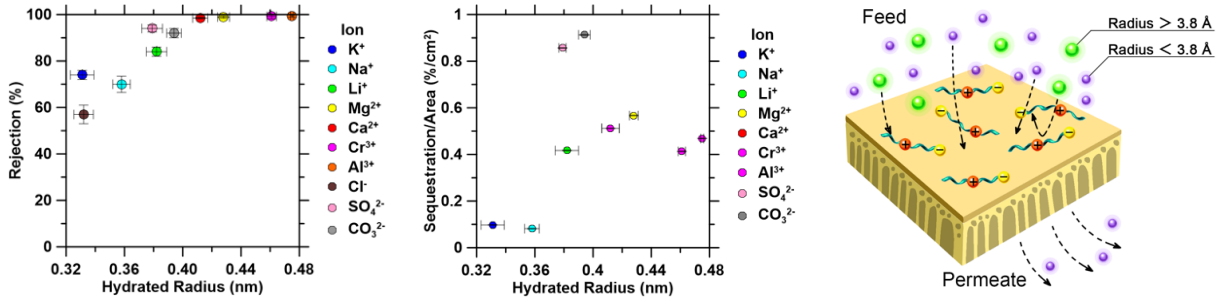

(a) **(b)** **(c)**

Figure 4-6. The behavior of PFPA-Z in dilute single-salt solutions ($\pi/P < 1$) at a concentration of 5 mM across a variety of individual salts showing: **(a)** ion rejection (i.e., ions in the permeate)

for a 2 mg/mL PFPA-Z coated NF90 membrane, and **(b)** ions that are electrosorbed by the membrane in a static solution. **(c)** An illustration of the proposed mechanism by which the macroscopically-neutral PFPA-Z coating ensures enhanced ion rejection via size exclusion and ion sequesteration.

First, it was observed that the PFPA-Z coated membrane rejects ions in relation to their hydrated radius (**Fig 6a**). In general, rejection was maximized (>90%) for hydrated radii greater than 0.38 nm, while for smaller hydrated radii, rejection varied approximately linearly with solvated ion radius. Interestingly, ions with a solvated radius >0.40 nm achieved nearly 100% rejection. Second, the amounts of ions sequestered did not show a dependence on size; although generally speaking, polyvalent ions featured higher levels of sequestration than univalent species (**Fig 6b**). Thus, it appears as though a combination of sequestration (a secondary effect), and size exclusion effects (the primary effect) which influences the kinetics of ion rejection (separation) explain why the neutral-zwitterion coated membrane, in spite of its lack of surface charge, is able to achieve excellent ion rejection performance (**Fig 6c**). Obtaining high rejections of both anions and cations also indicates the importance that diffusion plays in the separation of multivalent ions transporting within the pores of the grafted PFPA-Z membrane.[38] It should additionally be noted that the rejection of the PFPA-Z membrane appears to be especially sensitive in the 0.38-0.41 nm range of hydrated radii (**Fig. S6)**. Specifically, Li^+ has a hydrated radius of 0.38 nm and 17% of these ions sequester into the zwitterion (83% rejection), attributing to its respectable rejection of 85% via size exclusion and its being sequestered by the zwitterion. This range is believed to be relevant because it is on the order of the distance between the methylene groups in the zwitterion, which are responsible for sequestration of cations.[48] Significantly, this indicates that zwitterionic polymers could be *fine-tuned* to reject different ions based on ion-solvated size by elongating or

shortening the hydrocarbon chain in the polymer.[48] This approach could find use across a wide range of applications wherein ion separations are industrially required or desirable.

4.4 Summary and conclusions

Charged copolymers were grafted onto NF membranes to alter the properties of the membranes. Compared to a commercial (*pristine*) NF90 membrane, the modified membranes showed altered surface charges, lower surface roughness, lower pore size, and substantially improved performance in terms polyvalent ion rejection. It was established that high rejection of polyvalent ions can be successfully achieved by altering the charge on the membrane surface, making the membrane more hydrophilic and reducing the membrane pore size from porous to nonporous. The increase in ion rejection between the NF90 membrane, PFPA-S and PFPA-QA rely heavily on electrostatic repulsion and dielectric exclusion between the functional groups and the ions in a single salt system. Significantly, and in contrast to typical Donnan effects, the rejection mechanism of PFPA-Z coatings relies on aperture sieving of the compact polymer via a size exclusion mechanism. Thus, the PFPA-Z traps polyvalent ions while letting the mono-valent ions pass through the membrane. Lower loadings of the PFPA-Z modified membrane demonstrate superior rejection of polyvalent cations, while increasing the flux compared to larger grafting doses. PFPA-Z coated membrane performance was also evaluated at high ionic strengths wherein these membranes show substantially higher rejection than native NF90 membranes. The observations indicate that zwitterion grafting is especially well-suited for NF membranes that display low divalent cation rejections (<60%) but larger permeate flux than NF90 membranes. Importantly, the zwitterion rejection mechanism implies that the grafting of copolymer can be altered to selectively reject ions based on hydrated radii.

4.5 References

(1) Elimelech, M.; Phillip, W. A. The Future of Seawater Desalination: Energy, Technology, and the Environment. *Science (80-.).* **2011**, *333* (6043), 712–717.

(2) Zhao, X.; Zhang, R.; Liu, Y.; He, M.; Su, Y.; Gao, C.; Jiang, Z. Antifouling Membrane Surface Construction: Chemistry Plays a Critical Role. *J. Memb. Sci.* **2018**, *551*, 145–171.

(3) Diawara, C. K. Nanofiltration Process Efficiency in Water Desalination. *Sep. Purif. Rev.* **2008**, *37* (3), 302–324.

(4) Schäfer, A. I.; Richards, B. S. Testing of a Hybrid Membrane System for Groundwater Desalination in an Australian National Park. *Desalination* **2005**, *183* (1–3), 55–62.

(5) Dashtpour, R.; Al-Zubaidy, S. N. Energy Efficient Reverse Osmosis Desalination Process. *Int. J. Environ. Sci. Dev.* **2011**, *3* (4), 339–345.

(6) Costa, A. R.; de Pinho, M. N. Performance and Cost Estimation of Nanofiltration for Surface Water Treatment in Drinking Water Production. *Desalination* **2006**, *196* (1–3), 55–65.

(7) Werber, J. R.; Osuji, C. O.; Elimelech, M. Materials for Next-Generation Desalination and Water Purification Membranes. *Nature Reviews Materials*. 2016, pp 1–15.

(8) Nedela, O.; Slepicka, P.; Švorcík, V. Surface Modification of Polymer Substrates for Biomedical Applications. *Materials (Basel).* **2017**, *10* (10), 1115.

(9) Sun, H. S.; Chiu, Y. C.; Chen, W. C. Renewable Polymeric Materials for Electronic Applications. *Polym. J.* **2017**, *49* (1), 61–73.

(10) Maitz, M. F. Applications of Synthetic Polymers in Clinical Medicine. *Biosurface and Biotribology* **2015**, *1* (3), 161–176.

(11) Rana, D.; Matsuura, T. Surface Modifications for Antifouling Membranes. *Chem. Rev.* **2010**, *110* (4), 2448–2471.

(12) Kochkodan, V. M.; Goncharuk, V. V.; Al-Khatib, L.; Levadna, T. I.; Hilal, N. Effect of the Surface Modification of Polymer Membranes on Their Microbiological Fouling. *Colloid J.* **2006**, *68* (3), 267–273.

(13) Liu, L. H.; Yan, M. Perfluorophenyl Azides: New Applications in Surface Functionalization and Nanomaterial Synthesis. *Acc. Chem. Res.* **2010**, *43* (11), 1434–1443.

(14) Brase, S.; Gil, C.; Knepper, K.; Zimmermann, V. Organic Azides: An Exploding Diversity of a Unique Class of Compounds. *Angew. Chemie Int. Ed.* **2005**, *44*, 5188–5240.

(15) Lin, C. W.; Aguilar, S.; Rao, E.; Mak, W. H.; Huang, X.; He, N.; Chen, D.; Jun, D.; Curson, P. A.; McVerry, B. T.; Kaner, R. Direct Grafting of Tetraaniline: Via Perfluorophenylazide Photochemistry to Create Antifouling, Low Bio-Adhesion Surfaces. *Chem. Sci.* **2019**, *10* (16), 4445–4457.

(16) Siegmann, K.; Inauen, J.; Villamaina, D.; Winkler, M. Photografting of Perfluoroalkanes onto Polyethylene Surfaces via Azide/Nitrene Chemistry. *Appl. Surf. Sci.* **2017**, *396*, 672–680.

(17) Pandey, V. C.; Singh, V. Exploring the Potential and Opportunities of Current Tools for Removal of Hazardous Materials From Environments. In *Phytomanagement of Polluted*

Sites; Elsevier, 2019; pp 501–516.

(18) Al-Zoubi, H.; Omar, W. *Rejection of Salt Mixtures from High Saline by Nanofiltration Membranes*; 2009; Vol. 26.

(19) Cheng, W.; Liu, C.; Tong, T.; Epsztein, R.; Sun, M.; Verduzco, R.; Ma, J.; Elimelech, M. Selective Removal of Divalent Cations by Polyelectrolyte Multilayer Nanofiltration Membrane: Role of Polyelectrolyte Charge, Ion Size, and Ionic Strength. *J. Memb. Sci.* **2018**, *559*, 98–106.

(20) Ba, C.; Economy, J. Preparation and Characterization of a Neutrally Charged Antifouling Nanofiltration Membrane by Coating a Layer of Sulfonated Poly(Ether Ether Ketone) on a Positively Charged Nanofiltration Membrane. *J. Memb. Sci.* **2010**, *362* (1–2), 192–201.

(21) Han, R.; Zeng, J.; Wang, Y.; Chang, Q.; Zhang, X.; Zhou, J. Preparation and Application of Positively Charged Quaternized Chitosan/PEI Composite Nanofiltration Membranes. *Desalin. Water Treat.* **2014**, *52* (31–33), 5790–5795.

(22) Teixeira, M. R.; Rosa, M. J.; Nyström, M. The Role of Membrane Charge on Nanofiltration Performance. *J. Memb. Sci.* **2005**, *265* (1–2), 160–166.

(23) He, M.; Gao, K.; Zhou, L.; Jiao, Z.; Wu, M.; Cao, J.; You, X.; Cai, Z.; Su, Y.; Jiang, Z. Zwitterionic Materials for Antifouling Membrane Surface Construction. *Acta Biomater.* **2016**, *40*, 142–152.

(24) Zhou, Q.; Lei, X. P.; Li, J. H.; Yan, B. F.; Zhang, Q. Q. Antifouling, Adsorption and Reversible Flux Properties of Zwitterionic Grafted PVDF Membrane Prepared via Physisorbed Free Radical Polymerization. *Desalination* **2014**, *337* (1), 6–15.

(25) Shao, Q.; Jiang, S. Molecular Understanding and Design of Zwitterionic Materials. *Adv. Mater.* **2015**, *27* (1), 15–26.

(26) Liu, Y. ling; Wang, X. mao; Yang, H. wei; Xie, Y. F. Adsorption of Pharmaceuticals onto Isolated Polyamide Active Layer of NF/RO Membranes. *Chemosphere* **2018**, *200*, 36–47.

(27) Hideo Nakae; Ryuichi Inui; Yosuke Hirata; Hiroyuki Saito. Effects of Surface Roughness on Wettability. *Acta Mater.* **1998**, *46* (7), 2313–2318.

(28) Kubiak, K. J.; Wilson, M. C. T.; Mathia, T. G.; Carval, P. Wettability versus Roughness of Engineering Surfaces. *Wear* **2011**, *271*, 523–528.

(29) Boussu, K.; Van Der Bruggen, B.; Volodin, A.; Snauwaert, J.; Van Haesendonck, C.; Vandecasteele, C. Roughness and Hydrophobicity Studies of Nanofiltration Membranes Using Different Modes of AFM. *J. Colloid Interface Sci.* **2005**, *286* (2), 632–638.

(30) Fan, Z.; Wang, Z.; Duan, M.; Wang, J.; Wang, S. Preparation and Characterization of Polyaniline/Polysulfone Nanocomposite Ultrafiltration Membrane. *J. Memb. Sci.* **2008**, *310* (1–2), 402–408.

(31) Salis, A.; Ninham, B. W. Models and Mechanisms of Hofmeister Effects in Electrolyte Solutions, and Colloid and Protein Systems Revisited. *Chem. Soc. Rev.* **2014**, *43* (21), 7358–7377.

(32) Wilhelm, F. G.; Pünt, I. G. M.; Van Der Vegt, N. F. A.; Strathmann, H.; Wessling, M. Cation Permeable Membranes from Blends of Sulfonated Poly(Ether Ether Ketone) and Poly(Ether Sulfone). *J. Memb. Sci.* **2002**, *199*, 167–176.

(33) Hower, J. C.; Bernards, M. T.; Chen, S.; Tsao, H. K.; Sheng, Y. J.; Jiang, S. Hydration of

"Nonfouling" Functional Groups. *J. Phys. Chem. B* **2009**, *113* (1), 197–201.

(34) Nesterenko, P. N.; Haddad, P. R. Zwitterionic Ion-Exchangers in Liquid Chromatography. *Anal. Sci.* **2005**, *16* (6), 565–574.

(35) Chou, Y. N.; Wen, T. C.; Chang, Y. Zwitterionic Surface Grafting of Epoxylated Sulfobetaine Copolymers for the Development of Stealth Biomaterial Interfaces. *Acta Biomater.* **2016**, *40*, 78–91.

(36) Abitoye, J. O.; Mukherjee, P.; Jones, K. Ion Implantation: Effect on Flux and Rejection Properties of NF Membranes. *Environ. Sci. Technol.* **2005**, *39* (17), 6487–6493.

(37) Déon, S.; Escoda, A.; Fievet, P.; Dutournié, P.; Bourseau, P. How to Use a Multi-Ionic Transport Model to Fully Predict Rejection of Mineral Salts by Nanofiltration Membranes. *Chem. Eng. J.* **2012**, *189–190*, 24–31.

(38) Yaroshchuk, A.; Bruening, M. L. An Analytical Solution of the Solution-Diffusion-Electromigration Equations Reproduces Trends in Ion Rejections during Nanofiltration of Mixed Electrolytes. *J. Memb. Sci.* **2017**, *523*, 361–372.

(39) Bera, A.; Jewrajka, S. K. Tailoring Polyamide Thin Film Composite Nanofiltration Membranes by Polyethyleneimine and Its Conjugates for the Enhancement of Selectivity and Antifouling Property. *RSC Adv.* **2016**, *6* (6), 4521–4530.

(40) Lowe, A. B.; McCormick, C. L. Synthesis and Solution Properties of Zwitterionic Polymers. *Chem. Rev.* **2002**, *102* (11), 4177–4189.

(41) Georgiev, G. S.; Kamenska, E. B.; Vassileva, E. D.; Kamenova, I. P.; Georgieva, V. T.; Iliev, S. B.; Ivanov, I. A. Self-Assembly, Antipolyelectrolyte Effect, Nonbiofouling

Properties of Polyzwitterions. *Biomacromolecules* **2006**, *7* (4), 1329–1334.

(42) Pérez-González, A.; Ibáñez, R.; Gómez, P.; Urtiaga, A. M.; Ortiz, I.; Irabien, J. A. Nanofiltration Separation of Polyvalent and Monovalent Anions in Desalination Brines. **2014**.

(43) Tansel, B. Significance of Thermodynamic and Physical Characteristics on Permeation of Ions during Membrane Separation: Hydrated Radius, Hydration Free Energy and Viscous Effects. *Sep. Purif. Technol.* **2012**, *86*, 119–126.

(44) Stamm, M. Polymer Surfaces and Interfaces: Characterization, Modification and Applications. *Polym. Surfaces Interfaces Charact. Modif. Appl.* **2008**, 1–324.

(45) Maity, P.; Saha, B.; Suresh Kumar, G.; Karmakar, S. Effect of Zwitterionic Phospholipid on the Interaction of Cationic Membranes with Monovalent Sodium Salts. *Langmuir* **2018**, *34* (33), 9810–9817.

(46) Ernst, M.; Bismarck, A.; Springer, J.; Jekel, M. Zeta-Potential and Rejection Rates of a Polyethersulfone Nanofiltration Membrane in Single Salt Solutions. *J. Memb. Sci.* **2000**, *165* (2), 251–259.

(47) Bernards, M. T. Environmentally Responsive Polyelectrolytes and Zwitterionic Polymers. *Switch. Responsive Surfaces Mater. Biomed. Appl.* **2015**, 45–64.

(48) Shao, Q.; Jiang, S. Effect of Carbon Spacer Length on Zwitterionic Carboxybetaines. *J. Phys. Chem. B* **2013**, *117* (5), 1357–1366.

CHAPTER 5: PFPA-ETHYLENEIMINE MODIFIED SEPARATORS FOR LITHIUM SULFUR BATTERIES

5.1 INTRODUCTION

5.1.1. Lithium-sulfur batteries background

The 2019 Nobel Prize in Chemistry was awarded for work on developing lithium-ion batteries (LiBs) to Akira Yoshino, M. Stanley Whittingham and John B. Goodenough. LiBs are a leading energy storage technology for electric vehicles, portable electronics and smart-grid applications. They have many advantages over other batteries because they typically have high energy density, low self-discharge and zero memory effects. LiBs are made of a traditional metal oxide cathode and a graphite anode.[1] However, they are typically unable to keep up with the demand for advanced energy storage technologies that have high-energy density and long life that is required for portable electronics and electric vehicles.[2]

Lithium-sulfur (Li-S) batteries are considered to be high performance batteries (i.e. more so than lithium-ion batteries) because of their extremely high theoretical capacity, energy density, good environmental protection and low cost.[3] They are being used to develop electric vehicle batteries and for large-scale grid applications because of their high density and low-cost. Li-S have a high specific capacity of 1675 mA h g^{-1} and an energy density of 2600 Wh kg^{-1}, which are around five times higher than those of conventional LiBs.[4] Elemental sulfur is naturally abundant and an inexpensive side product of industrial processes making it an ideal material to use.[5]

5.1.2 Limitations of Li-S batteries

Li-S batteries are excellent for new generation batteries, however, practical applications of Li-S batteries are hindered by the low electrical and ionic conductivity of elemental sulfur, the "shuttle effect" caused by the dissolved polysulfide species, the discharge product Li_2S from lithium anode deterioration due to passivation, and the formation of a solid electrolyte interlayer (SEI).[3,6] A criticism of Li-S batteries is that the energy density is not good enough for long driving distances.[2] The "shuttle effect" involves large-chain polysulfides that diffuse to the anode and react to form shorter polysulfides that diffuse back to the cathode and jeopardize the energy density and cycle life of the Li-S batteries.[7] Polysulfide shuffling is described as "a variety of polysulfide anions can freely migrate between the cathode and anode in the charge-discharge process".[8] The intermediate redox product Li_2S_x ($6 < x < 8$) is soluble in most of the liquid electrolytes used and can then can precipitate onto the electrode surface as a solid sediment.[6,9] Polysulfide shuffling causes low Coulombic efficiency of Li-S batteries and also leads to corrosion of the lithium anode.[3,10] The loss of active material is the main reason for rapid capacity fading in Li-S batteries.[2,11]

5.1.3 Solving polysulfide shuffling

Solving the issue of polysulfide shuffling has been attempted by altering the cathode and separators of Li-S batteries.[12–14] Abbas *et al.* created a bifunctional poly(3,4-ethylenedioxythiophene) polysulfonate polymer (PEDOT:PSS) separator that obtained long ranged polysulfides.[13] The sulfonate acted as an electrostatic shield for the soluble lithium polysulfides through mutual Coulombic repulsion, while the PEDOT portion of the polymer provided chemical interactions with insoluble polysulfides.[13] Wang *et al.* created a cationic polymer binder to inhibit the shuttle effect through electrostatic confinement in Li-S batteries.[15] They developed a branched polyethylene imide (PEI) polymer and a cationic methylated PEI

polymer that attracted long chained polysulfides to achieve high capacity and high loading. PEI can be used as a chelating agent with the ability to complex metal ions, like Mn^{2+}. Cationic PEI, is also designed to confine lithium sulfide through interactions with both Li^{+} and S^{2-} ions. Specifically, primary, secondary and tertiary amines possess strong electronegativity which attracts Li^{+} and anchors S^{2-} anions. The amido- heads can easily adhere to negative or partially negative charged surfaces. We propose to synthesize 1) small molecules of PEI and methylated PEI like polymers that trap lithium polysulfides; 2) a small molecule that would mimic the electrostatic interactions of a polystyrenesulfonate polymer that will create a negative charge on the surface; and 3) a small molecule zwitterion that has both a cationic amine and an anionic sulfonate. These small molecules will all utilize perfluorophenylazide (PFPA) photochemistry to graft onto the polyolefin separators.

5.2 Synthesis of small molecules and modification of separators

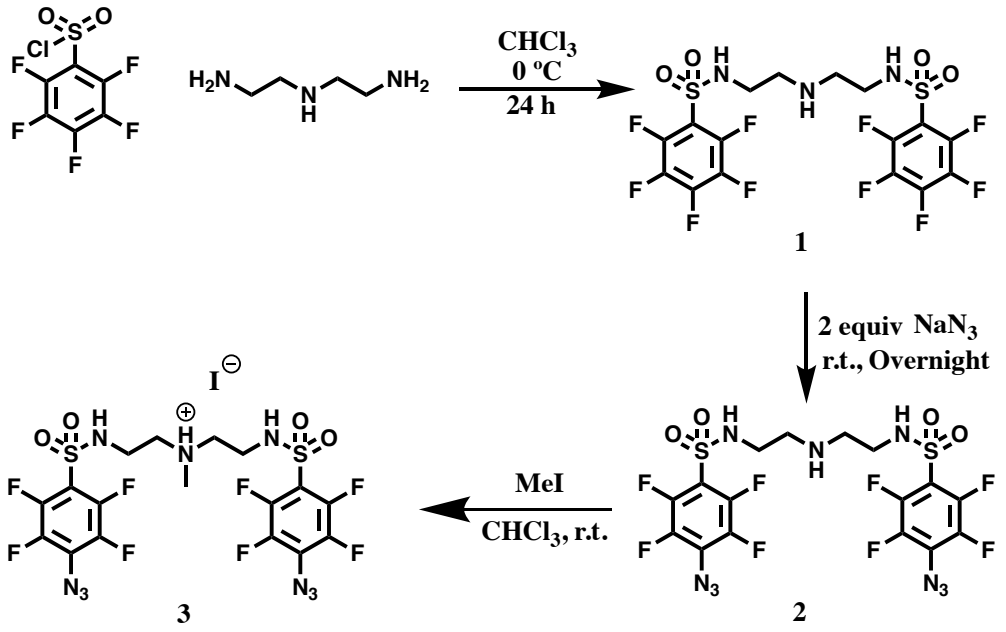

Figure 5-1. Synthesis of products 2 and 3, PFPA-PEI like and methylated PEI.

The synthesis of each small molecule was composed of two or three steps (**Figures 1-3**). A detailed synthetic procedure is described in the supporting information section. PFPA photochemistry covalently binds the azide to the polyolefin chain of the separator (polypropylene, PE), inside and outside the pores accomplished by low-power UV light. Each small molecule was dissolved in 10 mL of ethanol and poured on top of a commercially available PE separator. A hand-held UV light was placed above the separator in solution and irradiated for ten minutes. After the 10 minutes, the separator was removed from the perfluorophenylazide monomer solution and cleaned with DI water to remove any residual uncoated monomer and side products.

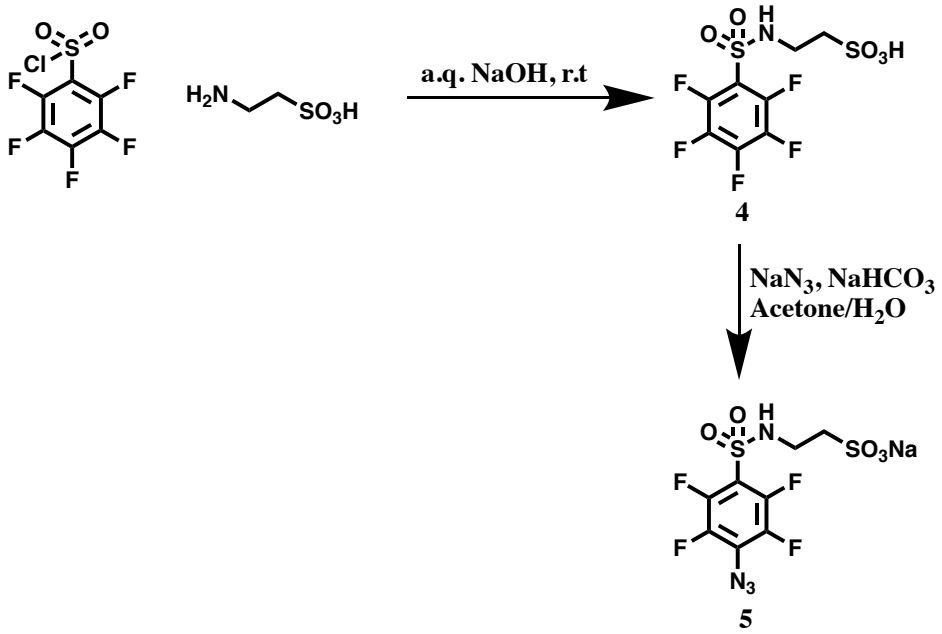

Figure 5-2. Synthesis of compound 5, PFPA-sulfonate.

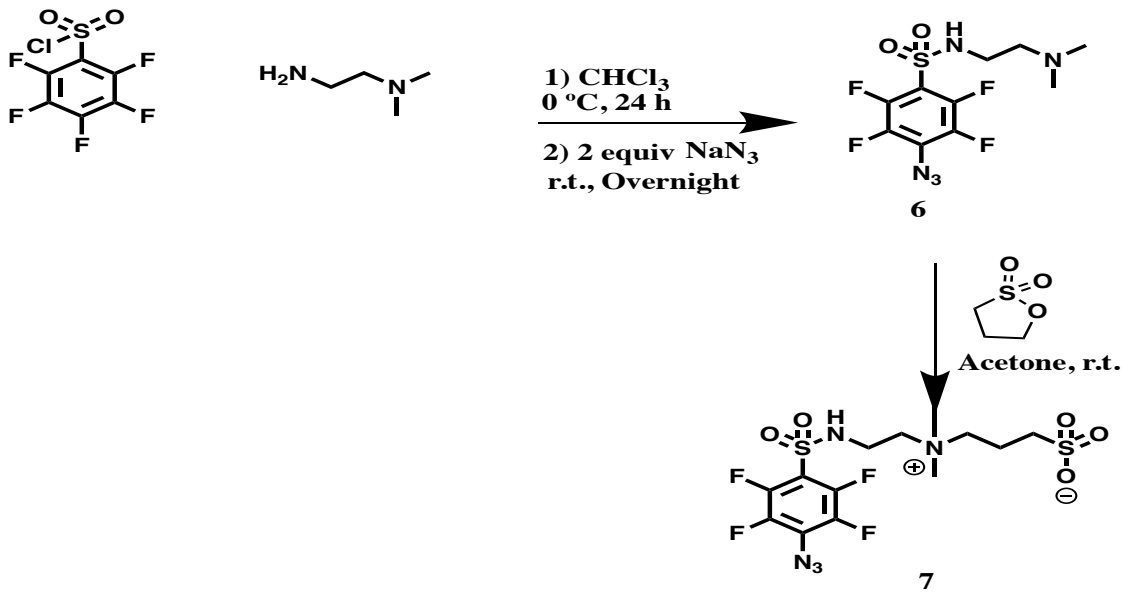

Figure 5-3. Synthesis of compound 7, PFPA-sulfobetaine.

5.3 Results and Discussion

5.3.1 Wettability

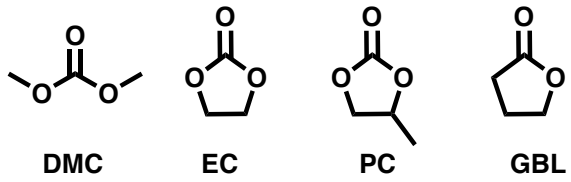

Figure 5-4. Electrolytes.

Once the separators were modified with the three small molecules and the PFPA-sulfonate polymer a wettability test was performed. A mixture of common electrolytes from **Figure 4** were used to wet the separator.

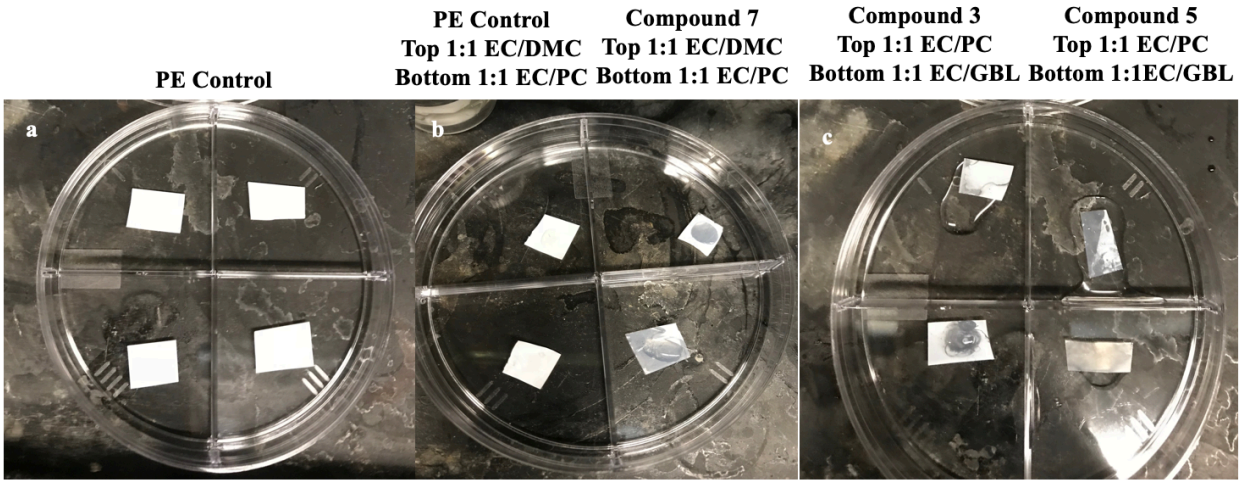

Figure 5-5. Wettability test of **a)** polyethylene control, **b)** PE control and compound 7 with EC/DMC and EC/PC as the electrolyte mixture, and **c)** Compound 3 and Compound 5 with EC/PC and EC/GBL as the electrolyte mixture. The control separator did not pass the wettability test, while compounds 3, 5 and 7 did pass with the given electrolytes.

As can be seen in **Figure 5**, the unmodified PE membrane was not wet by either mixture of EC/DMC or EC/PC. This is not surprising because the polyolefin PE is very non-polar and the two mixtures used are polar. The PFPA-sulfobetaine (compound 7) did show wettability after modification in a 1:1 mixture of EC/DMC and EC/PC (**Figure 5b**). Zwitterions are known to be hydrophilic by forming a hydration later allowing the polar electrolyte to wet the separator. The methylated PEI like small molecule (compound 3) demonstrated its ability to be wet in a 1:1 mixture of EC/PC and EC/GBL as seen in **Figure 5c**. This indicates that the cationic species enhance the hydrophilic nature of the hydrophobic polyolefin, which correlates to the hydrophilicity of cationic species that form a hydration layer with polar species. The anionic nature of PFPA-sulfonate in **Figure 5c** shows that it is also hydrophilic, enabling a 1:1 mixture of EC/PC and EC/GBL to wet the separator.

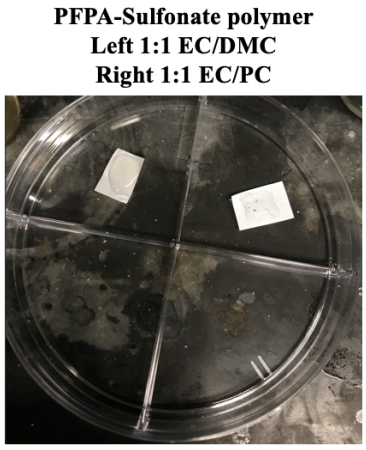

Figure 5-6. Wettability test for the PFPA-sulfonate polymer that did not penetrate the separator using EC/DMC and EC/PC as the electrolyte mixture.

Figure 6 indicates that the PFPA-sulfonate polymer modified onto the PE separator has no wettability. The PFPA-sulfonate polymer is hydrophilic; however, the large polymer might block the pores of the separator, not allowing for the polar solvents to penetrate through. Because of these results, we decided against using the PFPA-sulfonate polymer further in testing.

5.3.2 Polysulfide Diffusion Test

In order to investigate the influence of the modified and unmodified separators with dissolved polysulfides a diffusion test was created. The polysulfide blocking effect was investigated by comparing the polysulfide diffusion behavior with the native PE separator and the modified separators in an H-type cell as shown in **Figure 7**. A solution of 0.5 M Li_2S_4 (polysulfides) dissolved in electrolyte containing 1.0 M LiTFSI in a binary solvent of DME and DOL (1:1 in volume ratio) was prepared. The polysulfide solution was filled in one chamber, and the pure electrolyte mixture was filled in the other. The native and modified PE separators were inserted between the two chambers as shown in **Figures 7 and 8**. Because this test was conducted

in air and not under inert conditions, after 24 hours the bright red color of the polysulfides faded to orange/brown in color. The duration of these tests was performed up to a 96-hour period. A visual comparison of polysulfide diffusion in a double-cell reactor is shown in **(Figures 7 and 8).** The native PE separator does not prevent the polysulfides from diffusing through the separator. The color changed from colorless to yellow within a 24-hour period (**Figures 7a,b**). This indicated that the polysulfide penetrates the separator and migrated to the opposite chamber filled with the electrolyte solution.

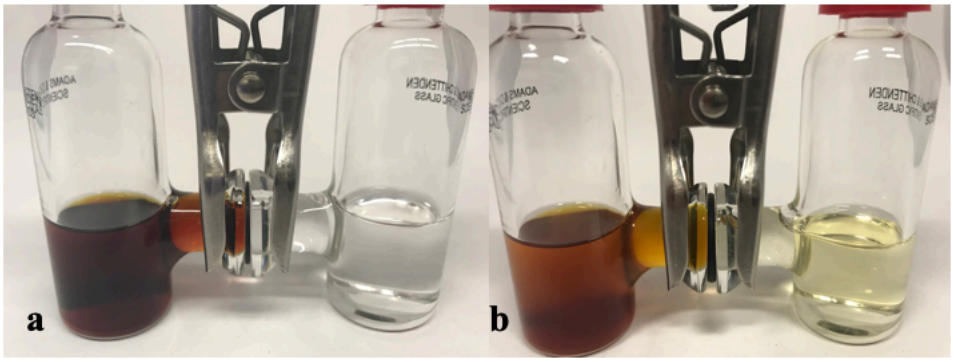

Figure 5-7. Polysulfide diffusion test with a 5.0 M polysulfide solution recorded by a digital camera in air. **a)** Initial setup with a native PE separator; **b) The** native PE separator after 48 hours.

In contrast, the functionalized modified separators were also tested. With the PFPA-methylated ethyleneimine, PFPA-sulfonate, and PFPA-sulfobetaine modified separators the diffusion of the polysulfide is much slower and not as apparent as in the native PE separator (**Figures 8a-h**). The comparison between the unmodified and modified separators clearly demonstrates the polysulfide shielding capability of the modified separators. This blocking effect of the separators is attributed to the chemical bonding between the polysulfides and the functional groups on the surface or from electrostatic repulsion. For example, the positively charged PFPA-

methylated ethyleneimine will attract the negatively charged polysulfide. In contrast, the negatively charged PFPA-sulfonate surface will electrostatically repel the anionic polysulfides. Therefore, the chemical interactions of the polysulfide form a negatively charged polysulfide layer on the separator surface that repels polysulfide anions, resulting in prohibiting the shuttling of polysulfides.

Figure 5-8. Polysulfide diffusion test with a 5.0 M polysulfide solution recorded by a digital camera in air. **a)** Initial setup with PFPA-methylated ethyleneimine; **b)** PFPA-methylated ethyleneimine after 48 hours; **c)** Initial setup with PFPA-sulfonate; **d)** PFPA-sulfonate after 48 hours; **e)** PFPA-sulfonate after 96 hours; **f)** Initial setup with PFPA-sulfobetaine; **g)** PFPA-sulfobetaine after 48 hours; and **h)** PFPA- sulfobetaine after 96 hours.

5.3.3 Capacity of Li-S batteries

Battery capacity is important because it's the amount of electrical charge that can be stored under specific conditions and is measured by discharging a fully charged battery through a load at a constant rate. The capacity is calculated by integrating the current in time. This is dependent on the discharge conditions. Capacity loss is due to physical and chemical degradation of the positive and negative electrodes and electrolyte. Capacity tests are made to measure the maximum charge that a cell can supply between two predefined voltage limits. These voltage limits are dependent on the materials of the electrodes used.[16]

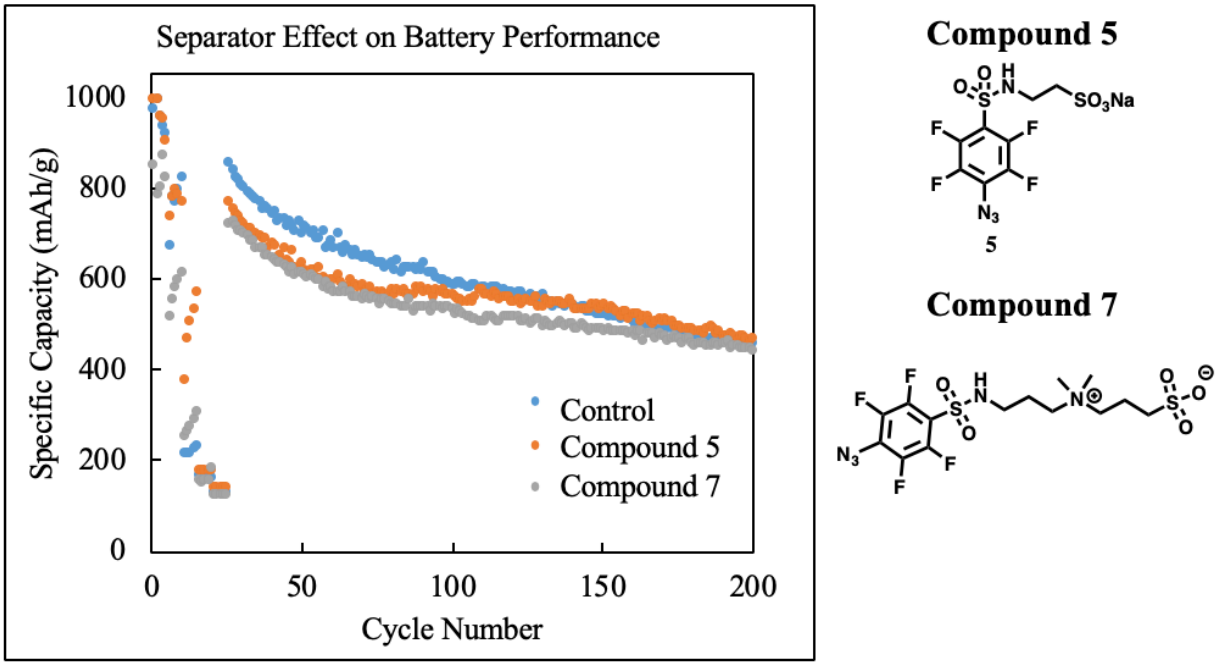

Figure 5-9. Specific capacity of a Li-S cell with an unmodified separator and negatively charged compounds 5 and 7.

The long-term cycling performance of the Li-S cell was evaluated based on the functional separator performance. A combination of the suppression of polysulfide shuttling and wettability of these separators endows the Li-S battery with better performance and capacity retention after

200 cycles (**Figure 9**). Compounds 5 and 7 reduce the overall capacity of the batteries to start and they then eventually equalize at around 200 cycles (**Figure 10**).

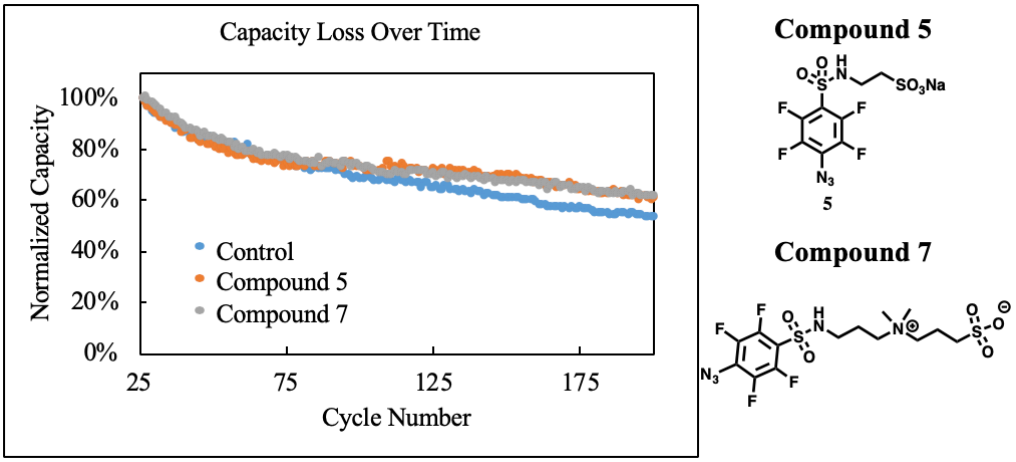

Figure 5-10. Capacity loss over time. Compounds 5 and 7 show enhanced capacity retention compared to the control.

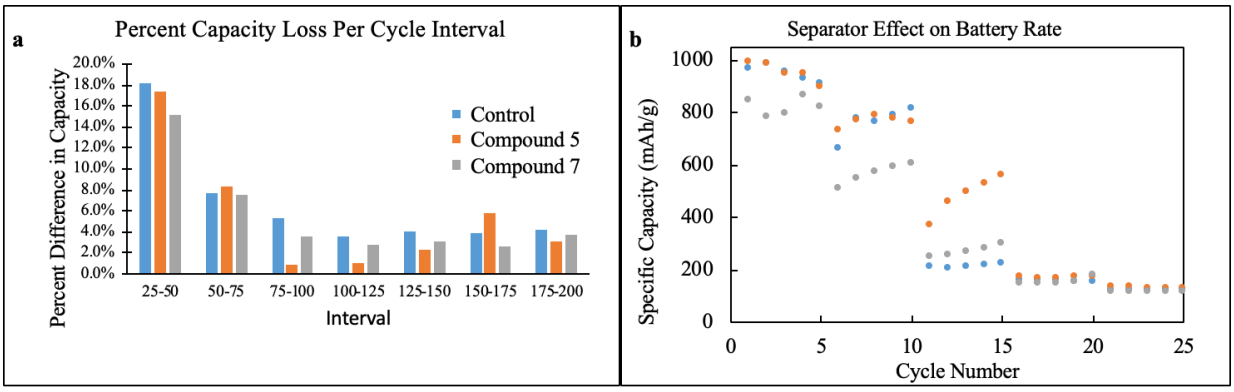

Figure 5-11. Comparing the unmodified separator used with compounds 5 and 7 to **a)** the capacity loss over 200 cycles and the **b)** separator effect on the battery rate. Compound 5 shows variable capacity loss and compound 7 has consistently lower loss per 25 cycle intervals.

Figure 10 shows that once the capacity is normalized both compounds 5 and 7 have a capacity loss per cycle that is lower than the unmodified native PE separator. Both modified separators have about the same capacity loss. **Figure 11** indicates that compound 5 shows a variable capacity loss and compound 7 has consistently lower loss per 25 cycle intervals (**Figure 11a)**. The high capacity in the beginning cycles may be due to the reaction of the functionalized separators with the Li^+ ions (**Figure 11b**). The formation of an SEI layer is also observed in the beginning cycles. Overall, there is about an 8% higher capacity retention of the modified over the unmodified separators (53% vs 61%).

5.4 Conclusions

The PFPA coatings for Li-S battery separators were created to functionalize the surface of the PE separator. The chemical interactions between the anionic polysulfides and the modified separators are important in restraining polysulfides from dissolving into the electrolyte and disturbing the anode. The PFPA-sulfonate and PFPA-sulfobetaine are both good at suppressing the dissolved polysulfides from migrating through the separator. Both showed an improvement in capacity retention over 200 cycles compared to the native PE separator. This work utilizes a promising strategy in easily modifying battery separators to improve their properties and life of the battery.

Supporting Information

S5-1. Synthesis of compound 1

Diethylenetriamine (3.82 mmol, 1 eq.) and 520 μL of triethylamine were dissolved in 5 mL of $CHCl_3$ and cooled to 0 ºC in an ice bath. Separately, pentafluorobenzenesulfonyl chloride (3.83 mmol, 1 mL) was dissolved in 5 mL $CHCl_3$ and cooled to 0 ºC. The two solutions were slowly combined by adding the solution containing the pentafluorobenzenesulfonyl chloride dropwise to the diethylenetriamine solution at 0 ºC. The ice bath was allowed to stir at room temperature. After 24 hours, the crude mixture was partitioned between $CHCl_3/H_2O$ and washed 3 times with DI water. The organic layer was concentrated under reduced pressure to give product **1** (70% yield) as a white solid.

S5-2. Synthesis of compound 2

To a solution of **1** (2.23 mmol) in an acetone/H_2O mixture (24 mL acetone, 8 mL H_2O) was added 524 mg of sodium azide (8.34 mmol, 3.75 eq.). The cloudy reaction mixture was allowed to stir overnight in the dark. The crude mixture was diluted with $CHCl_3$ and partitioned between $CHCl_3/H_2O$, then washed three times with copious amounts of H_2O. The organic layer was concentrated under reduced pressure to give product **2** (75% yield) as an off-white solid.

S5-3. Synthesis of compound 3

To a solution of **2** (0.88 mmol, 1 eq.) in $CHCl_3$ (4 mL, 0.2 M) at room temperature was added methyl iodide (1.7 mmol, 2 eq.) in one partition. The mixture was allowed to stir overnight at room temperature. In the morning the mixture was concentrated to dryness to give product **3** (92 % yield) as an off-white solid.

S5-4. Synthesis of compound 4 and 5

Taurine (3.4 mmol, 1 eq.) was dissolved in water (4 mL, 1.0 M) and 2.0 M NaOH (2mL, 1.0 M) was added to reach a pH of 10 in a round bottom flask. The sulfonyl chloride (3.75 mmol) was added in one portion to the taurine solution. The mixture was stirred at room temperature with periodic additions of 2.0 M NaOH to maintain a pH of ~10 for 6 hours and then allowed to stir undisturbed overnight. An additional aliquot of 2.0 M NaOH was added after overnight stirring and allowed to stir for an addition 2 hours. Concentrated HCl was added to achieve a pH of 1 and the mixture was placed in a 0 ºC freezer to precipitate for 4 hours. The solids were removed by filtration, washed quickly with ice-water and dissolved in methanol. The solids were then concentrated and dried to give the sulfonic acid product **4** as a white solid (49% yield). Product **4** (0.28 mmol, 1 eq.) was added to a round bottom flask followed by addition of acetone/H_2O (3:1, 8 mL, 0.05 M). Solid $NaHCO_3$ (0.28 mmol, 1 eq.) was added in one portion followed by addition of sodium azide (0.34 mmol, 1.2 eq.) in one portion and allowed to stir overnight. The mixture was filtered and the filtrate was concentrated to produce compound **5** as a while solid (90% yield).

S5-5. Synthesis of compound 6

N,N-dimethylethylenediamine (3.82 mmol, 1 eq.) and 520 µL of triethylamine was dissolved in 5 mL of $CHCl_3$ and cooled to 0 ºC in an ice bath. Separately, pentafluorobenzenesulfonyl chloride (3.82 mmol, 1 eq) was dissolved in 5 mL of $CHCl_3$ and cooled to 0 ºC. The two solutions were slowly combined by adding the solution containing the pentafluorobenzenesulfonyl chloride dropwise into the *N,N*-dimethylethylenediamine solution at 0 ºC. The ice was replaced every 15 minutes for 1 hour. After 1 hour, the reaction was removed from the ice bath and was allowed to stir at room temperature. After 2 hours, the crude mixture was partitioned between $CHCl_3$/H_2O

and washed 3x with DI water. The organic layer was concentrated under reduced pressure to obtain a white solid. The white solid (2.23 mmol, 1 eq.) was dissolved in an acetone/H_2O mixture (24 mL of acetone, 8 mL of H_2O) and sodium azide (8.34 mmol, 3.75 eq.) was added in one portion. The cloudy reaction mixture was allowed to stir overnight in the dark. The crude mixture was diluted with $CHCl_3$ and partitioned between $CHCl_3$/H_2O, then washed three times with copious amounts of H_2O. The organic layer was concentrated under reduced pressure to give product **6** (80% yield) as an off-white solid.

S5-7. Synthesis of compound 7

Anhydrous acetone (16 mL, 0.15 M) was added to produce **6** (2.3 mmol, 1 eq.), followed by an addition of 1,3-propane sultone (2.8 mmol, 1.2 eq.) in one portion. The mixture was allowed to stir overnight in the dark. The mixture was filtered and the filtrate returned to the initial reaction vessel, covered and allowed to continue stirring. The filtered product was washed three times with acetone and dried. This process was repeated three times over the course of 4 days to provide (52% yield) of product **7** as a white powder after drying under high vacuum.

S5-8. Making Li-S batteries

The mass loading for each sample was around 1 mg/cm^2 of active material. Batteries were cycled at 0.1 C with the theoretical capacity of sulfur being 1675 mAh/g. Slurries were made as follows:

1) Sulfur and Ketjen Black conductive carbon were ground in a 80:20 ratio. This composite was melt diffused (sulfur melts into carbon pores) in an autoclave at 155 ºC for 4 hours. This composite was then mixed with super P conductive carbon and polyvinylidene fluoride (PVDF) binder in N-methyl-2-pyrrolidone (NMP) at a ratio of 75:10:15, respectively. The slurry was blade cast onto an Al foil current collector, and dried at 60 ºC in an oven for 2 hours. The electrolyte was a 50:50

mix of DOL (1,3-dioxane) and DME (dimethoxyethane) with 1.0 M lithium bis(trifluoromethanoesulfonyl)imide (LiTFSI) and 1% by weight $LiNO_3$ (the additives make a nice, stable SEI).

5.5 References

(1) Blomgren, G. E. The Development and Future of Lithium Ion Batteries. *J. Electrochem. Soc.* **2017**, *164* (1), A5019–A5025.

(2) Wild, M.; O'neill, L.; Zhang, T.; Purkayastha, R.; Minton, G.; Marinescu, M.; Offer, G. J. Lithium Sulfur Batteries, a Mechanistic Review. *Energy Environ. Sci* **2015**, *8*, 3477.

(3) Deng, N.; Kang, W.; Liu, Y.; Ju, J.; Wu, D.; Li, L.; Hassan, B. S.; Cheng, B. A Review on Separators for Lithium Sulfur Battery: Progress and Prospects. *J. Power Sources* **2016**, *331*, 132–155.

(4) Wang, H.; Ling, M.; Bai, Y.; Chen, S.; Yuan, Y.; Liu, G.; Wu, C.; Wu, F. Cationic Polymer Binder Inhibit Shuttle Effects through Electrostatic Confinement in Lithium Sulfur Batteries. *J. Mater. Chem. A* **2018**, *6* (16), 6959–6966.

(5) Bucur, C. B.; Jones, M.; Kopylov, M.; Spear, J.; Muldoon, J. Inorganic-Organic Layer by Layer Hybrid Membranes for Lithium-Sulfur Batteries. *Energy Environ. Sci.* **2017**, *10* (4), 905–911.

(6) Fotouhi, A.; Auger, D.; O'Neill, L.; Cleaver, T.; Walus, S. Lithium-Sulfur Battery Technology Readiness and Applications—A Review. *Energies* **2017**, *10* (12), 1937.

(7) Chang, C. H.; Chung, S. H.; Han, P.; Manthiram, A. Oligoanilines as a Suppressor of Polysulfide Shuttling in Lithium-Sulfur Batteries. *Mater. Horizons* **2017**, *4* (5), 908–914.

(8) Drvarič Talian, S.; Moškon, J.; Dominko, R.; Gaberšček, M. Reactivity and Diffusivity of Li Polysulfides: A Fundamental Study Using Impedance Spectroscopy. *ACS Appl. Mater. Interfaces* **2017**, *9* (35), 29760–29770.

(9) Pang, Q.; Liang, X.; Kwok, C. Y.; Nazar, L. F. JES COLLECTION OF INVITED BATTERY REVIEW PAPERS Review—The Importance of Chemical Interactions between Sulfur Host Materials and Lithium Polysulfides for Advanced Lithium-Sulfur Batteries. *J. Electrochem. Soc.* **2015**, *162* (14), 2567–2576.

(10) Chen, X.; Peng, H. J.; Zhang, R.; Hou, T. Z.; Huang, J. Q.; Li, B.; Zhang, Q. An Analogous Periodic Law for Strong Anchoring of Polysulfides on Polar Hosts in Lithium Sulfur Batteries: S- or Li-Binding on First-Row Transition-Metal Sulfides? *ACS Energy Lett.* **2017**, *2* (4), 795–801.

(11) Pang, Q.; Liang, X.; Kwok, C. Y.; Nazar, L. F. Review—The Importance of Chemical Interactions between Sulfur Host Materials and Lithium Polysulfides for Advanced Lithium-Sulfur Batteries. *J. Electrochem. Soc.* **2015**, *162* (14), A2567–A2576.

(12) Ma, L.; Zhuang, H. L.; Wei, S.; Hendrickson, K. E.; Kim, M. S.; Cohn, G.; Hennig, R. G.; Archer, L. A. Enhanced Li-S Batteries Using Amine-Functionalized Carbon Nanotubes in the Cathode. *ACS Nano* **2016**, *10* (1), 1050–1059.

(13) Abbas, S. A.; Ibrahem, M. A.; Hu, L. H.; Lin, C. N.; Fang, J.; Boopathi, K. M.; Wang, P. C.; Li, L. J.; Chu, C. W. Bifunctional Separator as a Polysulfide Mediator for Highly Stable Li-S Batteries. *J. Mater. Chem. A* **2016**, *4* (24), 9661–9669.

(14) Zhang, L.; Ling, M.; Feng, J.; Liu, G.; Guo, J. Effective Electrostatic Confinement of Polysulfides in Lithium/Sulfur Batteries by a Functional Binder. *Nano Energy* **2017**, *40*, 559–565.

(15) Wang, H.; Ling, M.; Bai, Y.; Chen, S.; Yuan, Y.; Liu, G.; Wu, C.; Wu, F. Cationic

Polymer Binder Inhibit Shuttle Effects through Electrostatic Confinement in Lithium Sulfur Batteries. *J. Mater. Chem. A* **2018**, *6* (16), 6959–6966.

(16) Whittingham, M. S. Lithium Batteries and Cathode Materials. *Chem. Rev.* **2004**, *104* (10), 4271–4301.

CHAPTER 6: PFPA-ZWITTERIONS ON PDMS FOR BIOMEDICAL DEVICES

6.1 INTRODUCTION

6.1.1 Hospital Infections

Estimates from the Centers for Disease Control and Prevention observe that 1.7 million patients suffer from hospital-acquired infections each year and about 100,000 of them die (one in 17).[1,2] These medical errors are also preventable, resulting in up to $4.5 billion in additional healthcare expenses annually. Health-care associated infections (HCAIs) are "infections that occur while receiving health care, developed in a hospital or other health care facility that first appear 48 hours or more after hospital admission, or within 30 days after having received health care.[2] HCAIs are the most common complications of hospital care and one of the top 10 leading causes of death in the USA as stated by the Agency for Health Care Research and Quality.[2] The most common HCAIs are surgical site infections, urinary tract infections, pneumonia and bloodstream infections. The patients are typically given antibiotics and antimicrobials to treat these infections.[3] There's about 12-17 microorganisms that cause ~85% of HCAIs: *S. aureus, Enterococcus species, E. coli, Staphylococci, Candida* species*, K. pneumoniae, A. baumannii, P. aeuruginosa, Bacteroides* species, and other pathogens.[2] From these pathogens, about 16-10% are multidrug-resistant (MDR) phenotypes and some of the Gram-negative microorganisms have a higher rate of resistance than others. One common way to get an HCAIs is via medical devices.

6.1.2 Medical Devices

Medical devices are defined by the FDA as an "apparatus, instrument, implement, machine, contrivance, implant, *in vitro* agent, or other similar or related article, including a component part, or accessory which is intended for use in the diagnosis of disease, in man or other animals, or intended to affect the structure or any function of the body of man or other animals, and which does not achieve any of its primary intended purposes though chemical action within or on the body of man or other animals and which is not dependent upon being metabolized for the achievement of any of its primary intended purposes".[4,5] These medical devices can be divided into implantable devices and indwelling dependent upon intended function and duration of its use.[5] These medical devices that can be implanted in the body can cause infections due to biofouling.

6.1.3 Fouling

Fouling is typically divided into four different categories: 1) mineral scaling, 2) colloidal fouling, 3) organic fouling and 4) microbial fouling.[6,7,8] Microbial fouling, which is known as biofouling, refers to the deposition of bacterial cells (biological species) and their formation and growth into biofilms.[6] Biofouling occurs when micro-organisms make a transition from free-floating planktonic to stationary, and adhere to one another and a hard surface with an adhesive called the extracellular substance (EPS).[9] Ultimately, a layer of proteins on the surface of a device becomes a microbial colonization (biofilm).[10] Biofouling depends on a number of surface factors like microtexture, wettability, charge and contours.[11] It's biofouling that causes infections in the body resulting in HCAIs and protein fouling on implants reduces the efficacy of the device.[10] Treatments for biofilms on devices include surgical replacement of the device and antibiotic therapy.[10] Nonspecific adsorption of proteins and bacteria is what occurs on these medical devices that starts the formation of biofilms.

6.1.4 Nonspecific adsorption

Nonspecific adsorption of proteins onto synthetic surfaces is important in biomedical devices.[12] Hence, the need to develop materials that resist adsorption of proteins. Surfaces that resist nonspecific adsorption of proteins and microbes therefore are vital. Typically, surfaces with low density and high molecular weight have resistance towards adsorption of proteins. It has been shown that good characteristics for nonspecific adsorption surfaces should be 1) hydrophilic, 2) electrically neutral, 3) hydrogen bond acceptors, and 4) not hydrogen bond donors.[13,14] There are two different ways to prevent biofouling: by preventing biofoulants from attaching or by degrading them.[10]

Charged polymers have also been used for nonspecific adsorption because of their physicochemical properties.[15] Quaternary ammonium (QA) groups have been studied due to their antibacterial properties.[3] QA groups kill microorganisms through ionic interactions and by attacking the cytoplasmic membranes resulting in leakage of intracellular components.

4.1.5 Developing an antimicrobial coating

Antimicrobial coatings are used to either prevent adsorption, kill on contact or a combination of the two.[16] The biocidal approach will either leach a biological or organic biocidal into its environment via the solid and liquid interface to kill any bacteria in the environment.[16] However, some of these biocides may be harmful to the environment.[17] There is also the resistance approach that relies on either hydrophilic materials or hydrophobic materials.[18] The hydrophobic materials are inspired by nature like the lotus leaf. This type of coating does not prevent bacteria from adhering to the surface, it only makes the surface so hydrophobic that the material is easy to clean. In contrast, hydrophilic coatings work by forming a hydration layer to prevent bacteria from

adhering onto the surface.[19,20] There is also a combination of utilizing a biocide and the resistance approach. We decided to utilize both the killing on contact approach in case the bacteria does contact the surface and the preventative approach of trying to prevent bacteria from adhering to the surface.

6.1.6 Interactions of proteins in solution at varied pHs

Molecular interactions are forces, either attractive or repulsive, between molecules and non-bonded atoms.[21] They are noncovalent/intermolecular interactions that are not bonds, but "attraction between likes".[22] These molecular interactions are important in drug design, nanotechnology, and protein folding, to only name a few.[21] Electrostatic interactions are important for all biological macromolecules. Only 5 of 20 amino acids that make up proteins are charged at physiological pH.[23] As there are both positively and negatively charged amino acids, the net charge on most proteins tends to be small. Repulsive energy is when you force two atoms together and they push back. This occurs because when two atoms are close together, their occupied orbitals on the atom surfaces overlap, causing electrostatic repulsion between the surface electrons.[24] Electrostatic interactions are between cations and anions, that can either be attractive or repulsive, where like charges repel and unlike charges attract. Electrostatic interactions are highly attenuated by water, for example in DNA annealing, electrostatic interactions are dependent on salt concentration and pH.[25] Changing the pH disrupts hydrogen bonding and ionic bonds and will change the shape of the protein because various amino acid chains can hydrogen bond to each other. This means that a change in pH will change the attractions between the groups in the side chains of proteins.[26] Changes in molecular interactions are when proteins unfold, DNA strands separate and membranes disassemble. The surface of a protein has a net charge that depends on the number and identities of the charged amino acids and on pH.[23,27]

6.1.7 Isoelectric Point

The isoelectric point is the pH value of a buffer solution is exactly zero and the surface charge is neutral. For example, at a particular pH (the isoelectric point of the amino acid), each amino acid exists in solution as a zwitterion because a proton transfers from the carboxylic group to the amine group, balancing the charges and making it have a net charge of zero. The isoelectric point for most proteins occur at a pH range of 5.5 - 8.[21,24] The lowest solubility of a protein is at its isoelectric point. At the isoelectric point, a protein has no net charge (i.e. it is neutral).[27] Above the isoelectric point, a protein carries a net negative charge and below the isoelectric point it carries a net positive charge. If there is a charge at the protein surface, the protein will prefer to interact with water instead of other protein molecules, making the protein more soluble. Therefore, without a net charge, protein-protein interactions and precipitation are more likely to occur.[28,29]

6.1.8 Modifications of Medical Devices

Common ways to alter medical devices are imbibing implants in antimicrobial solutions or by using coatings to control infection.[30,31] However, sometimes antimicrobial agents leach from surfaces and cause toxicity in the body.[31] Anti-fouling surfaces can achieve antimicrobial performances without these risks.[5] Polybetaines, for example, have been shown to significantly reduce protein adsorption to a level that can inhibit thrombus formation or other complications.[32] Biomaterials such as catheters come into contact with protein-rich biological materials where nonspecific protein adsorption can either partially or entirely compromise functionality.[9] When a surface is antifouling it is well hydrated (e.g. hydrophilic), and it tends to repel protein binding through a combination of steric repulsion and formation of a structured water layer.[5] These hydrophilic surfaces are intended to prevent biofouling. A variety of strategies have been studied

to enhance the hydrophilicity of materials, one of them being modification of the materials surface chemistry.[33] Hydrophilic polymers (charged or nonionic) or hydrophobic polymers can be coated onto devices to impart fouling resistance. Increasing the hydrophilicity of a material is a common way to reduce the initial biological response of nonspecific protein adsorption and subsequent cellular events.[9] Antibiofouling polymers are polymers that prevent the adsorption of proteins.[34] Superhydrophobicity or superhydrophilicity are often considered to be the best methods for creating microbial resistance. A limitation to these surface modifications is that these anti-fouling coatings cannot inhibit the growth of microorganisms in the surrounding environment or kill them. Ideally, to enhance the antimicrobial efficacy and reduce the possibility of complications on medical devices, anti-fouling modifications should be combined with antimicrobial techniques.[9] Therefore, a combination of an anti-fouling coating and an antimicrobial agent is a promising technique to investigate to achieve a long-term multiple fouling-resistant surface in a complex environment.

6.1.9 SAMs and Polymer brushes

Self-assembled monolayers (SAMs) and polymer brushes are both common ways to add an antifouling surface.[35,36] SAMs, however, are prone to surface defects, possess non-covalent interactions and have limited applications to metal surfaces.[37] Polymer brushes are more versatile as they can be covalently attached to a variety of surfaces, unlike SAMs. There are two types of hydrophilic polymers: 1) un-dissociated polymers and 2) dissociated polymers. Un-dissociated polymers in the presence of a salt can enhance the polymer and water mixing conditions (salting-in) or salting out. Dissociated polymers are polymers that are acid derivatives and exhibit "polyelectrolyte behavior" characterized by a marked de-swelling in salt solution. The most studied polymer is poly(ethylene glycol) (PEG) because it's a non-ionic polymer for increasing

hydrophilicity on the surface of a material that has both antifouling and biocompatibility properties.[38] However, even though PEG does well in preventing biofouling, it is susceptible to autoxidation in the presence of dioxygen and transition metal ions. Also, the terminal hydroxy group in PEG is susceptible to oxidation by alcohol dehydrogenase to an aldehyde (this aldehyde can react with proteins *in vivo* and with other molecules with amines).[12,36,39] Dioxane is an ether, and the proportioning of dispersion, polar and hydrogen forces greatly influence its ability to swell elastomers like poly(dimethylsiloxane) PDMS, that can ultimately destroy the material.[37,40]

6.2 Materials and Methods

6.2.1 Poly(dimethylsiloxane)

PDMS have a broad range of biological applications due to its unique physical properties; mechanical durability, optical transparency, flexibility, chemical inertness, high gas permeability, nontoxicity, and ease of microfabrication.[33] PDMS is commonly used in biomedical devices such as contact lenses, pacemakers, microfluidic devices, catheters, and breast implants. However, even though PDMS is used in a variety of applications, it has one big disadvantage in biomedical applications, the hydrophobicity of PDMS creates protein adsorption onto its surface causing fouling.[33] It has been well studied that hydrophobic surfaces tend to adsorb high levels of bacteria and proteins. PDMS is a hydrophobic elastomer that can be oxidized in order to become hydrophilic. Oxidized PDMS occurs via exposure to UV radiation, air plasma or oxygen plasma.[33] This treatment generates silanol groups (Si-OH) on the surface by oxidizing the methyl groups of PDMS, changing the contact angle from ~120º to <60º. However, these Si-OH groups are only temporary and will ultimately revert back to PDMS ($Si\text{-}CH_3$), called the hydrophobic recovery phenomenon.[41,42] This is an effect that renders a hydrophilic PDMS surface hydrophobic with a

half-life of one day due to the surface rearrangement that brings new hydrophobic groups to the surface to lower the surface free energy when exposed to air.[35] Due to the short half-life of this treatment, the Si-OH groups on the surface can be functionalized to keep the surface hydrophilic. The modified hydrophilic PDMS can be used in a variety of applications in biomaterials. PDMS is an ideal candidate for a biomaterial because the compatibility of a biomaterial ideally would require: 1) no thrombogenic, allergic or inflammatory reactions; 2) no change in plasma proteins or enzymes; 3) no immunological reactions; 4) no carcinogenic effects; and 5) no deterioration of adjacent tissues.[41–43] Because of PDMS's excellent properties, we suggest using our novel modification for medical devices. Adding hydrophobic or hydrophilic side chains onto PDMS can insert various chemical functionalities. This is one of the key reasons PDMS is used, as a variety of chemical functionalities can be established on PDMS, compared to other polymers that are more limited towards generalized surface functionalization.

6.2.2 PDMS in Medical Devices

PDMS is widely used as a silicon based organic polymer because it is optically clear, non-toxic, nonflammable and biocompatible.[42] The uses for PDMS range from contact lenses, medical devices to elastomers.[44–46] However, PDMS is a popular material that has its downfalls, limiting it's applicability. It suffers from fouling problems because of its hydrophobic nature that allows protein adsorption.[47] Plasma treatment of PDMS has been utilized before to overcome the hydrophobic surface by increasing the number of surface silanol bonds (increasing hydrophilicity), however, this treatment is very short-lived and is readily reversed due to thermodynamic instability.[48] This phenomenon is known as hydrophobic recovery and is caused by the low glass transition temperature (-120 ºC).[48] Coating the surface of PDMS can create anti-fouling surfaces that rely on steric repulsion and a hydration layer mechanism.[47] Our work relies on coating the

surface of PDMS by adding zwitterion polymers to reject bacterial adhesion by making the surface hydrophilic. The hydrophilic surface will lead to preventing nonspecific protein absorption.

6.2.3 Sulfobetaine and Carboxybetaine Zwitterions

Zwitterions have no net charge, two of the main types of zwitterions are sulfobetaine and carboxybetaine. Zwitterions are dissociable polymers (**Figure 1**). The sulfobetaine has a quaternary amine (positive charge) and a sulfoxide group (negative charge), while the carboxybetaine has a quaternary amine (positive charge) and a carboxy group (negative charge). These different charged species result in a non-charged overall compound. Non-ionic species are known to have less adsorption/absorption of foulants, compared to charged species.[49] Zwitterions specifically have been studied because they tend to create a strong water layer that surrounds them, preventing any adhesion by being more hydrophilic than a neutral substrate.[50]

The polymerization procedure does not require inert conditions and can be carried out in air.[50] Polymerization kinetics suggest that the polymerization is controlled well with linear pseudo first-order kinetic plots to high monomer consumption. The molar mass of the polymer can be controlled by the monomer to initiator ratio (primary amine) and can be easily controlled up to a degree of polymerization from 10-200, aiming for a chain length of 20 repeating units.[9,51] The molar mass and grafted chain density will be varied to test which chain density produces the best results.[49,51] However, we anticipate seeing a decrease in protein adsorption with increased grafted chain densities.[50,52] High chain lengths and density of zwitterion brushes have been shown to resist to a variety of proteins and bacteria attachment due to their high hydrophilic character.[49] Contact angle measurements will be carried out on each polymer brush, comparing uncoated PDMS to coated PDMS. It is expected that the uncoated hydrophobic PDMS will have a contact angle of

about ~120º, while the coated hydrophilic PDMS should have a contact angle near 20º. The trend is expected to be that the contact angle will decrease (increased hydrophilicity) with higher densities and longer lengths. This is justified because the mechanism for preventing protein adsorption by the zwitterion brush is due to steric repulsions, i.e. the restriction on the number of zwitterion conformations and the high local osmotic pressure that results from protein insertion into the zwitterion layer.

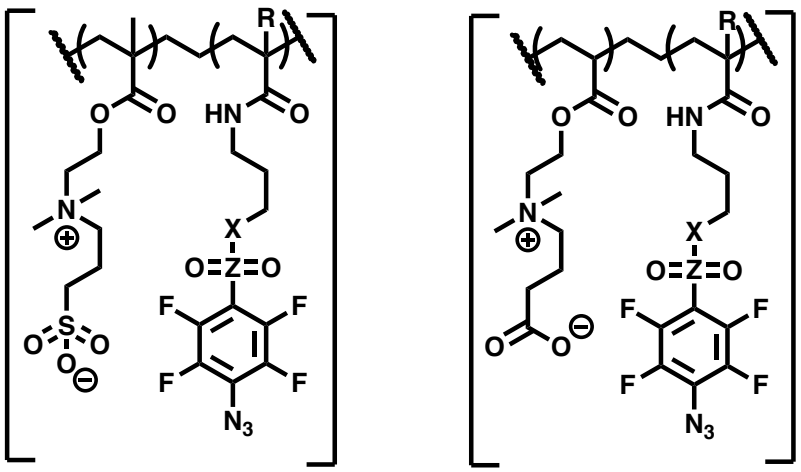

Figure 6-1. a) Sulfobetaine and **b)** Carboxybetaine zwitterion copolymers.

6.3 Results and Discussion

6.3.1 Contact Angle Measurements

Water contact angle measurements were obtained to see the changes in hydrophilicity. PDMS is very hydrophobic with a contact angle of ~100º. 2, 5 and 10 mg/mL concentrations of

each zwitterion polymer were grafted onto PDMS films. The different grafting densities had no impact on the contact angle of the samples so just 10 mg/mL as representative samples are shown (**Figure 2**). The water contact angle decreased from unmodified PDMS of >100º to ~20º for the PFPA-sulfobetaine and ~30º for the PFPA-carboxybetaine (**Figure 2**). This shows that both modified zwitterions make the PDMS material hydrophilic, PFPA-sulfobetaine more so than PFPA-carboxybetaine. Both zwitterions have the same cation (quaternary ammonium), but differ in the anion.

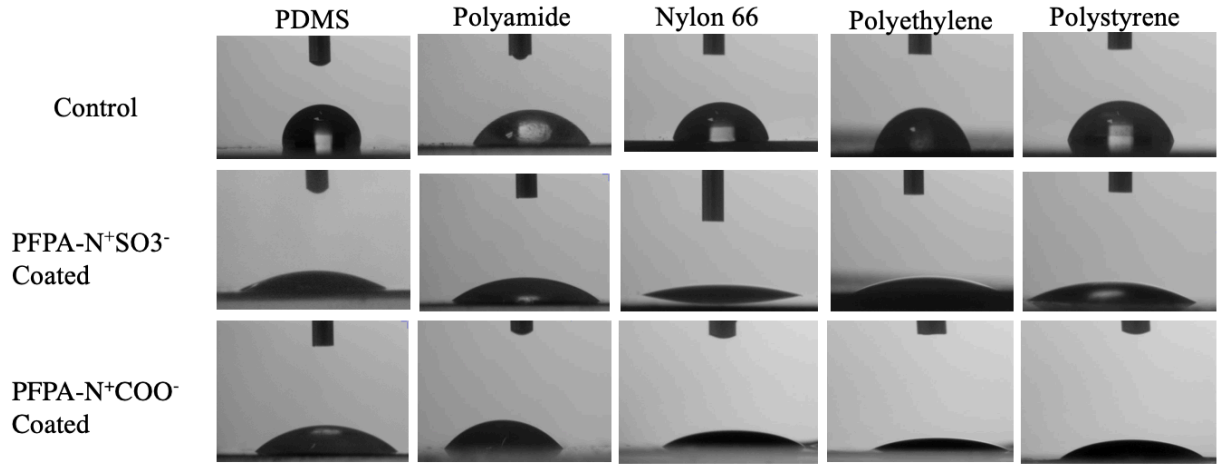

Figure 6-2. Contact angles of unmodified materials, and modified with either 10 mg/mL PFPA-sulfobetaine or 10 mg/mL PFPA-carboxybetaine.

Contact angle measurements of a variety of materials were measured to test the hydrophilicity of the grafted PFPA-zwitterions. The contact angle (hydrophilicity) of each material significantly dropped with the modifications. Each unmodified material was hydrophobic before modification with the zwitterions at 10 mg/mL and turned superhydrophilic with the grafted zwitterions.

6.3.2 X-Ray Photoelectron Spectroscopy (XPS)

Attenuated total reflectance infrared (ATR-IR) spectroscopy did not show the difference between the unmodified and modified PDMS, likely due to the small amount of PFPA-zwitterion attached to the surface. A more sensitive and precise surface technique, such as X-ray photoelectron spectroscopy (XPS) was needed. To determine the elemental analysis of the PDMS films, XPS was used to accurately determine if the PFPA-sulfobetaine and PFPA-carboxybetaine were successfully bound to the PDMS surface. **Table 1** shows that both PFPA-sulfobetaine and PFPA-carboxybetaine did successfully bind to PDMS. There is a clear sulfur peak on the modified surface, compared to the unmodified PDMS. Most importantly, there is a N 1s peak indicating that there is a new nitrogen bond to PDMS at 400 eV. This signifies that the azide of PFPA formed a covalent bond with PDMS through C-H insertion.

Material	**O 1S (eV)**	**N 1s (eV)**	**C 1s (eV)**	**S 2s and 2p (eV)**	**Si 2s and 2p (eV)**
PDMS	534		285		153 and 104
PDMS PFPA-S	534	400	285	263 and 167	153 and 104
PDMS PFPA-C	534	400	285	263 and 167	153 and 104

Table 6-1. Summary of XPS characterization of modified and unmodified PDMS with PFPA-zwitterions.

6.3.3 Atomic Force Microscopy (AFM)

Atomic force microscopy (AFM) was performed to see if surface roughness changed after the modification of the PDMS (**Table 2**). There was no large observable change after running

AFM of the samples, the native PDMS already had a smooth surface and the modification of the zwitterions only slightly increased the smoothness of the surface. Comparing the AFM with the water contact angle we can see that the wettability of the PDMS was increased with the modification of both zwitterion copolymers.

Material	**Root-mean-square roughness (nm)**
PDMS	6.13 ± 0.54
PDMS PFPA-S	2.87 ± 0.68
PDMS PFPA-C	4.85 ± 0.42

Table 6-2. AFM of modified and unmodified PDMS with PFPA-zwitterions.

6.3.4 Zeta Potential

Zeta potential is an important surface characterization technique to determine the charge on the surface of a material. PDMS is a very hydrophobic and negatively charged surface starting from pH 3.1. The modification of PFPA-sulfobetaine and PFPA-carboxybetaine make the surface hydrophilic and also change the charge of the surface. PFPA-sulfobetaine is close to neutral (from pH 5.5-6.4) with the highest zeta potential being 5.79 mV at pH 3.23, and the lowest being at pH 7.91 with a zeta potential of -16.65 mV. The isoelectric point of PFPA-sulfobetaine is pH 6.4, meaning that below pH 6.4 the surface of the modified PDMS is slightly more positively charged and above pH 6.4 the surface is slightly negatively charged. When the surface becomes negative the sulfonate group at the end of the zwitterion is deprotonated becoming more negative at high pH (**Figure 3**). PFPA-carboxybetaine starts off more positivity charged compared to PFPA-sulfobetaine with the highest zeta potential being 18.5 mV at pH 3.5. The isoelectric point of

PFPA-carboxybetaine is at pH 5.4, where the carboxylic acid deprotonates above pH 5.4 to a carbonylate and dramatically gets more negative with the lowest zeta potential being -29.84 at pH 7.24 (**Figure 3**). These results correlate well with the contact angle measurements where PFPA-sulfobetaine has a lower contact angle (e.g. more hydrophilic) compared to PFPA-carboxybetaine. It is believed that the almost neutral surface of PFPA-sulfobetaine makes the surface more hydrophilic.

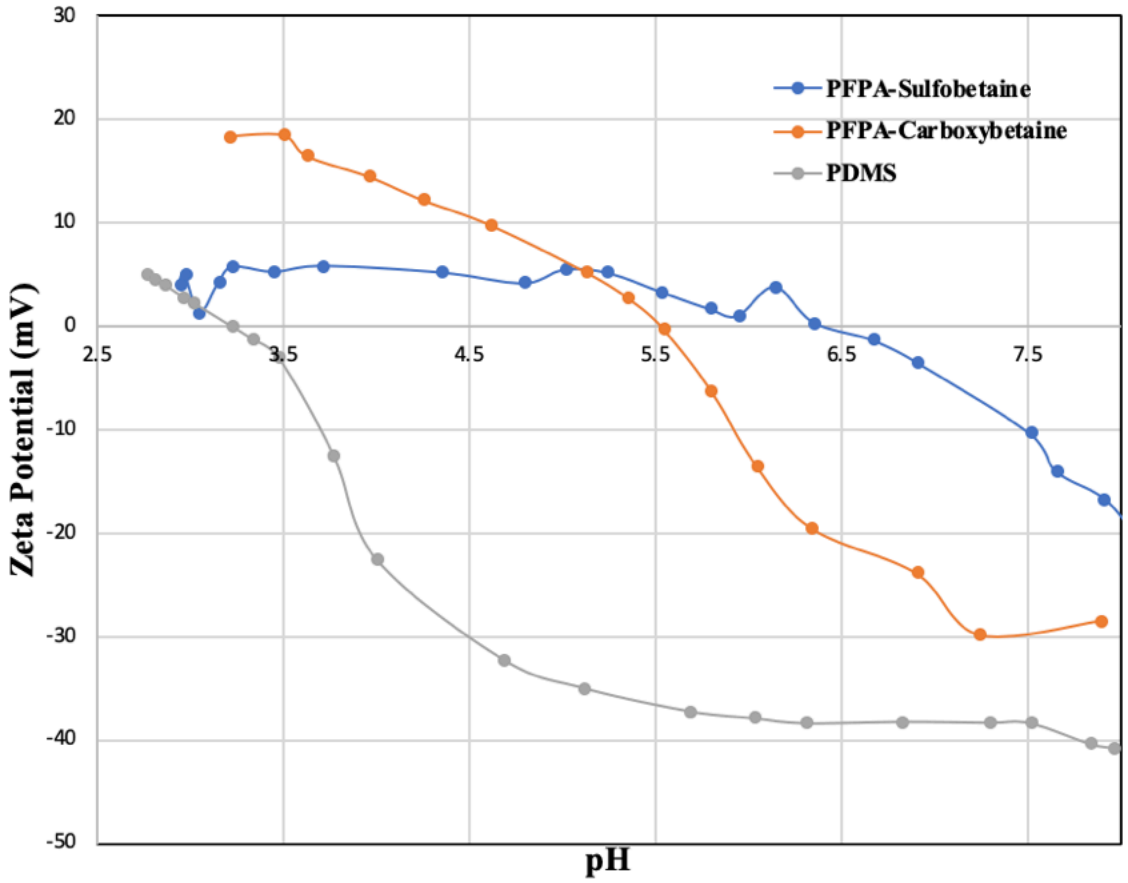

Figure 6-3. Zeta potential of unmodified PDMS, PFPA-sulfobetaine and PFPA-carboxybetaine from pH 2.5-8.

6.3.5 Surface Energy Calculations

Wettability of a material is an important parameter affecting protein absorption on a surface, with hydrophobic surfaces having more adsorption than hydrophilic ones. Because of this, surface free energy measurements are one way to quantify the hydrophilicity of a modified surface.

Thomas Young described the relationship between contact angle θ, the face free energy of a solid σ_s, the surface tension of a liquid σ_l, and the interfacial tension between the liquid and the solid σ_{sl} in **Equation 6.1**.[53]

$$\sigma_s = \sigma_{sl} + \sigma_l * \cos\theta \qquad [6.1]$$

This however, is not practical as it is for an ideal surface where the interfacial tension and surface free energy of the solid are both unknown. There have been a few different methods that have been developed for calculating surface free energy. The Fowkes method says that the surface free energy of a system can be separated into two main components, polar (σ^p) and dispersive (σ^d) with the sum of the two parts equaling the total surface energy as seen in **Equation 6.2**.[54]

$$\sigma = \sigma^d + \sigma^p \qquad [6.2]$$

The dispersive coefficient (σ^d) is calculated using the contact angle of one dispersive liquid and the polar coefficient (σ^p) is determined using a different liquid that is polar. The solvents that are typically used are water for the polar liquid and diiodomethane for the dispersive liquid. Each solvent is unique because it has a different interaction with the solid substrate and their contact angles differ. For example, if the solid substrate is polar itself, it would be more similar to water and have better adhesion and thus a smaller contact angle. By testing these two very different coefficients, we can better characterize the type of solid material.

Wu also developed a method for calculating surface free energy for polymers. This method uses a series of nonlinear **Equations (6.3)** and **(6.4)** to solve for both the polar and dispersive coefficients.[55]

$$(b_1 + c_1 - a_1)\sigma^d\sigma^p + c_1(b_1 - a_1)\sigma^d + b_1(c_1 - a_1)\sigma^p - a_1b_1c_1 = 0 \quad [6.3]$$

$$(b_2 + c_2 - a_2)\sigma^d\sigma^p + c_2(b_2 - a_2)\sigma^d + b_2(c_2 - a_2)\sigma^p - a_2b_2c_2 = 0 \quad [6.4]$$

With $a_n = (1/4)\ \sigma_n(1 + \cos\theta_n)$, $b_n = \sigma_1^d$, $c_n = \sigma_n^p$ (n = 1 or 2); σ_1 = the contact angle of water and σ_2 = the contact angle of diiodomethane. σ_1 = 72.8 dynes/cm, σ_1^d = 22.1 dynes/cm, σ_1^p = 50.7 dynes/cm, σ_2 = 50.8 dynes/cm, σ_2^d = 44.1 dynes/cm, σ_2^p = 6.7 dynes/cm. By solving the dispersive and the polar components separately we use **Equation 2** to calculate the total surface free energy.

Substrate	**Water θ**	**Diiodomethane θ**	$\boldsymbol{\gamma^p}$**(dynes/cm)**	$\boldsymbol{\gamma^d}$**(dynes/cm)**	$\boldsymbol{\gamma}$ **(dynes/cm)**
Control PDMS	107.5º	66.56º	29.99	0.02	30.01
PFPA-Sulfobetaine	22.0º	38.31º	27.37	41.57	69.14
PFPA-Carboxybetaine	37.5º	48.7º	34.87	45.87	58.67

Table 6-3. Surface free energy calculations of unmodified PDMS and PDMS modified with PFPA-sulfoxybetaine and PFPA-carboxybetaine.

6.3.6 Bacterial Adhesion

The first step in biofilm formation is bacterial adhesion. Bacterial adhesion of PDMS and modified PDMS were studied to see if the zwitterions were anti-biofouling once we observed the

contact angle of the modified PDMS showed a super-hydrophilic surface. A 24-hour fibroblast cell culture and live/dead staining was performed to show how the coatings compared to the native PDMS film.

The native PDMS film had over 100% cell adhesion, indicating that the cells reproduced over the 24-hour period. The PFPA-sulfobetaine modified PDMS sample had almost no cell adhesion on the surface. There were also no live cells and very few dead cells in the PFPA-sulfobetaine sample. This indicated that there was no adhesion and ability for these cells to grow and reproduce, while the few cells that did adhere died.

6.4 Conclusions

Herein, we describe successful modification of PDMS with a carboxybetaine and sulfobetaine coating. The native PDMS is hydrophobic and forms biofilms, while the coated PDMS shows super-hydrophilic properties and shows relatively non-adhesion or reproduction of cells. The coating was examined via XPS, IR and AFM to ensure the coating is on the membrane along with determining the charge of the surface via zeta potential measurements. These are successful initial studies that show how useful zwitterion coatings can be used for preventing biofilm formation.

S.6 Supplementary Information

S.6-1 Synthesis of Zwitterion Polymers

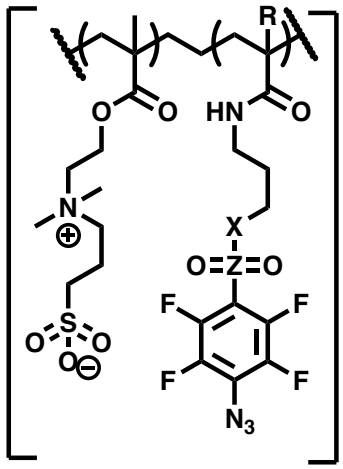

Figure 6S-1: Synthesis of PFPA-Sulfobetaine

PFPA-Sulfobetaine: See Chapter 2 Supplementary Information for complete synthesis.

PFPA-Carboxybetaine: Synthesis was modified by the procedure used by Zhang e*t al.*[32] *N*-(3-dimethylainopropyl)acrylamide (50 mmol), ethyl 4-bromobutraye (60 mmol) and acetonitrile (30 mL) were reacted for three days at 45 ºC under argon. The product was purified by washing with anhydrous ether and hydrolyzed immediately by dissolving in water and passing the monomer through a column packed with Amberlite IRA-400 (hydroxide form) resin. Water was then removed under reduced pressure and washed with anhydrous acetone (50 mL) and anhydrous ether (50 mL) once. The solvent was removed under reduced pressure to obtain a colorless oil, **Product 1.**

PFPA-Carboxybetaine: Product 1 was immediately used after synthesis and polymerized.

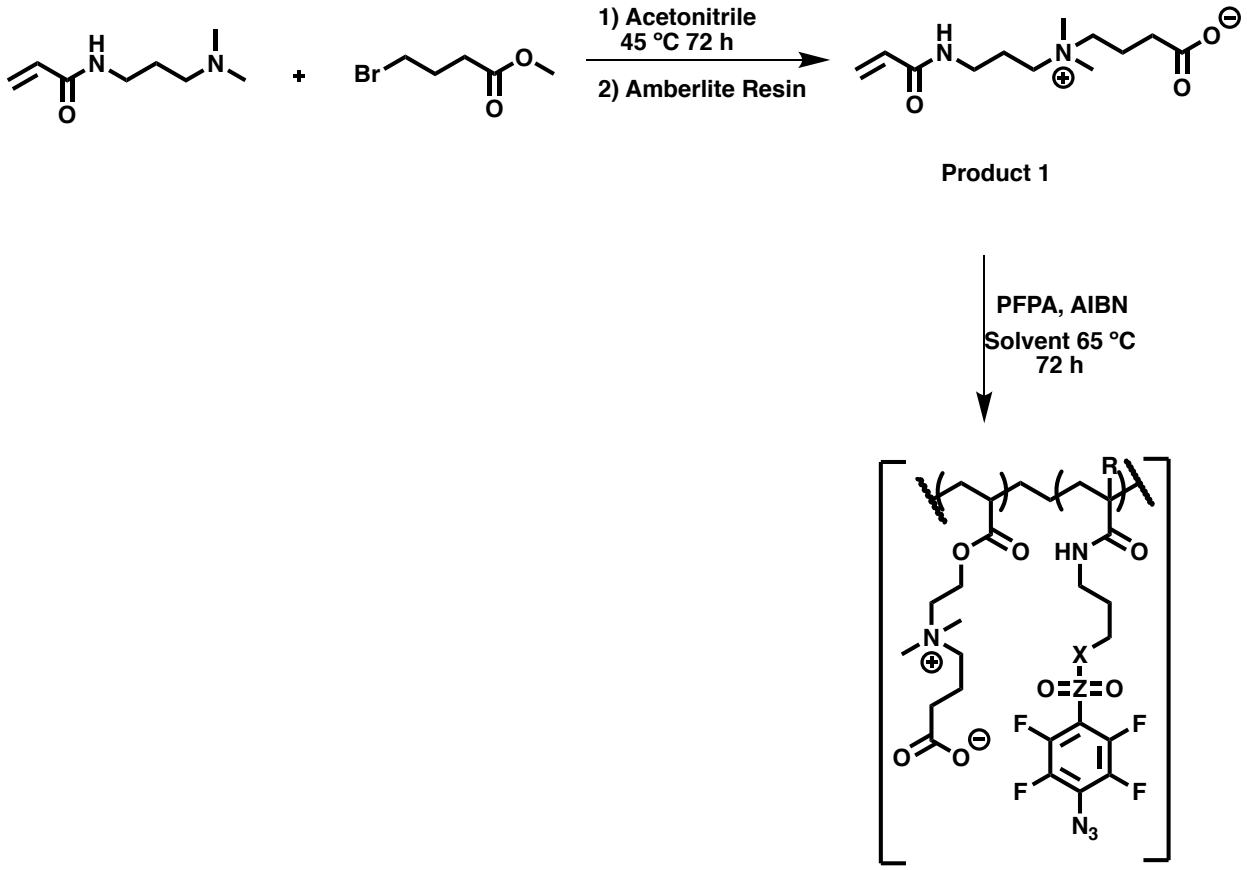

Figure S6-2: Synthesis of PFPA-carboxybetaine.

S6-2 Synthesis of PDMS Films: A 10:1 ratio of elastomer to curing agent (Syglard 184), was mixed together for 10 minutes before pouring into 3 mm Petri dishes and curing at 80 ºC for 1 hour.

S6-3 Modification of PDMS Films with PFPA-Sulfobetaine and PFPA-Carboxybetaine: 2 mL of PFPA polymer was dissolved in water at three different concentrations (2, 5, or 10 mg/mL).

The polymer solution was placed and spread onto the surface of a PDMS disk, followed by exposure to 254 nm UV light for 10 minutes. After 10 minutes, the disk was rinsed with DI water three times and dried under vacuum.

S6-4 Contact Angle Measurements: Water and diiodomenthane contact angle measurements were taken on PDMS and modified PDMS. Also, water contact angles were taken for a variety of substrates including PDMS, polystyrene, nylon 66, polyamide and polyethylene. ~20 microliter of DI water or diiodomethane was placed on the flat substrate at room temperature followed by imaging. To measure the contact angle, the images were analyzed using FTA32 version 2.1 software. Hydrophobic recovery of water contact angles on PDMS was also studied on: 1) PDMS; 2) unmodified PDMS treated with O_2 plasma using a Plasma Etch PE25-JW Plasma Cleaner, NV, US for 1 minute; 3) PDMS modified with PFPA-sulfobetaine at a concentration of 10 mg/mL; and 4) PDMS modified with PFPA-carboxybetaine at a concentration 10 mg/mL. Contact angles for each of these samples was measured after 1, 2, 4, 7 and 10 days.

S6-5 X-Ray Photoelectron Spectroscopy (XPS): A Kratos AXIS Ultra DLD with a monochromatic Al K X-ray source operated at 10 mA and 15 kV was used to perform the measurements. Individual high-resolution spectra and survey spectra were collected using 20 and 160 eV pass energies. The data were processed using CasaXPS 2.3 software. Each spectrum was calibrated using binding energies by realizing the hydrocarbon peak in the C 1s high-resolution spectra at 284.6 eV.

S6-6 Zeta Potential Measurements: Zeta potential of each membrane was determined by streaming potential measurements with an electrokinetic analyzer (SurPASS, Anton Paar) with an adjustable gap cell. Two membrane samples of 20 mm x 10 mm were used with a gap height of 100 microns and the streaming potential was measured in a 0.1 mM KCl solution at 25 ºC. Four measurements of each PDMS sample were performed between a pH of 2.5-8 by adjusting the pH of the electrolyte solution through the addition of 0.1 M NaOH solution. The zeta potential was then calculated using the Fairbrother-Mastin equation, **Equation 5**:

$$\left(\frac{\Delta\varphi}{\Delta P}\right) = \zeta \frac{\varepsilon_0 \varepsilon_r}{\eta \lambda_0} \left(\frac{\lambda_h R_h}{R}\right) \quad [5]$$

where ζ is the zeta potential (mV), $\Delta\varphi$ is the measured streaming potential in the flow cell (mV), ΔP is the applied pressure (mbar), ε_0 is the vacuum permittivity (F m^{-1}), ε_r is the relative dielectric constant of the electrolyte solution, λ_0 is the bulk conductivity of the circulating electrolyte (mS m^{-1}), and R and R_h are the measured electrical resistances (mV A^{-1}) across the flow channel with the electrolyte solution and the saline reference solution, respectively.

S6-7 Surface roughness: PDMS surface topography and roughness were evaluated by Atomic Force Microscopy (AFM, Bruker, USA) with a scanasyrt-air probe. Each membrane was cut into a 1 x 1 cm^2 piece and attached onto a glass slide with tape. The AFM results were further analyzed using Nanoscope Analysis for surface roughness.

6.5 References

(1) Reed, D.; Kemmerly, S. A. *Infection Control and Prevention: A Review of Hospital-Acquired Infections and the Economic Implications*; 2009; Vol. 9.

(2) Haque, M.; Sartelli, M.; McKimm, J.; Bakar, M. A. Health Care-Associated Infections – An Overview. *Infect. Drug Resist.* **2018**, *11*, 2321–2333.

(3) Liu, Y.; Ren, X.; Huang, T. S. Antimicrobial Cotton Containing N-Halamine and Quaternary Ammonium Groups by Grafting Copolymerization. *Appl. Surf. Sci.* **2014**, *296*, 231–236.

(4) How to Determine if Your Product is a Medical Device | FDA https://www.fda.gov/medical-devices/classify-your-medical-device/how-determine-if-your-product-medical-device (accessed Mar 27, 2020).

(5) Zhang, Z.; Wagner, V. E. *Antimicrobial Coatings and Modifications on Medical Devices*; 2017.

(6) Bogler, A.; Lin, S.; Bar-Zeev, E. Biofouling of Membrane Distillation, Forward Osmosis and Pressure Retarded Osmosis: Principles, Impacts and Future Directions. *Journal of Membrane Science*. Elsevier B.V. 2017, pp 378–398.

(7) Bixler, G. D.; Bhushan, B. Biofouling: Lessons from Nature. *Phil. Trans. R. Soc. A 370*, 2381–2417.

(8) Rana, D.; Matsuura, T. Surface Modifications for Antifouling Membranes. *Chem. Rev.* **2010**, *110*, 2448–2471.

(9) Krishnamoorthy, M.; Hakobyan, S.; Ramstedt, M.; Gautrot, J. E. Surface-Initiated Polymer Brushes in the Biomedical Field: Applications in Membrane Science, Biosensing, Cell Culture, Regenerative Medicine and Antibacterial Coatings. *Chem. Rev.* **2014**, *114*, 10976–11026.

(10) Banerjee, I.; Pangule, R. C.; Kane, R. S. Antifouling Coatings: Recent Developments in the Design of Surfaces That Prevent Fouling by Proteins, Bacteria, and Marine Organisms. *Adv. Mater.* **2011**, *23*, 690–718.

(11) Salta, M.; Wharton, J. A.; Stoodley, P.; Dennington, S. P.; Goodes, L. R.; Werwinski, S.; Mart, U.; Wood, R. J. K.; Stokes, K. R. Designing Biomimetic Antifouling Surfaces. *Phil. Trans. R. Soc. A* **2010**, *368*, 4729–4754.

(12) Holmlin, R. E.; Chen, X.; Chapman, R. G.; Takayama, S.; Whitesides, G. M. Zwitterionic SAMs That Resist Nonspecific Adsorption of Protein from Aqueous Buffer. *Langmuir* **2001**, *17*, 2841–2850.

(13) Ostuni, E.; Chapman, R. G.; Liang, M. N.; Meluleni, G.; Pier, G.; Ingber, D. E.; Whitesides, G. M. Self-Assembled Monolayers That Resist the Adsorption of Proteins and the Adhesion of Bacterial and Mammalian Cells. *Langmuir* **2001**, *17*, 6336–6343.

(14) Nezakati, T.; Seifalian, A.; Tan, A.; Seifalian, A. M. Conductive Polymers: Opportunities and Challenges in Biomedical Applications. *Chem. Rev.* **2018**, *118*, 6766–6843.

(15) Mendona, P. V.; Konkolewicz, D.; Averick, S. E.; Serra, A. C.; Popov, A. V.; Guliashvili, T.; Matyjaszewski, K.; Coelho, J. F. J. Synthesis of Cationic Poly((3-Acrylamidopropyl)Trimethylammonium Chloride) by SARA ATRP in Ecofriendly

Solvent Mixtures. *Polym. Chem.* **2014**, *5*, 5829–5836.

(16) Song, B.; Zhang, E.; Han, X.; Zhu, H.; Shi, Y.; Cao, Z. Engineering and Application Perspectives on Designing an Antimicrobial Surface. *ACS Appl. Mater. Interfaces* **2020**, *12*, 21330–21341.

(17) Mozetič, M. Surface Modification to Improve Properties of Materials. *Materials (Basel).* **2019**, *12*, 441.

(18) P., S. V. V. S. N.; P., S. V. V. S. A Review on Surface Modifications and Coatings on Implants to Prevent Biofilm. *Regen. Eng. Transl. Med.* **2019**.

(19) Roy, S.; Das, T.; Yue, C. Y. High Performance of Cyclic Olefin Copolymer-Based Capillary Electrophoretic Chips. *ACS Appl. Mater. Interfaces* **2013**, *5*, 5683–5689.

(20) Stachowiak, T. B.; Mair, D. A.; Holden, T. G.; Lee, L. J.; Svec, F.; Fréchet, J. M. J. Hydrophilic Surface Modification of Cyclic Olefin Copolymer Microfluidic Chips Using Sequential Photografting. *J. Sep. Sci.* **2007**, *30*, 1088–1093.

(21) Wong, G. C. L.; Pollack, L. Electrostatics of Strongly Charged Biological Polymers: Ion-Mediated Interactions and Self-Organization in Nucleic Acids and Proteins. *Rev. Adv. Annu. Rev. Phys. Chem* **2010**, *61*, 171–189.

(22) Rilbe, H. Historical and Theoretical Aspects of Isoelectric Focusing. *Ann. N. Y. Acad. Sci.* **1973**, *209*, 11–22.

(23) Lipfert, J.; Doniach, S.; Das, R.; Herschlag, D. Understanding Nucleic Acid–Ion Interactions. *Annu. Rev. Biochem.* **2014**, *83*, 813–841.

(24) Sillero, A.; Ribeiro, J. M. Isoelectric Points of Proteins: Theoretical Determination. *Anal. Biochem.* **1989**, *179*, 319–325.

(25) Arakawa, T.; Timasheff, S. N. [3]Theory of Protein Solubility. *Methods Enzymol.* **1985**, *114*, 49–77.

(26) Dumetz, A. C.; Chockla, A. M.; Kaler, E. W.; Lenhoff, A. M. Effects of PH on Protein-Protein Interactions and Implications for Protein Phase Behavior. *Biochim. Biophys. Acta - Proteins Proteomics* **2008**, *1784*, 600–610.

(27) Pergande, M. R.; Cologna, S. M. Isoelectric Point Separations of Peptides and Proteins. *Proteomes* **2017**, *5*.

(28) Shaw, K. L.; Grimsley, G. R.; Yakovlev, G. I.; Makarov, A. A.; Pace, C. N. The Effect of Net Charge on the Solubility, Activity, and Stability of Ribonuclease Sa. *Protein Sci.* **2001**, *10*, 1206–1215.

(29) Patrickios, C. S.; Yamasaki, E. N. Polypeptide Amino Acid Composition and Isoelectric Point: II. Comparison between Experiment and Theory. *Anal. Biochem.* **1995**, *231*, 82–91.

(30) Satpathy, S.; Sen, S. K.; Pattanaik, S.; Raut, S. Review on Bacterial Biofilm: An Universal Cause of Contamination. *Biocatal. Agric. Biotechnol.* **2016**, *7*, 56–66.

(31) Høiby, N.; Bjarnsholt, T.; Givskov, M.; Molin, S.; Ciofu, O. Antibiotic Resistance of Bacterial Biofilms. *Int. J. Antimicrob. Agents* **2010**, *35*, 322–332.

(32) Zhang, Z.; Vaisocherová, H.; Cheng, G.; Yang, W.; Xue, H.; Jiang, S. Nonfouling Behavior of Polycarboxybetaine-Grafted Surfaces: Structural and Environmental Effects. *Biomacromolecules* **2008**, *9*, 2686–2692.

(33) Wong, I.; Ho, C. M. Surface Molecular Property Modifications for Poly(Dimethylsiloxane) (PDMS) Based Microfluidic Devices. *Microfluid. Nanofluidics* **2009**, *7*, 291–306.

(34) Lowe, S.; O 'brien-Simpson, N. M.; Connal, L. A. Antibiofouling Polymer Interfaces: Poly(Ethylene Glycol) and Other Promising Candidates. *Polym. Chem* **2015**, *6*.

(35) Prime, K. L.; Whitesides, G. M. Self-Assembled Organic Monolayers: Model Systems for Studying Adsorption of Proteins at Surfaces. *Science (80-.).* **1991**, *252*, 1164–1167.

(36) Prime', K. L.; Whitesides', G. M. *Adsorption of Proteins onto Surfaces Containing End-Attached Oligo(Ethylene Oxide): A Model System Using Self-Assembled Monolayers*; 1993; Vol. 115.

(37) Stetsyshyn, Y.; Fornal, K.; Raczkowska, J.; Zemla, J.; Kostruba, A.; Ohar, H.; Ohar, M.; Donchak, V.; Harhay, K.; Awsiuk, K.; et al. Temperature and PH Dual-Responsive POEGMA-Based Coatings for Protein Adsorption. *J. Colloid Interface Sci.* **2013**, *411*, 247–256.

(38) Lowe, S.; O'brien-Simpson, N. M.; Connal, L. A. Antibiofouling Polymer Interfaces: Poly(Ethylene Glycol) and Other Promising Candidates. *Polym. Chem.* **2014**, *6*.

(39) Liang, M. N.; Meluleni, G.; Ingber, D. E.; Chapman, R. G.; Whitesides, G. M.; Ostuni, E.; Pier, G. Self-Assembled Monolayers That Resist the Adsorption of Proteins and the Adhesion of Bacterial and Mammalian Cells. *Langmuir* **2002**, *17*, 6336–6343.

(40) Whitesides, G. M. The Origins and the Future of Microfluidics. *Nature*. 2006.

(41) McDonald, J. C.; Whitesides, G. M. Poly(Dimethylsiloxane) as a Material for Fabricating

Microfluidic Devices. *Acc. Chem. Res.* **2002**, *35*, 491–499.

(42) C.M.Kuo, A. Poly(Dimethylsiloxane). *Polym. Data Handb.* **1999**, 411–435.

(43) Trantidou, T.; Elani, Y.; Parsons, E.; Ces, O. Hydrophilic Surface Modification of PDMS for Droplet Microfluidics Using a Simple, Quick, and Robust Method via PVA Deposition. *Microsystems Nanoeng.* **2017**, *3*.

(44) Lin, C.-H.; Yeh, Y.-H.; Lin, W.-C.; Yang, M.-C. Novel Silicone Hydrogel Based on PDMS and PEGMA for Contact Lens Application. *Colloids Surfaces B Biointerfaces* **2014**, *123*, 986–994.

(45) Xue, P.; Li, Q.; Li, Y.; Sun, L.; Zhang, L.; Xu, Z.; Kang, Y. Surface Modification of Poly(Dimethylsiloxane) with Polydopamine and Hyaluronic Acid to Enhance Hemocompatibility for Potential Applications in Medical Implants or Devices. *ACS Appl. Mater. Interfaces* **2017**, *9*, 33632–33644.

(46) Maitz, M. F. Applications of Synthetic Polymers in Clinical Medicine. *Biosurface and Biotribology* **2015**, *1*, 161–176.

(47) Zhang, H.; Chiao, • Mu. Anti-Fouling Coatings of Poly(Dimethylsiloxane) Devices for Biological and Biomedical Applications. *J. Med. Biol. Eng.*

(48) Bausch, G. G.; Stasser, J. L.; Tonge, J. S.; Owen, M. J. Behavior of Plasma-Treated Elastomeric Polydimethylsiloxane Coatings in Aqueous Environment. *Plasmas Polym.* **1998**, *3*, 23–34.

(49) Guo, S.; Jan, D.; Zhu, X.; Quintana, R.; He, T.; Gee Neoh, K.; Jan, D. Surface Charge Control for Zwitterionic Polymer Brushes: Tailoring Surface Properties to Antifouling

Applications. *J. Colloid Interface Sci.* **2015**, *452*, 43–53.

(50) Lowe, A. B.; McCormick, C. L. Synthesis and Solution Properties of Zwitterionic Polymers. *Chem. Rev.* **2002**, *102*, 4177–4189.

(51) Chou, Y. N.; Wen, T. C.; Chang, Y. Zwitterionic Surface Grafting of Epoxylated Sulfobetaine Copolymers for the Development of Stealth Biomaterial Interfaces. *Acta Biomater.* **2016**, *40*, 78–91.

(52) Shao, Q.; Jiang, S. Molecular Understanding and Design of Zwitterionic Materials. *Adv. Mater.* **2015**, *27*, 15–26.

(53) III. An Essay on the Cohesion of Fluids. *Philos. Trans. R. Soc. London* **1805**, *95*, 65–87.

(54) Fowkes, F. M. *THE INTERFACE SYMPOSIUMS Attractive Forces at Interfaces Calculation of a New Prop-Erty Unifies Several Previously Unrelated Fields of Surface Chemistry and Permits Rapid Determination of Several de-Sign Variables. Most Note-Worthy of These Are the Heats* ; UTC, 2020; Vol. 20.

(55) Wu, S. Calculation of Interfacial Tension in Polymer Systems. *J. Polym. Sci. Part C Polym. Symp.* **2007**, *34*, 19–30.

CHAPTER 7: CONCLUSIONs AND FUTURE WORK

7.1 Conclusions

Polymeric materials have been proposed for applications in a variety of fields including: biomedical applications, electronics, biosensor devices and water treatment. Covalent functionalization of these materials provides an effective means to adjust surface properties. These covalent approaches benefit more than noncovalent alternatives because they are more robust and create stable attachment of groups with specific functional properties. Specifically, photo-initiated grafting can be performed under mild reaction conditions and low temperatures with high selectivity compared to other grafting techniques. PFPA chemistry has been used as a coupling agent for fluorinated phenylazides, which are capable of forming stable covalent bonds to sp^2 or sp^3 hybridized carbons or nitrogens.

Perfluorophenylazides (PFPA) are known for their highly reactive nitrene ($-N_3$) moiety that allows them to make chemical bonds with rather unreactive substrates. The nitrene group is activated thermally or with photo-excitation that expels nitrogen gas and affords a reactive singlet nitrogen that attacks –NH-, C=C, and C-H bonds. A PFPA can be synthesized with a carbonyl in the *para* position relative to the nitrene group that enables the attachment of a variety of amine or alcohol terminated molecules, particles, or surfaces via amide or ester bond formation. The azide functional group is activated by photo-excitation producing a highly reactive singlet nitrene that can, for example, undergo C-H insertion within the hydrocarbon backbone of a polyamide membrane, thus creating a covalent bond between the polymer and the membrane. Via intersystem crossing, the singlet nitrene gives a triplet nitrene that dimerizes to a diazo-compound, or gives a ring expansion to an azepine.

PFPA has shown great potential to be used as a favorable coupling agent for a variety of materials. The modifications were all done via a handheld UV lamp; in the future it would be advantageous to attempt modification inside of an actual device (e.g. a microfluidic device) to be able to use this technique in industry.

The PFPA-zwitterions described in Chapter 6 have great potential to become high impact. Zwitterions have shown great potential in preventing biofouling in biomedical devices. Initial studies were conducted with two types of zwitterions (sulfobetaine and carboxybetaine). Both zwitterions were able to coat PDMS surfaces and showed an increase in wettability by a decrease in contact angle. Preliminary biofouling experiments were conducted with the sulfobetaine zwitterion, but were not conducted with the carboxybetaine. Carboxybetaines are known to have higher hydration potential compared to sulfobetaine. Future experiments should include conducting biofouling tests on both zwitterions because it is believed that carboxybetaine would have higher potential to prevent biofouling compared to sulfobetaine. Also, it is known that the methylene group in the zwitterion can be lengthened or shortened to tune the hydration potential of a zwitterion. Therefore, synthesizing a variety of zwitterions with different lengths between the charges could be beneficial.

Chapter 3 described a project regarding the octamer of aniline (two tetramers combined). The octamer was synthesized via two different methods and the purification was optimized. Preliminary crystallization studies were conducted to test the conductivity of the aniline octamer. We believe the conductivity of the crystalline octamer should be higher than conventional polyaniline and the tetramer. Future experiments should include testing different crystallization parameters to try to crystallize the octamer. Once the octamer is crystallized, the conductivity should be compared to both the tetramer and the polyaniline.